System-Level UWB Interference Impact Analysis and Coexistence Limitations

Dr. Jay E. Padgett (P.I.)
Dr. Anthony A. Triolo
Dr. John C. Koshy

Wireless Systems and Networks Research,
Telcordia Technologies, Inc.

August 11, 2003

Sponsored by
Defense Advanced Research Projects Agency
Advanced Technology Office
Analysis and Simulation of UWB Interference Effects – NETEX Program
Issued by DARPA/CMO under Contract #MDA972-02-C-0056

Distribution

DARPA/CMO Attn: Mr. Anthony E. Cicala 3701 North Fairfax Drive Arlington, VA 22203-1714 acicala@darpa.mil (one copy)	DARPA/ATO Attn: Mr. Steve Griggs 3701 North Fairfax Drive Arlington, VA 22203-1714 sgriggs@darpa.mil (two copies)
DARPA/ATO Attn: Mr. Patrick Bailey 3701 North Fairfax Drive Arlington, VA 22203-1714 (one copy)	Defense Contract Management Agency DCMA Springfield DCMAE-GXTB DCMA Springfield Bldg 1, ARDEC Picatinny Arsenal, NJ 07086-5000 (one copy)

Contact information:

Dr. Jay Padgett
Senior Research Scientist
Telcordia Technologies
Room 2Z-465
331 Newman Springs Road
Red Bank, NJ 07701

tel: 732-758-2043
fax:732-758-4372
jpadgett@telcordia.com

Executive Summary

Phase I of the NETEX program is designed to develop an understanding of the effects of interference from ultra-wideband (UWB) transmitters on legacy military radio receivers, nearly all of which are narrowband (NB) relative to the UWB signal. UWB-to-NB interference is being investigated via two parallel activities: (1) extensive testing and (2) analysis/simulation. This document is the third major report on the continuing work of the analysis/simulation program. This report builds on the results of the first and second reports [1][2], which focused primarily on the impact of a single UWB transmission on a NB receiver at the physical layer.

The first report developed physical-layer models to quantify the effect of interference from a UWB transmitter to a narrowband receiver. There were two main components: (1) a detailed analysis of the UWB power spectral density (PSD), which gives the average power-per-Hz vs. frequency for the UWB signal; and (2) a set of models describing the effect of UWB interference on performance for several different communications receiver types. Performance is quantified using the usual measures such as bit error rate (BER) for digital communications receivers, and baseband signal-to-noise ratio (SNR) or signal-to-interference ratio (SIR) for analog receivers.

The second report provides an initial analysis of the coexistence between UWB and legacy NB systems, quantifying the tradeoff between UWB transmit power and the interference impact on a narrowband receiver that is a fixed distance from the UWB transmitter. Aggregate interference impact (additive interference from multiple randomly-distributed UWB transmitters) is analyzed separately but not included in the coexistence analysis. The second report also enhances the work of the first report by introducing additional interference models, including (1) digital communications systems using frequency shift keying (FSK) with coding in the presence of UWB interference; (2) the effects of the UWB interference on pulsed radar systems; and (3) the effect of low pulse-rate UWB interference on an FM receiver, below the FM threshold.

The first Chapter of this report provides an analysis of the impact on a NB receiver of a group of UWB transmitters that are randomly located in two dimensions. The total UWB interference power is taken as the sum of the power levels received from all active UWB transmitters, and the desired signal to the NB receiver is assumed to be Rayleigh-faded due to multipath propagation over a non-line-of-sight path. Two cases are considered: (1) no constraint on the placement of the UWB transmitters relative to the NB receiver, and UWB transmitter locations are governed by a two-dimensional uniform random distribution (a Poisson point distribution); and (2) an "exclusion zone" of some specified size surrounding the NB receiver, within which there cannot be any UWB transmitters, and outside the exclusion zone, the transmitter location distribution is uniform random.

Closed-form expressions are derived for the cumulative distribution functions (CDFs) of the carrier-to-interference ratios (CIRs) and the carrier-to-interference plus noise ratios (CINRs) for each of these two cases, with the size of the exclusion zone being a

parameter in the second case. The outage probability is the probability that the CIR or CINR is below some critical threshold (e.g., the CIR or CINR necessary to support some target bit error rate or baseband signal to noise ratio). Simplified approximations are developed for low outage probabilities (below about 10%) and used to analyze the tradeoff between UWB transmit power and UWB transmitter density (active transmitters per square meter) for each of the two cases, for a given outage impact on the NB receiver. Numerical examples are provided showing the benefit of the exclusion zone in increasing the allowable UWB density and/or transmit power.

To continue adding to the base of physical-layer interference models, Chapter 2 analyzes the effect of UWB interference on a CW radar altimeter using linear FM (chirp) modulation. The scope was limited to cases for which the pulse rate is no greater than the IF bandwidth. The receiver was assumed to be an ideal discriminator followed by baseband filtering, which may be an integral part of the display or control mechanism associated with altimeter. The effective baseband bandwidth will be very narrow, because the process being tracked (the aircraft altitude) is slowly varying, and any high frequency components at the discriminator output will be due to noise or interference. As a result, most of the energy at the discriminator output due to the UWB pulse is rejected by the baseband filtering and the UWB signal has little effect on the altitude estimate.

UWB signals with pulse rates that are high relative to the IF bandwidth will appear as combinations of CW tones and noise-like components. A CW tone within the IF passband can cause a DC component at baseband (at the discriminator output) which cannot be rejected by the baseband filtering. However, CW interference is not unique to UWB signals, and any well-designed altimeter receiver should have capabilities for recognizing and removing the effects of CW interference.

To continue enhancing the understanding of physical-layer UWB interference effects, Chapter 3 provides a detailed analysis and explanation of the abrupt threshold phenomenon that occurs when an FM receiver is subjected to UWB signal with a pulse rate less than the receiver channel bandwidth. This was first observed during the analysis described in Chapter 6 of [2]. The mechanism underlying this phenomenon is explained, and using physical reasoning based on that mechanism, a closed-form approximation is derived for the curve showing the baseband output interference energy per pulse as a function of the carrier-to-interference ratio times the ratio of the pulse rate to the receiver bandwidth (the parameter denoted N_u). Agreement with numerically-derived results is excellent, as can be seen from the curves below. The effects of this phenomenon were observed in the tests on an FM receiver, and are seen in the analysis of Chapter 2 in this report as well.

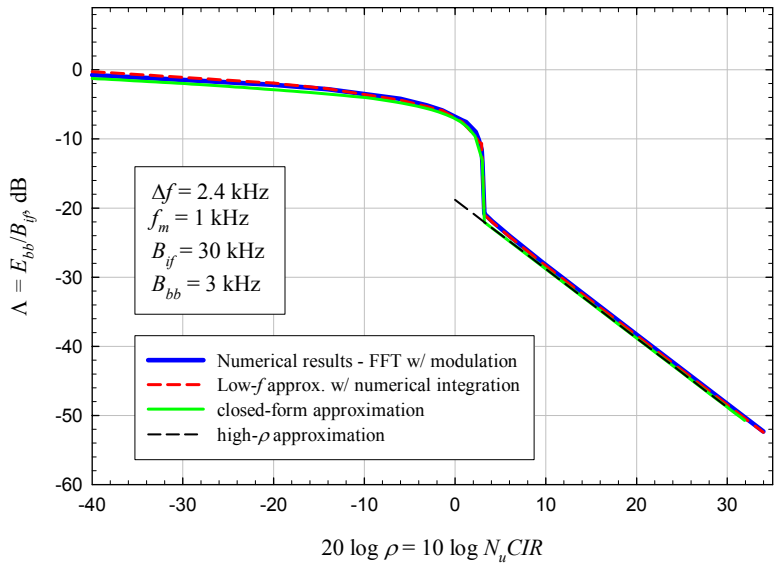

References

[1] "Physical-Layer Modeling of UWB Interference Effects," J. E. Padgett, J. C. Koshy, A. A. Triolo, January 10, 2003, sponsored by DARPA under contract MDA972-02-C-0056.

[2] "Physical-Layer UWB Interference Impact Analysis," J. E. Padgett, A. A. Triolo, J. C. Koshy, August 8, 2003, sponsored by DARPA under contract MDA972-02-C-0056.

Contents

Chapter 1: System-Level UWB Interference Analysis

1.1. Introduction

Previous reports [1][2] have developed physical-layer models for analysis of interference from UWB transmitters to narrowband (NB) receivers, and provided physical-layer analyses of the interference impact. These analyses generally considered the effect of a single UWB transmitter on a single narrowband receiver, although Chapter 3 of [2] discussed aggregate interference from multiple UWB transmitters. Annex 3A of [2] derived an expression for the cumulative distribution function (CDF) of the total power received from multiple UWB transmitters that are distributed around the victim receiver in a uniform random fashion.

One major goal of this report is to develop a modeling framework for a system-level interference analysis and to provide some initial results and conclusions about UWB/NB coexistence. For the present, the focus will be limited to UWB-to-NB interference, rather than NB-to-UWB interference. It is assumed that the UWB devices are randomly-scattered spatially in two dimensions, and operated as a network, performing some function of combination of functions such as local area data networking, position location, or local radar (e.g., a UWB radar net monitoring a protected area).

The analysis initially focuses on a victim narrowband receiver, which is assumed to be surrounded by the UWB transmitters. Figure 1-1 illustrates the concept.

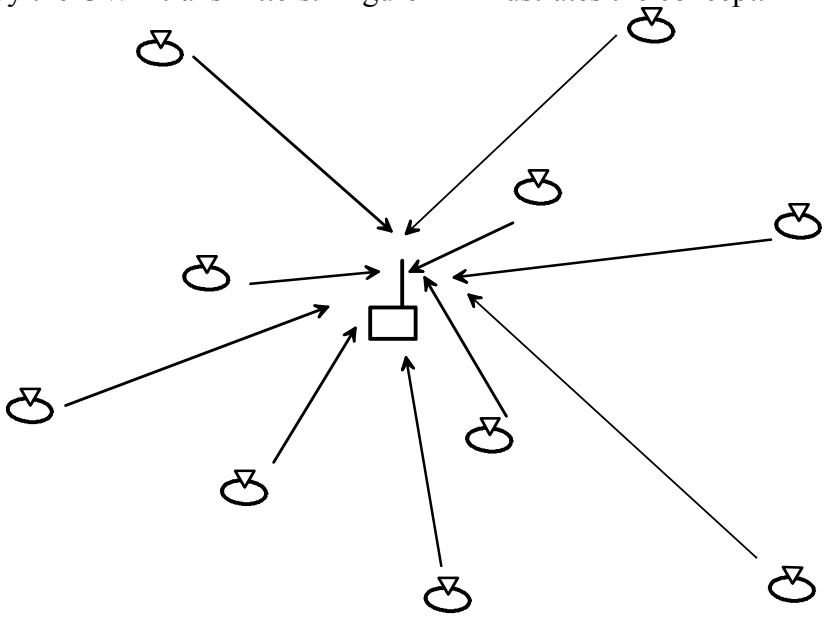

Figure 1-1: *Conceptual illustration of Interference to a NB transmitter from a UWB network*

1.2. Parameters and Assumptions

Key parameters of the analysis are shown in the table below for reference.

ρ_u	spatial density of UWB transmitters (transmitters per km^2)
a	average traffic intensity (transmit duty cycle) per UWB transmitter
$\rho_a = \rho a$	average density of UWB transmitters thar are transmitting at a given time
C_{nb}	carrier (desired signal) power received by the NB receiver
$\overline{C}_{nb}$	local mean (averaged over multipath fading) NB received carrier power
v_m	multipath fade factor; $C_{nb} = v_m \overline{C}_{nb}$
N_{nb}	effective thermal noise power as seen by the NB receiver
I_{UWB}	total UWB interference power seen by NB receiver
P_{tx}	UWB transmit power within the NB receiver passband
f_0	NB receiver channel center frequency
γ	path loss exponent (path loss proportional to d^{γ})
Λ	carrier to interference plus noise threshold for the NB receiver

It is assumed here that the carrier is Rayleigh-faded, which is appropriate to a signal subject to non-line-of-sight (NLOS) propagation with multipath. The interference is assumed to be the power sum of the signals received from all surrounding active UWB transmitters. It is assumed that in general, the UWB transmitters will transmit bursts measured in milliseconds or tens of milliseconds, so the interference will be time-varying. The carrier will vary as well due to motion of the transmitter and/or receiver, and movement of reflective objects in the environment. Thus, the carrier to interference plus noise ratio (CINR) is not static, but will vary at rates approximating those of typical digital communications frame rates (e.g., 100 Hz). What will be of interest here is the probability that the CINR drops below some critical threshold Λ. Thus, the results here take the form of a statistical "snapshot", such as the probability that at a given time, the CINR is below Λ. This condition is termed an "outage".

1.3. Propagation

1.3.1. Desired Signal to Victim Receiver

The desired signal is assumed to be subject to multipath fading, and the receive signal power can be represented at a given point in time as

$$C_{nb} = v_m \overline{C}_{nb} \tag{1-1}$$

where $\overline{C}_{nb}$ is the local mean received signal, and v_m is a random variable that represents the variation due to the multipath fading. Rayleigh fading is assumed, in which case the probability density function (PDF) of v_m is

$$f_{v_m}(v) = e^{-v} \quad v \geq 0 . \tag{1-2}$$

Although it will not be included in the initial analysis, shadow fading can also be incorporated into the model using

$$\overline{C}_{nb} = v_s \left\langle \overline{C}_{nb} \right\rangle \tag{1-3}$$

where $\left\langle \overline{C}_{nb} \right\rangle$ is the average value of the local mean, averaged over the shadow fade variations, and v_s is a random variable that represents the effects of shadow fading. The mean $\left\langle \overline{C}_{nb} \right\rangle$ will be a function of the distance of the narrowband receiver from its companion transmitter, the frequency f_0, the transmit power, and the antenna characteristics.

The relationship between $\left\langle \overline{C}_{nb} \right\rangle$ and distance can be based on models which apply to the antenna elevation, terrain, transmitter-receiver distance, and frequency range used by the NB victim systems. These models typically give the path loss in dB in the form

$$L(d) = A + 10\gamma \log d \tag{1-4}$$

where d is the distance between the transmitter and receiver, and the parameters A and γ depend generally on frequency, terrain, and the elevations of the transmit and receiver antennas. Some of these models are based on mathematical curve fitting to measured data, so their range of application (in terms of frequency, limits on d, antenna elevations, etc.) is limited to the range of conditions over which the measurements were made.

The random variable v_s is often modeled as lognormal, in which case $10 \log v_s$ is Gaussian with a standard deviation of σ dB, usually assumed to be 8 to 10 dB for frequencies in the UHF region. If $V_s = 10 \log v_s$ then

$$\overline{V}_s = 10 \log \overline{v}_s - \frac{\sigma^2 \ln 10}{20} \tag{1-5}$$

Clearly, from (1-3), $\overline{v}_s = 1$ by definition.

1.3.2. UWB-to-NB Interference Path

Propagation models used in system analysis are narrowband models, in that they assume that the signal center frequency far exceeds the bandwidth. With UWB signals, this is not the case, and traditional narrowband propagation models may not apply, at least without some adjustments. However, narrowband propagation models can be applied to the interference path, because the victim receiver only sees a narrowband signal and for most purposes, the propagation channel can be modeled as a linear channel as shown in Figure 1-2. An equivalent channel can be defined by passing the UWB signal through a narrowband filter with center frequency f_0 prior to transmission, which results in the same interference waveform being presented at the detector/demodulator block of the NB receiver. Hence, narrowband path loss models can be used for the interference analysis.

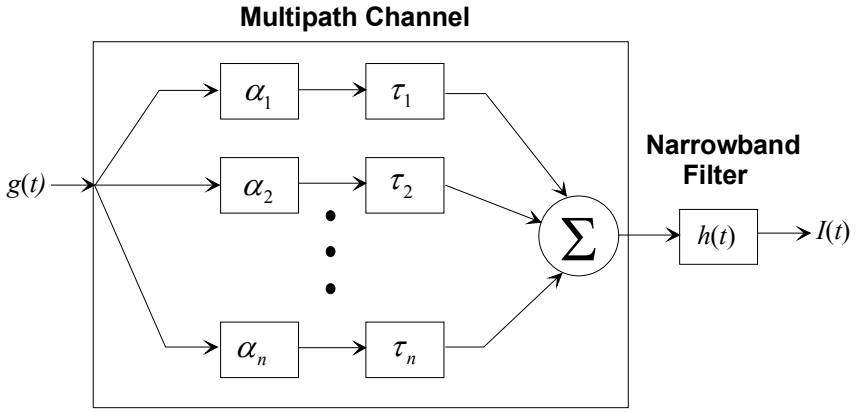

Figure 1-2: *UWB-to-NB propagation channel model*

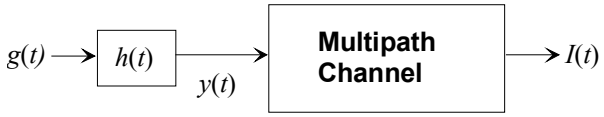

Figure 1-3: *Equivalent channel model*

The appropriate model will again depend on the conditions, including the distance between the UWB transmitter and the NB receiver, the NB receiver center frequency, the terrain, and the antenna elevations.

For this analysis, a general exponential path loss model will be used for the interference path, so that the interference power at the NB receiver from a UWB transmitter *d* meters away is

$$I_{rx}(d) = P_{tx} \cdot \alpha d^{-\gamma} \tag{1-6}$$

where the constant α depends on frequency. One way to define α is to assume free-space loss at 1 meter, giving

$$\alpha = \left(\frac{\lambda}{4\pi}\right)^2 = \left(\frac{c}{2\pi f_0}\right)^2 \tag{1-7}$$

where λ is the wavelength and *c* is the speed of light. For example, at 2.4 GHz, $10\log\alpha = -40$ dB. However, for the general formulation developed here, the exact value of α is not important.

In (1-6), P_{tx} is the UWB transmit power as seen through a filter with bandwidth B_{nb} and center frequency f_0. Initially it is assumed that P_{tx} is the same for each UWB transmitter that is actively transmitting a burst.

1.4. CDF of the Aggregate UWB Interference Power

The total UWB interference received by the NB receiver is

$$I_{UWB} = \alpha P_{tx} \sum_j d_j^{-\gamma} \tag{1-8}$$

and the $\{d_j\}$ are assumed to be randomly located with a uniform spatial distribution. This means that if the average density of active UWB transmitters is ρ_a, then on average there are $A \cdot \rho_a$ active UWB transmitters within some are *A*. The actual number of active UWB transmitters within the area is a Poisson-distributed random variable n_A; i.e.,

$$P_{n_A}(N) = \Pr\{n_A = N\} = e^{-A\rho_A} \frac{(A\rho_A)^N}{N!} \tag{1-9}$$

Clearly, $\sum_{N=0}^{\infty} P_{n_A}(N) = 1$.

It is useful to define a normalized version of I_{UWB}:

$$Z \equiv \frac{I_{UWB}}{\alpha P_{tx} (\pi\rho_a)^{\gamma/2}} \tag{1-10}$$

The cumulative distribution function (CDF) for *Z* is derived in Annex 3A of [2] and is shown to be (where $\nu = 2/\gamma$):

$$F_Z(z) = \Pr(Z < z) = 1 - \frac{1}{\pi}\sum_{k=1}^{\infty}\frac{\Gamma(k\nu)}{k!}\left[\frac{\Gamma(1-\nu)}{z^{\nu}}\right]^k \sin k\pi(1-\nu), \quad z > 0 \qquad (1\text{-}11)$$

For $z >> 1$, $F_Z(z) \cong 1 - z^{-\nu}$. As also shown in Annex 3A of [2], if only interference from the nearest transmitter is considered, then

$$F_Z(z) = \exp\left(-z^{-\nu}\right) \quad z > 0 \text{ (nearest interferer)} \qquad (1\text{-}12)$$

Again, for $z >> 1$, $F_Z(z) \cong 1 - z^{-\nu}$, from simply expanding the exponential. Thus, for high values of z (strong interference), the nearest-interferer and multiple-interferer distributions are nearly equal. Figure 1-4 shows the CDF of the aggregate interference for the multiple-interferer and nearest-interferer models (extracted from Figure 3-2 of [2]).

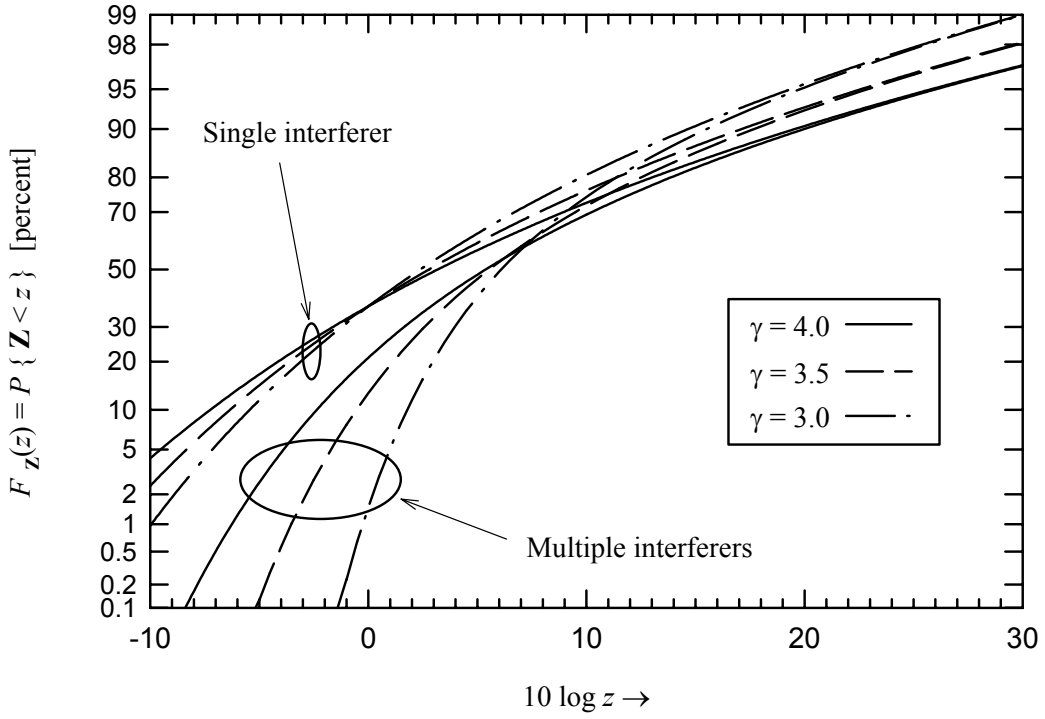

Figure 1-4: *CDF of the aggregate interference*

1.5. CDF of the Carrier-to-Interference Ratio

To understand the impact of the UWB transmitters on the performance of the NB receiver, it is useful to have an expression for the carrier-to-interference ratio as seen by the NB receiver. From such an expression, other measures of interest such as bit error rate (for digital communications systems) and baseband signal-to-interference ratio (for analog communications) can be derived.

Let a normalized version of the local mean NB carrier power be

$$\overline{X}_{nb} = \frac{\overline{C}_{nb}}{\alpha P_{tx} (\pi \rho_a)^{\gamma/2}} \tag{1-13}$$

and the faded normalized carrier power is

$$X_{nb} = v_m \overline{X}_{nb} . \tag{1-14}$$

What is of interest is the CDF of the carrier-to-interference ratio; that is

$$\Pr\left(\frac{C_{nb}}{I_{uwb}} < \Lambda \right) = \Pr\left(\frac{X_{nb}}{Z} < \Lambda \right) = \Pr\left(\frac{v_m \overline{X}_{nb}}{Z} < \Lambda \right) = \Pr\left(v_m < \frac{\Lambda Z}{\overline{X}_{nb}} \right) \tag{1-15}$$

Given that Z takes on a particular value z,

$$\Pr\left(v_m < \frac{\Lambda Z}{\overline{X}_{nb}} \middle| Z = z \right) = 1 - e^{-\frac{\Lambda z}{\overline{X}_{nb}}} \tag{1-16}$$

and removing the conditioning on Z gives

$$\Pr\left(v_m < \frac{\Lambda Z}{\overline{X}_{nb}} \right) = 1 - \int_0^\infty e^{-\frac{\Lambda z}{\overline{X}_{nb}}} f_Z(z) dz \tag{1-17}$$

Note that the integral in (1-17) is the moment generating function or characteristic function of Z. That is:

$$\Phi_Z(x) = \left\langle e^{xZ} \right\rangle = \int_0^\infty e^{xz} f_Z(z) dz \tag{1-18}$$

It is not necessary to know explicitly the PDF $f_Z(z)$; it is sufficient to know the moment generating function. Using eq. (10) in Annex 3A of [2] and substituting $\xi = -j\omega$, the characteristic function is

$$\Phi_Z(-\xi) = \exp\left(-\xi \int_0^\infty z^{-\nu} e^{-\xi z} dz\right) \tag{1-19}$$

The Gamma function is defined by Euler's integral as ([6], p. 255, eq. 6.1.1):

$$\Gamma(x) = \xi^x \int_0^\infty z^{x-1} e^{-\xi z} dz, \quad \operatorname{Re} x > 0, \operatorname{Re} \xi > 0 \tag{1-20}$$

Letting $x = 1 - \nu$, the argument of the exponential in (1-19) is

$$\xi \int_0^\infty z^{-\nu} e^{-\xi z} dz = \xi^\nu \cdot \xi^{1-\nu} \int_0^\infty z^{-\nu} e^{-\xi z} dz = \xi^\nu \Gamma(1-\nu) \qquad \nu < 1, \xi > 0 \tag{1-21}$$

and the characteristic function is

$$\Phi_Z(-\xi) = \exp\left[-\xi^\nu \Gamma(1-\nu)\right] \tag{1-22}$$

Letting $\xi = \dfrac{\Lambda}{\overline{X}_{nb}}$ gives the desired CDF as

$$\begin{aligned} \Pr\left(\frac{C_{nb}}{I_{UWB}} < \Lambda\right) &= 1 - \Phi_Z\left(-\frac{\Lambda}{\overline{X}_{nb}}\right) \\ &= 1 - \exp\left[-\left(\frac{\Lambda}{\overline{X}_{nb}}\right)^\nu \Gamma(1-\nu)\right] \\ &= 1 - \exp\left[-\left(\frac{\Lambda}{\overline{X}_{nb}}\right)^{\frac{2}{\gamma}} \Gamma\left(1-\frac{2}{\gamma}\right)\right] \qquad \gamma > 2 \end{aligned} \tag{1-23}$$

Figure 1-5 shows this CDF for four different values of γ, and also Monte Carlo results for $\gamma = 3$ for both the multiple-interferer and nearest-interferer cases. As can be seen, the multiple-interferer Monte Carlo results agree closely with the closed form CDF as would be expected. The nearest-interferer CDF matches closely only at for lower carrier-to-

interference ratios (high interference), which is consistent with Figure 1-4. However, as will become clear, it is this region of the CDF that normally is of most interest.

Applying the normalization factor $\overline{C}_{nb} = \alpha P_{tx} (\pi \rho_a)^{\gamma/2} \overline{X}_{nb}$ gives:

$$\Pr\left(\frac{C_{nb}}{I_{UWB}} < \Lambda\right) = 1 - \exp\left[-\pi\rho_a \left(\frac{\Lambda \alpha P_{tx}}{\overline{C}_{nb}}\right)^{\frac{2}{\gamma}} \Gamma\left(1 - \frac{2}{\gamma}\right)\right] \qquad \gamma > 2 \tag{1-24}$$

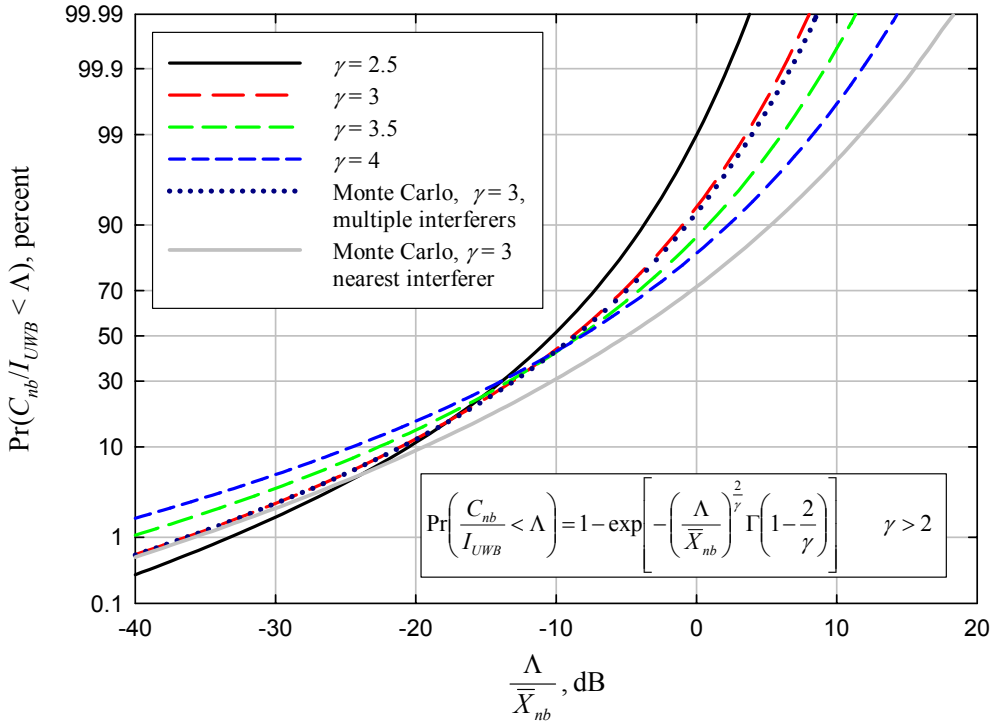

Figure 1-5: *CDF of the carrier-to-interference ratio*

1.5.1. Complementary CDF of the Bit Error Rate

For a digital communications system, the CDF of the bit error probability is of interest, and can be easily found from this expression. For example, consider a binary FSK NB system with non-coherent detection, for which the bit error probability (assuming the two signal frequencies are orthogonal with non-coherent detection) is given by:

$$P_b = \frac{1}{2} e^{-\frac{E_b}{2N_0}} \tag{1-25}$$

where E_b is the received energy per bit and $N_0/2$ is the two-sided noise power spectral density. Assuming that the UWB interference appears noise-like and assuming that $E_b/N_0 = C_{nb}/I_{UWB}$ (true if the NB system noise bandwidth is equal to the bit rate), then if $C_{nb}/I_{uwb} = \Lambda$ and $P_b = \frac{1}{2}e^{-\Lambda/2}$ as shown in Figure 1-6.

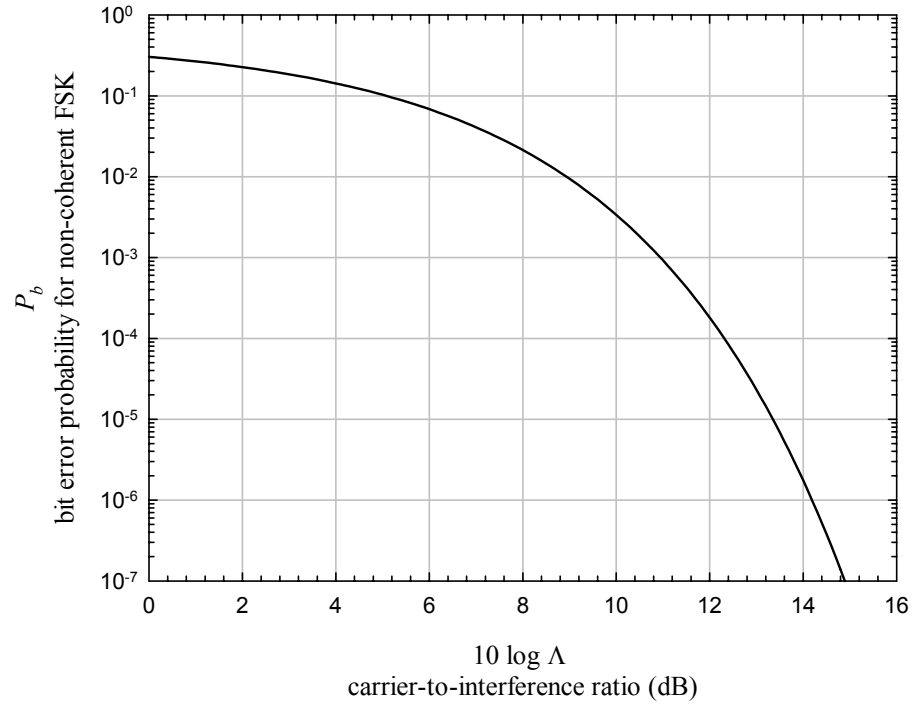

Figure 1-6: *Bit error probability for non-coherently detected FSK (orthogonal symbols)*

This relationship can be combined with (1-23) to give the CDF of the bit error probability. Letting $P_b = P$ and $\Lambda = -2\ln(2P)$, the complementary CDF of the bit error probability is:

$$\Pr(P_b > P) = \Pr\left(\frac{C_{nb}}{I_{UWB}} < -2\ln(2P)\right)$$

$$= 1 - \exp\left\{-\left[\frac{-2\ln(2P)}{\bar{X}_{nb}}\right]^{\frac{2}{\gamma}}\Gamma\left(1-\frac{2}{\gamma}\right)\right\}, \quad \gamma > 2, \quad 0 < P < 0.5 \tag{1-26}$$

or

$$\Pr(P_b > P) = 1 - \exp\left\{ -\pi\rho_a \left[\frac{-2\ln(2P)\cdot \alpha P_{tx}}{\overline{C}_{nb}} \right]^{\frac{2}{\gamma}} \Gamma\left(1 - \frac{2}{\gamma}\right) \right\}, \quad \gamma > 2, \quad 0 < P < 0.5 \qquad (1\text{-}27)$$

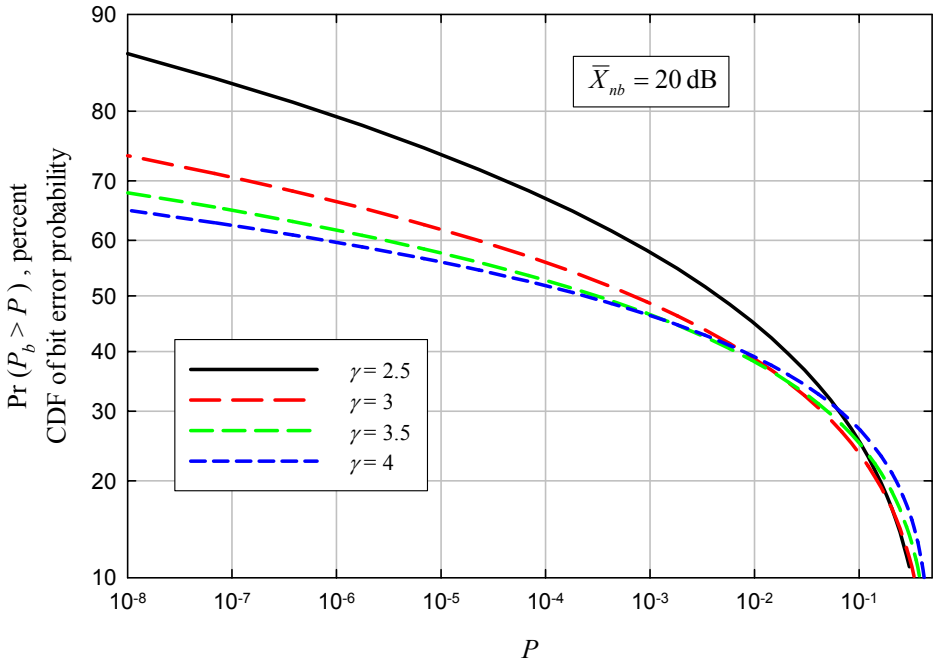

Figure 1-7: *Complementary CDF of the bit error probability for* $\overline{X}_{nb} = 20$ dB

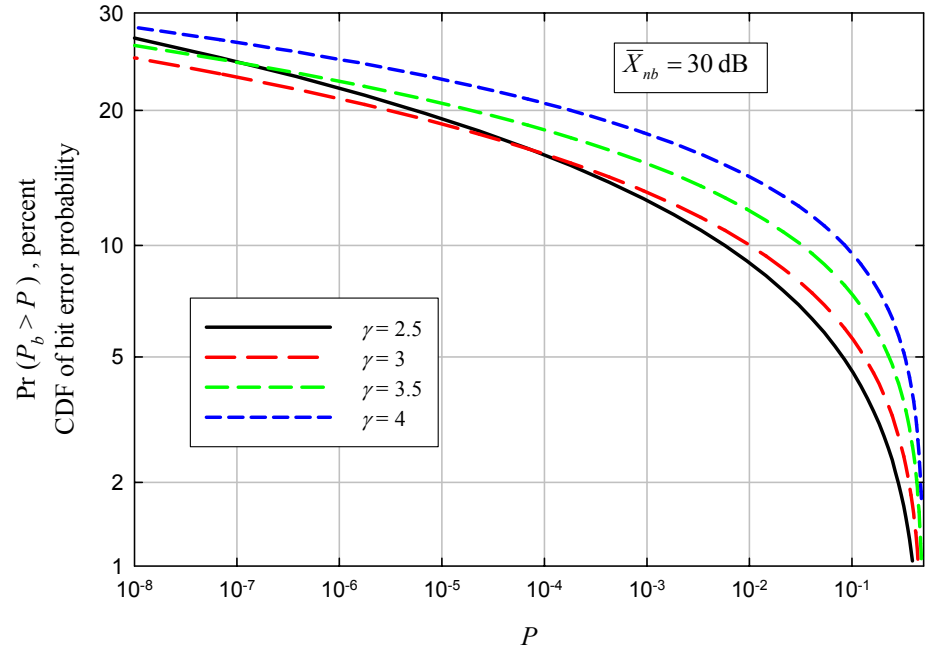

Figure 1-8: *Complementary CDF of the bit error probability for* $\overline{X}_{nb} = 30$ dB

1.5.2. Low Outage Probability Approximation

The probability $\Pr(C_{nb}/I_{UWB} < \Lambda)$ can be regarded as an "outage" probability (the probability that the bit error rate exceeds some threshold, or the probability that the baseband signal-to-noise ratio is below some threshold). Accordingly, the notation $P_{out} \equiv \Pr(C_{nb}/I_{UWB} < \Lambda)$ will be used. Typically it will be of interest to keep this outage probability low (e.g., in the range of 1% to 10%), with the target value depending on the specifics of the applications supported by the narrowband radios. Figure 1-9 shows P_{out} vs. $10\log(\overline{X}_{nb}/\Lambda)$ for $0.01 \le P_{out} \le 0.1$.

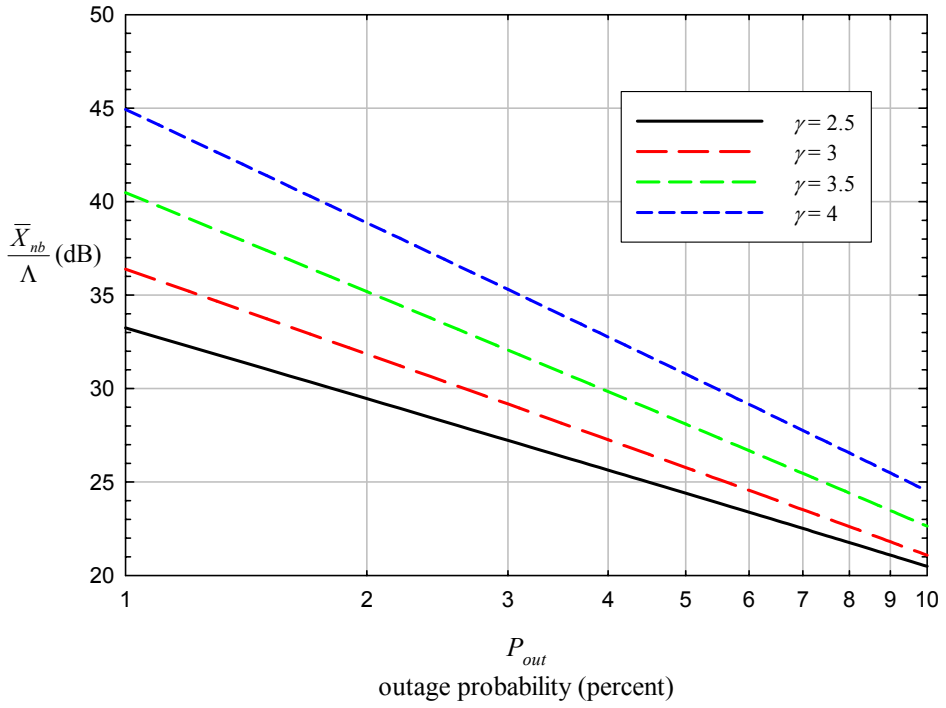

Figure 1-9: *Required $\overline{X}_{nb}/\Lambda$ to achieve a given outage probability for low outage*

In the low outage range, (1-17) can be approximated by recognizing that $P_{out} \cong -\ln(1 - P_{out})$ for $P_{out} << 1$, giving

$$P_{out} \cong \left(\frac{\Lambda}{\overline{X}_{nb}}\right)^{\frac{2}{\gamma}} \Gamma\left(1 - \frac{2}{\gamma}\right) \qquad P_{out} << 1\,, \tag{1-28}$$

which is useful because it allows any of the parameters to be used as the independent variable. For example, the normalized local mean signal power required at the narrowband receiver to achieve an outage probability of P_{out} is

$$\overline{X}_{nb} \cong \Lambda \cdot \left[\frac{\Gamma(1-2/\gamma)}{P_{out}} \right]^{\frac{\gamma}{2}} \qquad P_{out} << 1, \tag{1-29}$$

Hence, in terms of the curves in Figure 1-9,

$$10\log\left(\frac{\overline{X}_{nb}}{\Lambda}\right) \cong 5\gamma\left[\log\Gamma\left(1-\frac{2}{\gamma}\right) - \log P_{out}\right] \tag{1-30}$$

Figure 1-10 shows the approximation of (1-30) compared to the exact expression of (1-23); agreement is excellent over the range of interest.

Figure 1-11 shows the required $\overline{X}_{nb}/\Lambda$ vs. γ for different values of P_{out}, using (1-30).

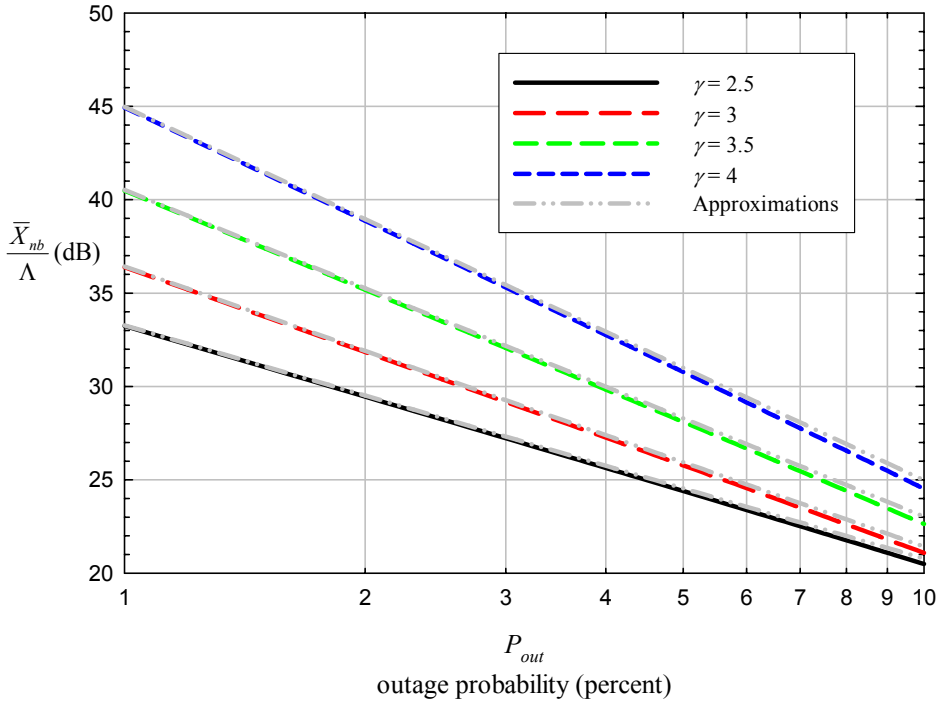

Figure 1-10: $\overline{X}_{nb}/\Lambda$ *vs. outage probability with low-outage approximations*

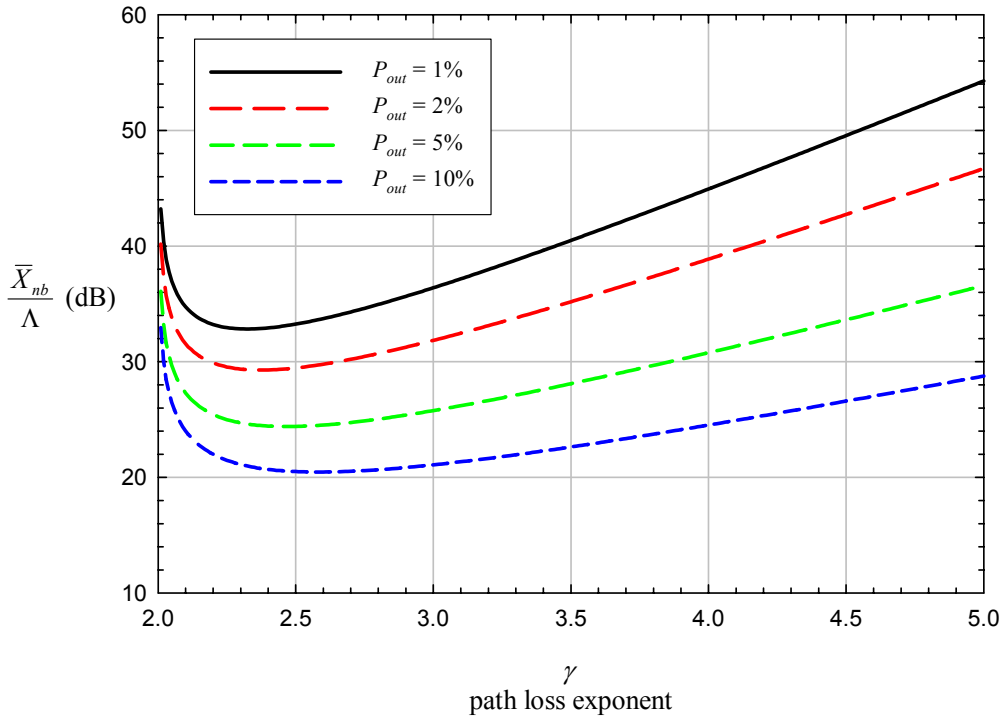

Figure 1-11: $\overline{X}_{nb}/\Lambda$ vs. γ for different outage probabilities

1.6. Outage Probability with an Interference Exclusion Zone

Suppose that by some means, an exclusion zone of radius $d_{\min}$ centered on the narrowband receiver can be ensured; that is, there will be no UWB transmitters within $d_{\min}$ meters of the NB receiver, as illustrated in Figure 1-12.

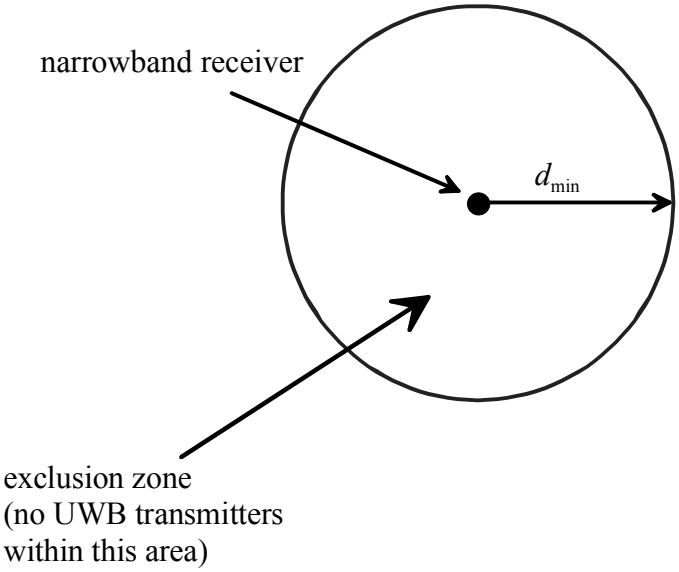

Figure 1-12: *Illustration of the UWB transmitter exclusion zone concept*

The area of this exclusion zone is $\pi d_{\min}^2$, and it is useful to define

$$n_x \equiv \rho_a \pi d_{\min}^2 \tag{1-31}$$

which is the average number of active UWB transmitters that *would have been* within this area without the exclusion.

1.6.1. CDF of the CIR with an Exclusion Zone

As in the previous case,

$$\Pr\left(\frac{C_{nb}}{I_{UWB}} < \Lambda\right) = 1 - \Phi_Z\left(-\frac{\Lambda}{\overline{X}_{nb}}\right) \tag{1-32}$$

As shown in the Annex to this Chapter, with the exclusion zone the characteristic function of the normalized aggregate interference is

$$\Phi_Z(-\xi) = \exp\left[n_x\left(1 - e^{-\xi n_x^{-1/\nu}}\right) - \xi^\nu \gamma\left(1-\nu, \xi\, n_x^{-1/\nu}\right)\right] \tag{1-33}$$

where

$$\gamma(a,x) = \int_0^x e^{-t} t^{a-1} dt \tag{1-34}$$

is the incomplete Gamma function (not to be confused with the path loss exponent γ).

The outage probability then becomes:

$$P_{out} = \Pr\left(\frac{C_{nb}}{I_{uwb}} < \Lambda\right) = 1 - \exp\left[n_x\left(1 - e^{-\frac{\Lambda}{\overline{X}_{nb}} n_x^{-1/\nu}}\right) - \left(\frac{\Lambda}{\overline{X}_{nb}}\right)^\nu \gamma\left(1-\nu, \frac{\Lambda}{\overline{X}_{nb}} n_x^{-1/\nu}\right)\right] \tag{1-35}$$

Figure 1-13 shows $\gamma(a,x)$ for $a = 1-\gamma/2$ where γ is the path loss exponent (2.5, 3.0, 3.5, and 4.0). Note that the asymptotic value is $\lim_{x\to\infty}\gamma(a,x) = \Gamma(a)$ as would be expected.

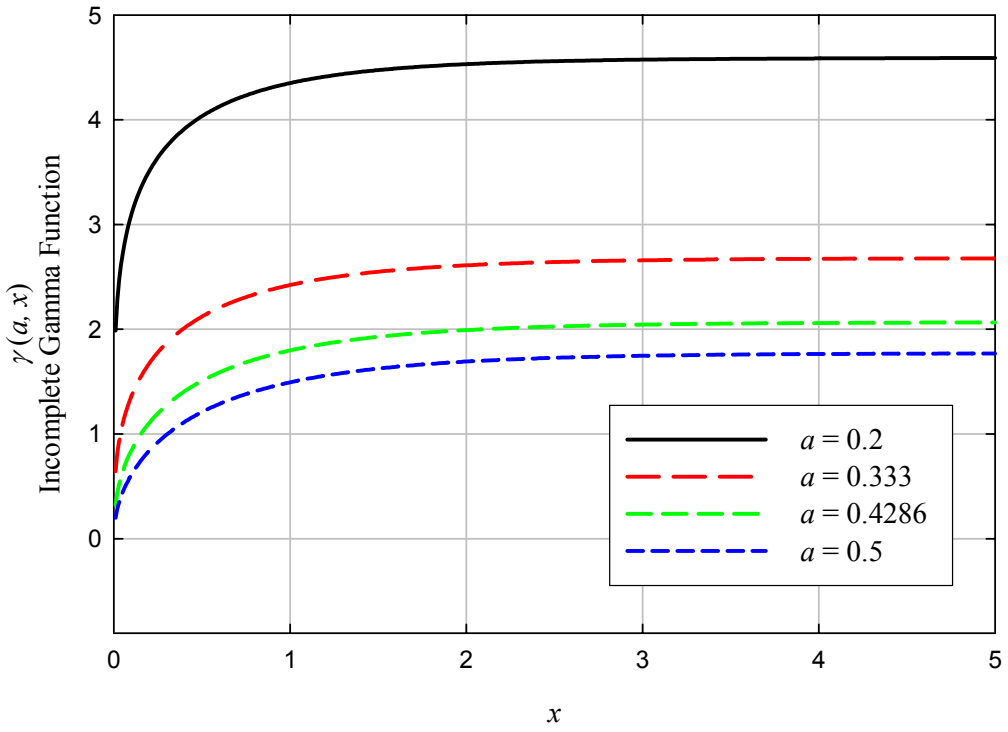

Figure 1-13: *The incomplete Gamma function for values of a corresponding to the path loss exponents 2.5, 3.0, 3.5, and 4.0.*

Figure 1-14 shows the CDF $\Pr(C_{nb}/I_{UWB} < \Lambda)$ with an exclusion zone for $n_x = 1$, for the usual values of the path loss exponent γ. Also shown are Monte Carlo results for $\gamma = 3$ for comparison, and the single-interferer CDF (also with the exclusion zone). With the exclusion zone, the nearest-interferer approximation begins to lose accuracy, because the total interference power is more often the sum of nearly equal contributions from several sources, rather than from a single dominant (nearby) interferer.

As for the non-exclusion case above, Figure 1-15 shows the value of $\overline{X}_{nb}/\Lambda$ required to achieve a given outage probability with $n_x = 1$, for outage probabilities ranging from 1% to 10%, and Figure 1-16 shows a similar set of curves for $n_x = 2$.

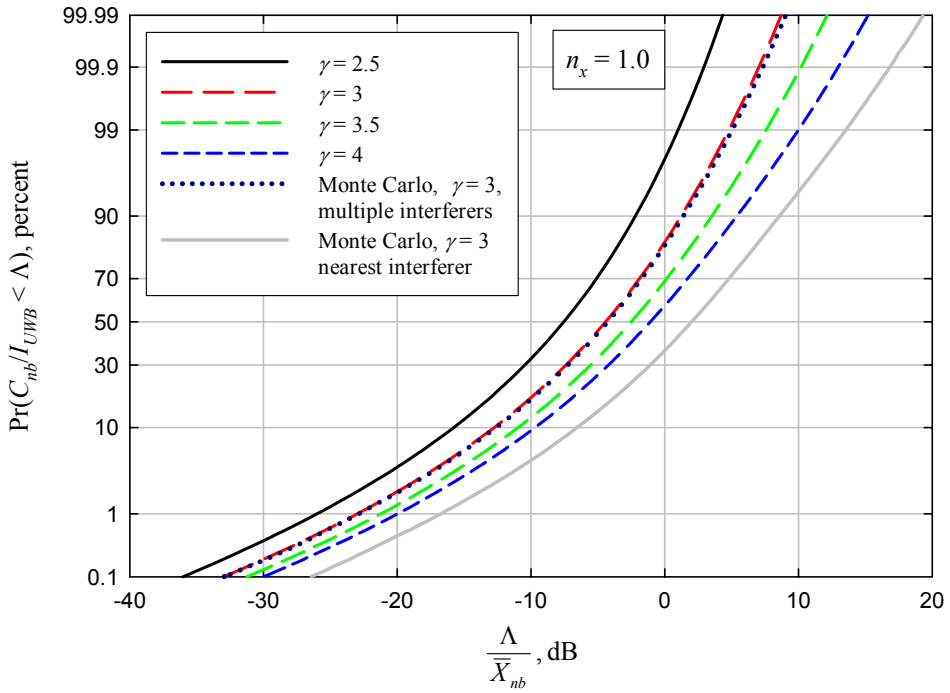

Figure 1-14: *CDF of the carrier-to-interference ratio with an exclusion zone of* $n_x = 1$.

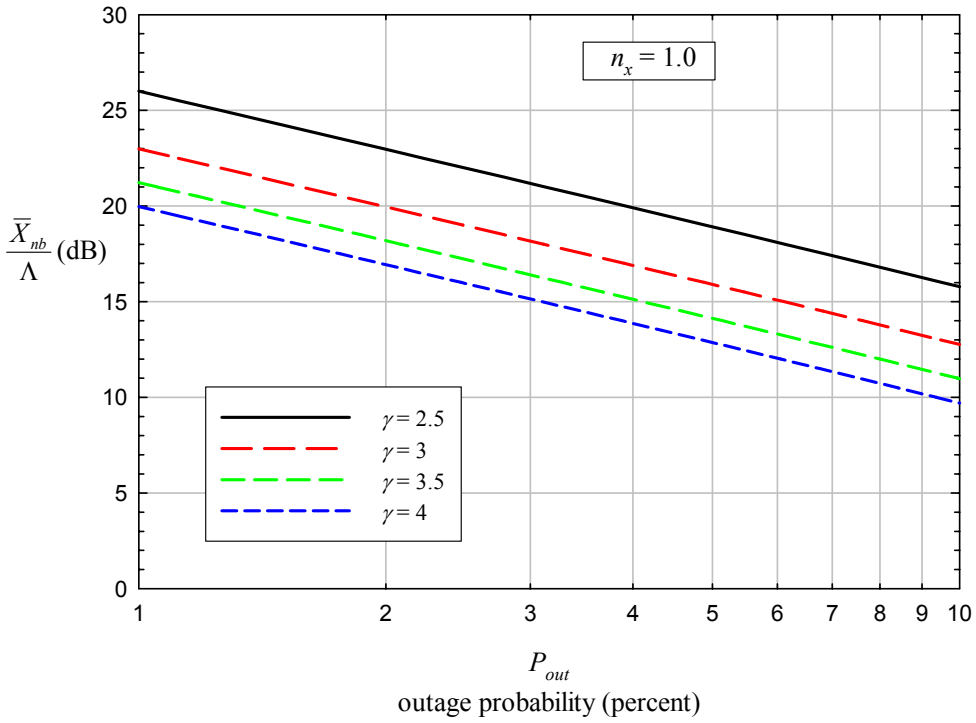

Figure 1-15: *Required* $\overline{X}_{nb}/\Lambda$ *to achieve a given outage probability for low outage with an exclusion zone,* $n_x = 1$.

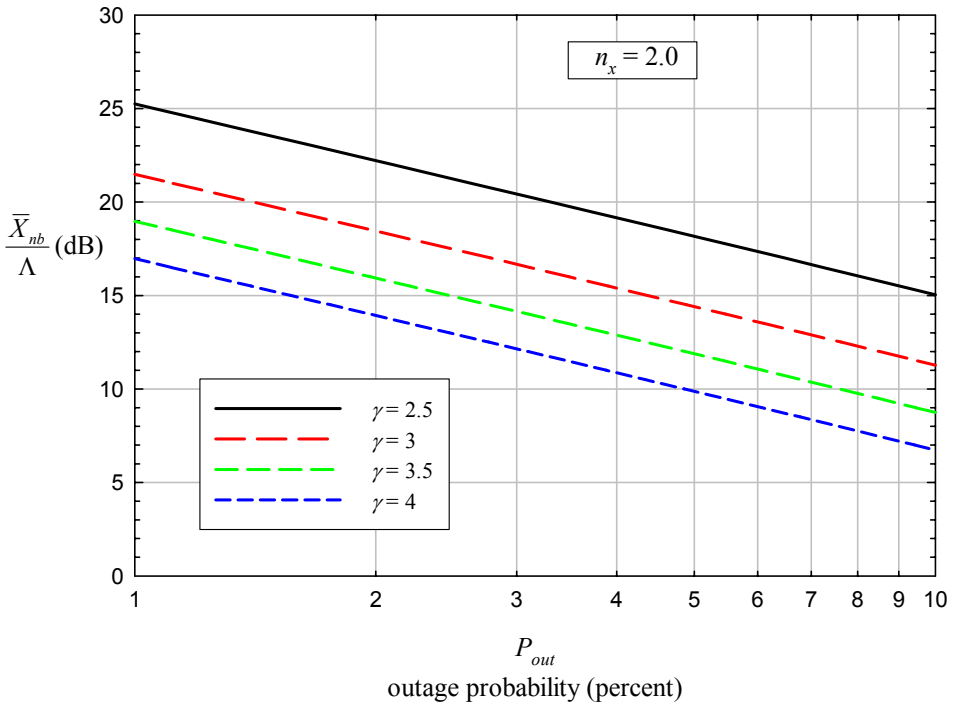

Figure 1-16: *Required* $\overline{X}_{nb}/\Lambda$ *to achieve a given outage probability for low outage with an exclusion zone,* $n_x = 2$.

1.6.2. Outage Probability Approximation with an Exclusion Zone

It is useful to develop an approximation for (1-35) that is invertible, so that the required $\overline{X}_{nb}/\Lambda$ can be expressed as a function of P_{out}, n_x, and γ.

In the range of interest, $\frac{\overline{X}_{nb}}{\Lambda} >> 1$, so unless $n_x << 1$, $\frac{\Lambda}{\overline{X}_{nb}} n_x^{-1/\nu} << 1$ and

$$1 - e^{-\frac{\Lambda}{\overline{X}_{nb}} n_x^{-1/\nu}} \cong \frac{\Lambda}{\overline{X}_{nb}} n_x^{-1/\nu} \tag{1-36}$$

The incomplete Gamma function $\gamma(a,x)$ can be approximated over a limited range of x by using the function (see e.g., [6] p. 260, eq. 6.5.4)

$$\gamma^*(a,x) = \frac{x^{-a}}{\Gamma(a)} \gamma(a,x) \tag{1-37}$$

which is shown in Figure 1-17, for values of $a = 1 - 2/\gamma$ corresponding to the usual values of the path loss exponent γ. In the range of small x of interest here, $\gamma^*(a,x) \cong 1.1$, so the incomplete Gamma function can be approximated as

$$\gamma(a,x) \cong 1.1 \times x^a \Gamma(a) \tag{1-38}$$

Using this approximation, as well as that of (1-36) and $\ln(1-P_{out}) \cong -P_{out}$ for $P_{out} << 1$ gives

$$\begin{aligned} P_{out} &\cong \left(\frac{\Lambda}{\overline{X}_{nb}}\right)^{\nu} \cdot 1.1 \times \left(\frac{\Lambda}{\overline{X}_{nb}} n_x^{-1/\nu}\right)^{1-\nu} \Gamma(1-\nu) - \frac{\Lambda}{\overline{X}_{nb}} n_x^{1-1/\nu} \\ &= \frac{\Lambda}{\overline{X}_{nb}} n_x^{1-1/\nu} \left[1.1 \times \Gamma(1-\nu) - 1\right] \end{aligned} \tag{1-39}$$

or

$$\frac{\overline{X}_{nb}}{\Lambda} \cong \frac{n_x^{1-\gamma/2}\left[1.1 \times \Gamma\left(1-\frac{2}{\gamma}\right) - 1\right]}{P_{out}} \tag{1-40}$$

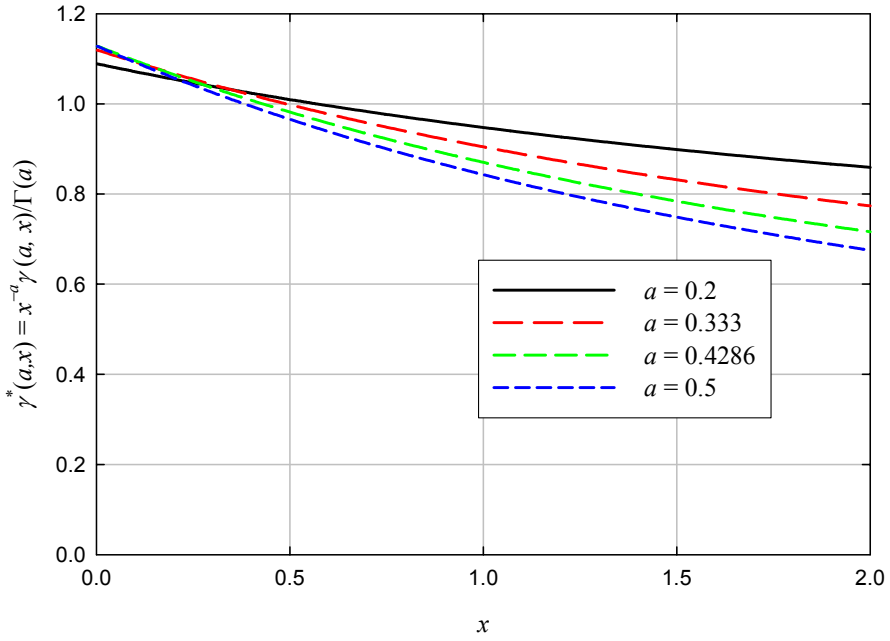

Figure 1-17: *The function $\gamma^*(a,x)$ used to approximate the incomplete Gamma function for low x.*

Figure 1-18 shows $\overline{X}_{nb}/\Lambda$ vs. P_{out} for $n_x = 1$ using both the exact formulation of (1-35) and the approximation of (1-40). As can be seen, agreement is excellent in this case. Figure 1-19 and Figure 1-20 show the same comparison for $n_x = 0.1$ and $n_x = 5$, respectively and agreement is excellent in both of these cases as well. Agreement is not as good, especially for the higher values of γ, in Figure 1-21, which shows the comparison for $n_x = 0.01$. This is because the assumption $\Lambda/\overline{X}_{nb}\, n_x^{-\gamma/2} << 1$ is no longer valid. For example, with $\gamma = 4$, $n_x^{-\gamma/2} = 10{,}000$, so even with $\overline{X}_{nb}/\Lambda = 10{,}000$ (40 dB), $\Lambda/\overline{X}_{nb}\, n_x^{-\gamma/2} = 1$. However, the approximation appears satisfactory for $n_x \geq 0.1$, which is more than adequate for the purposes of this analysis.

Of interest is the tradeoff between the size of the exclusion zone and the reduction in the required carrier power required by the narrowband receiver. Using the approximation of (1-40), the required value of $\overline{X}_{nb}/\Lambda$ can be shown as a function of n_x, as in Figure 1-22.

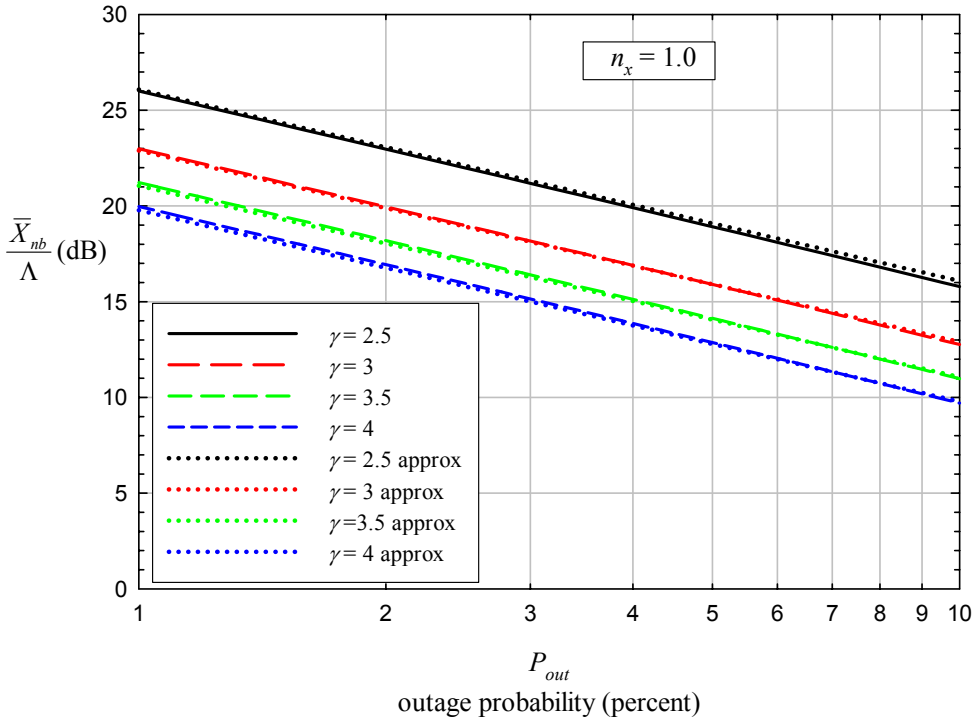

Figure 1-18: *Required* $\overline{X}_{nb}/\Lambda$ *to achieve a given outage probability for low outage with an exclusion zone,* $n_x = 1$ *and approximations from* (1-40).

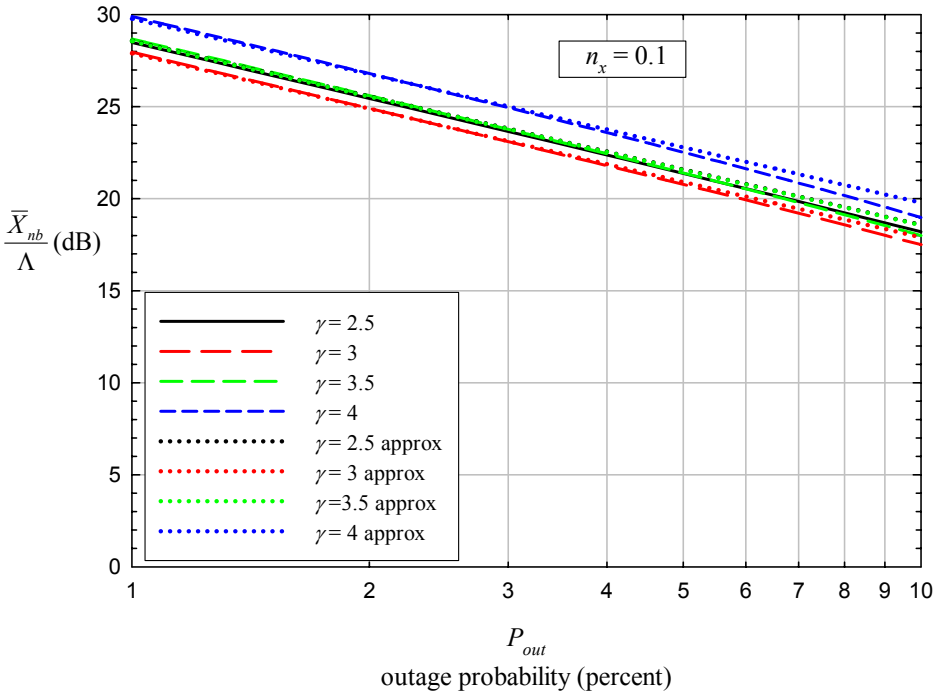

Figure 1-19: *Required* $\overline{X}_{nb}/\Lambda$ *to achieve a given outage probability for low outage with an exclusion zone,* $n_x = 0.1$ *and approximations from* (1-40).

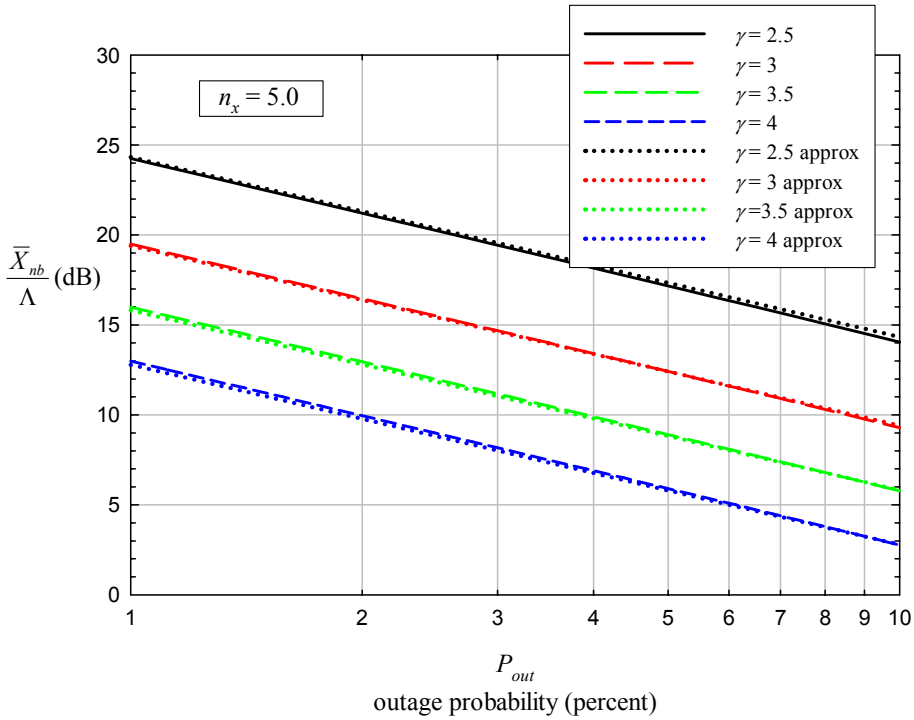

Figure 1-20: *Required* $\overline{X}_{nb}/\Lambda$ *to achieve a given outage probability for low outage with an exclusion zone,* $n_x = 5$ *and approximations from* (1-40).

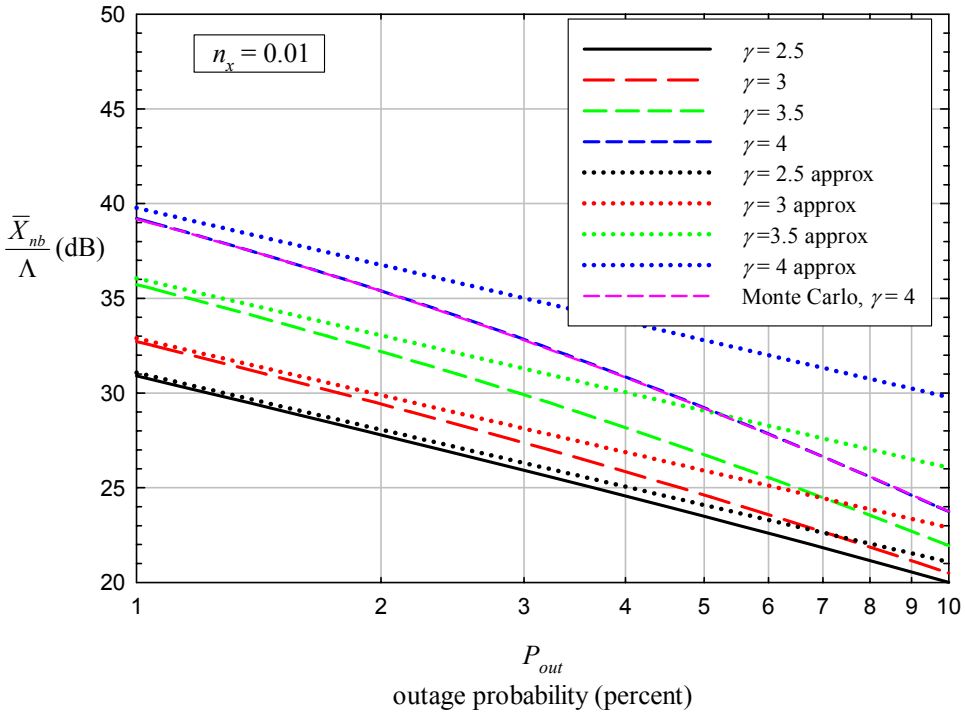

Figure 1-21: Required $\overline{X}_{nb}/\Lambda$ to achieve a given outage probability for low outage with an exclusion zone, $n_x = 0.01$ and approximations from (1-40), plus Monte Carlo results for $\gamma = 4$.

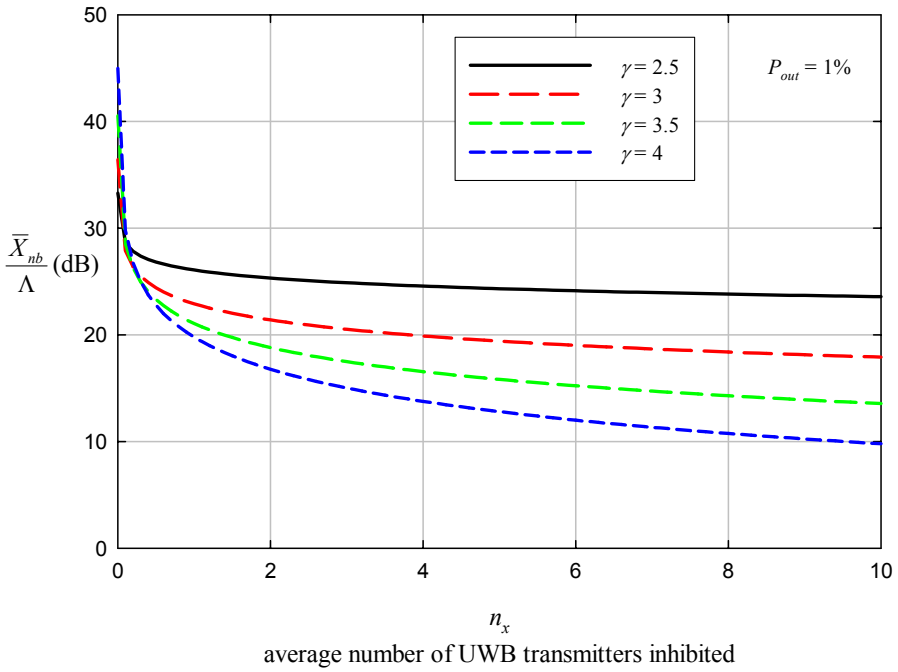

Figure 1-22: *Normalized local mean receive NB carrier power vs. the average number of inhibited UWB transmitters in the exclusion zone.*

1.6.3. Average Aggregate Interference with an Exclusion Zone

As shown in Chapter 3 of [2], eq. (3-5), the average interference is

$$I = I_{\max} \frac{\pi d_{\min}^2 \rho_a}{\gamma/2-1} = I_{\max} \frac{n_x}{\gamma/2-1} \tag{1-41}$$

where $I_{\max} = \alpha P_{tx} d_{\min}^{-\gamma}$; i.e., the interference from a transmitter just at the exclusion zone boundary. With the normalization $Z = I/\alpha P_{tx}(\pi\rho_a)^{\gamma/2}$, the average normalized interference power is

$$\begin{aligned} \overline{Z} &= Z_{\max} \frac{n_x}{\gamma/2-1} = \frac{1}{(\pi\rho_a d_{\min}^2)^{\gamma/2}} \frac{n_x}{\gamma/2-1} \\ &= \frac{n_x^{1-\gamma/2}}{\gamma/2-1} \end{aligned} \tag{1-42}$$

As can be seen from Table 1 and Figure 1-23, for γ in the range of interest here, $1.1\times\Gamma\left(1-\frac{2}{\gamma}\right)-1 \cong \frac{1}{\gamma/2-1}$.

Table 1

γ	$\frac{1}{\gamma/2-1}$	$1.1\times\Gamma\left(1-\frac{2}{\gamma}\right)-1$
2.5	4.0	4.05
3	2.0	1.95
3.5	1.33	1.28
4	1.0	0.95

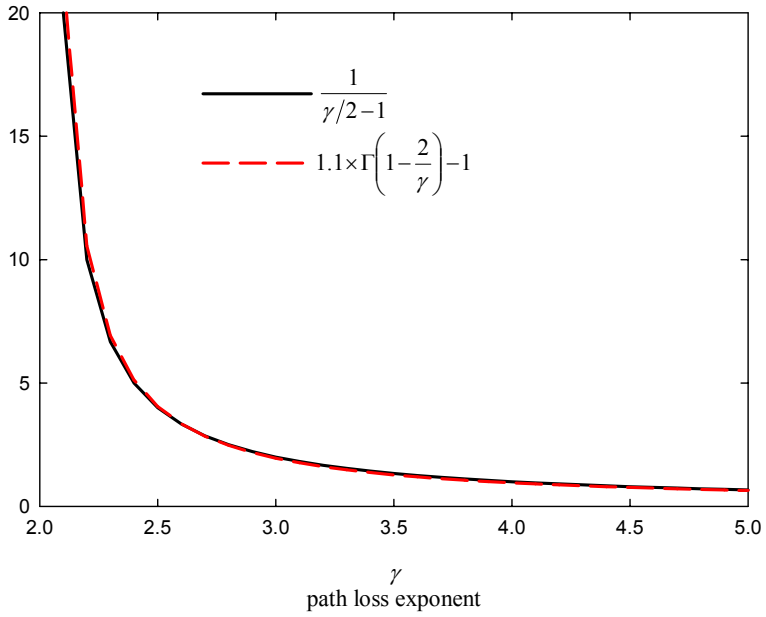

Figure 1-23: *Comparison of coefficient approximations for the case with an exclusion zone*

This leads to the approximation

$$\frac{\overline{X}_{nb}}{\Lambda} \cong \frac{n_x^{1-\gamma/2}}{(\gamma/2-1)P_{out}} = \frac{\overline{Z}}{P_{out}}. \tag{1-43}$$

This is an intuitively appealing form, because for a Rayleigh-faded carrier in the presence of interference level $\overline{Z}$,

$$\begin{aligned} P_{out} &= \Pr\left(v_m \overline{X}_{nb} < \Lambda \overline{Z}\right) = \Pr\left(v_m < \frac{\Lambda \overline{Z}}{\overline{X}_{nb}}\right) \\ &= 1 - \exp\left(-\frac{\Lambda \overline{Z}}{\overline{X}_{nb}}\right) \\ &\cong \frac{\Lambda \overline{Z}}{\overline{X}_{nb}} \text{ for } P_{out} << 1, \end{aligned} \tag{1-44}$$

which yields (1-43). Moreover, the factor $1/P_{out}$ corresponds to the fade margin imposed by the multipath variations. That is, the local mean signal must be $1/P_{out}$ times the target value to ensure that the fading signal remains about the target with probability $1 - P_{out}$. For example, if $P_{out} = 0.02$ (2%), then the fade margin is $20\log(1/P_{out}) = 17$ dB.

1.7. Outage Probability with UWB Interference Plus Noise

In general, the victim receiver will be subject to thermal noise as well as the UWB interference. The thermal noise is relatively constant, whereas the UWB interference fluctuates as the individual UWB transmitters turn on and off.

If the effect of thermal noise is included, the outage probability can be expressed as:

$$P_{out} = \Pr\left(\frac{C_{nb}}{I_{UWB} + N_{nb}} < \Lambda \right) \tag{1-45}$$

It is worth recalling that for a given performance level (e.g., bit error rate, baseband signal-to-noise ratio), the threshold Λ will in general depend on I_{UWB}/N_{nb} as well as the characteristics of the UWB interference into the NB receiver detector/demodulator. For purposes of this discussion, however, it is assumed that the UWB interference affects the receiver in the same way as Gaussian noise with the same average power over the NB receiver passband.

Defining a normalized noise level as

$$\eta = \frac{N_{nb}}{\alpha P_{tx} (\pi \rho_a)^{\gamma/2}}, \tag{1-46}$$

(1-45) becomes

$$\begin{aligned} P_{out} &= \Pr\left(\frac{X_{nb}}{Z + \eta} < \Lambda \right) \\ &= \Pr\left(v_m < \frac{\Lambda}{\bar{X}_{nb}} (Z + \eta) \right) \end{aligned} \tag{1-47}$$

Following (1-17)-(1-23), for the no-exclusion zone case this becomes:

$$\begin{aligned} P_{out} &= 1 - e^{-\frac{\Lambda}{\bar{X}_{nb}}\eta} \int_0^\infty e^{-\frac{\Lambda}{\bar{X}_{nb}}z} f_Z(z)\,dz \\ &= 1 - e^{-\frac{\Lambda}{\bar{X}_{nb}}\eta} \Phi_Z\left(-\frac{\Lambda}{\bar{X}_{nb}}\right) \\ &= 1 - \exp\left[-\eta\frac{\Lambda}{\bar{X}_{nb}} - \left(\frac{\Lambda}{\bar{X}_{nb}}\right)^{2/\gamma}\Gamma\left(1-\frac{2}{\gamma}\right)\right] \end{aligned} \tag{1-48}$$

which, for $P_{out} << 1$, can be approximated as:

$$P_{out} \cong \eta\frac{\Lambda}{\bar{X}_{nb}} + \left(\frac{\Lambda}{\bar{X}_{nb}}\right)^{2/\gamma}\Gamma\left(1-\frac{2}{\gamma}\right), \quad P_{out} << 1 \tag{1-49}$$

If an exclusion zone is assumed and thermal noise is included, the general form of (1-48) still holds, but the characteristic function of the normalized aggregate interference is given by (1-33), repeated here for convenience:

$$\Phi_Z(-\xi) = \exp\left[n_x\left(1 - e^{-\xi n_x^{-1/\nu}}\right) - \xi^\nu\gamma\left(1-\nu, \xi\, n_x^{-1/\nu}\right)\right] \tag{1-33}$$

so that the outage probability is:

$$\begin{aligned} P_{out} &= 1 - e^{-\frac{\Lambda}{\bar{X}_{nb}}\eta}\Phi_Z\left(-\frac{\Lambda}{\bar{X}_{nb}}\right) \\ &= 1 - \exp\left[-\eta\frac{\Lambda}{\bar{X}_{nb}} + n_x\left(1 - e^{-\frac{\Lambda}{\bar{X}_{nb}}n_x^{-1/\nu}}\right) - \left(\frac{\Lambda}{\bar{X}_{nb}}\right)^\nu\gamma\left(1-\nu, \frac{\Lambda}{\bar{X}_{nb}}n_x^{-1/\nu}\right)\right] \end{aligned} \tag{1-50}$$

which, using the usual approximation $P_{out} \cong -\ln(1-P_{out})$ for $P_{out} << 1$ can be approximated as:

$$\begin{aligned} P_{out} &\cong \eta\frac{\Lambda}{\overline{X}_{nb}} - n_x\cdot\frac{\Lambda}{\overline{X}_{nb}}n_x^{-1/\nu} + \left(\frac{\Lambda}{\overline{X}_{nb}}\right)^{\nu}\cdot 1.1\left(\frac{\Lambda}{\overline{X}_{nb}}n_x^{-1/\nu}\right)^{1-\nu}\Gamma(1-\nu) \\ &= \eta\frac{\Lambda}{\overline{X}_{nb}} - \frac{\Lambda}{\overline{X}_{nb}}n_x^{1-1/\nu} + \frac{\Lambda}{\overline{X}_{nb}}n_x^{1-1/\nu}\cdot 1.1\times\Gamma(1-\nu) \\ &\cong \eta\frac{\Lambda}{\overline{X}_{nb}} + \frac{\Lambda}{\overline{X}_{nb}}n_x^{1-1/\nu}\frac{1}{\gamma/2-1} \\ &= \frac{\Lambda}{\overline{X}_{nb}}\left(\eta + \frac{n_x^{1-1/\nu}}{\gamma/2-1}\right) \\ &= \frac{\Lambda}{\overline{X}_{nb}}\left(\eta+\overline{Z}\right) \end{aligned} \tag{1-51}$$

Thus,

$$\overline{X}_{nb} \cong \frac{\Lambda\left(\eta+\overline{Z}\right)}{P_{out}}, \quad P_{out} << 1 \tag{1-52}$$

which is not a surprising result.

1.8. Outage Probability Addition

Note that with noise only, the outage probability is

$$P_{out}\big|_{Z=0} = \Pr\left(\frac{C_{nb}}{N_{nb}} < \Lambda\right) = 1 - e^{-\frac{\Lambda}{\overline{X}_{nb}}\eta} \tag{1-53}$$

Thus, in both (1-48) and (1-50),

$$\begin{aligned} 1 - P_{out} &= \Pr\left(\frac{C_{nb}}{I_{UWB}+N_{nb}} > \Lambda\right) = \Pr\left(\frac{C_{nb}}{N_{nb}} > \Lambda\right)\times\Pr\left(\frac{C_{nb}}{I_{UWB}} > \Lambda\right) \\ &= e^{-\frac{\Lambda}{\overline{X}_{nb}}\eta}\Phi_Z\left(-\frac{\Lambda}{\overline{X}_{nb}}\right) \end{aligned} \tag{1-54}$$

This is a consequence of the PDF of the Rayleigh fade factor v_m, since if *W* and *Y* are independent non-negative (i.e., representing power) random variables with respective PDFs $f_W(w)$ and $f_Y(y)$, and *a* and *b* are positive constants, then

$$\begin{aligned}\Pr\left(v_m < aW + bY\right) &= 1 - \int_0^\infty \int_0^\infty e^{-(aw+by)} f_W(w) f_Y(y) dw dy \\ &= 1 - \Phi_W(-a)\Phi_Y(-b)\end{aligned} \tag{1-55}$$

Note that in the development presented here, $a = b$. However, this does not need to be the case, and different outage threshold can be used for the noise and interference to reflect the differences in impact that can occur between thermal noise and UWB interference. That is, the outage probability could be defined as

$$\begin{aligned}P_{out} &= \Pr\left(C_{nb} < \Lambda_U I_{UWB} + \Lambda_N N_{nb}\right) \\ &= \Pr\left(v_m < \frac{\Lambda_U}{\overline{X}_{nb}} Z + \frac{\Lambda_N}{\overline{X}_{nb}} \eta\right) \\ &= 1 - \Phi_Z\left(-\frac{\Lambda_U}{\overline{X}_{nb}}\right) e^{-\frac{\Lambda_N}{\overline{X}_{nb}}\eta}\end{aligned} \tag{1-56}$$

It is useful to define

$$P_{out,U} = \Pr\left(C_{nb} < \Lambda_U I_{UWB}\right) = \Pr\left(v_m < \frac{\Lambda_U}{\overline{X}_{nb}} Z\right) = 1 - \Phi_Z\left(-\frac{\Lambda_U}{\overline{X}_{nb}}\right) \tag{1-57}$$

$$P_{out,N} = \Pr\left(C_{nb} < \Lambda_N N_{nb}\right) = \Pr\left(v_m < \frac{\Lambda_N}{\overline{X}_{nb}} \eta\right) = 1 - e^{-\frac{\Lambda_N}{\overline{X}_{nb}}\eta} \tag{1-58}$$

and

$$\begin{aligned}P_{out} &= 1 - \left(1 - P_{out,U}\right)\left(1 - P_{out,N}\right) = P_{out,U} + P_{out,N} - P_{out,U} \cdot P_{out,N} \\ &\cong P_{out,U} + P_{out,N}, \quad P_{out,U} << 1, \; P_{out,N} << 1\end{aligned} \tag{1-59}$$

Clearly, for the low outage region, this may be approximated as

$$P_{out} \cong P_{out,U} + P_{out,N} \text{ for } P_{out,U} << 1 \text{ and } P_{out,N} << 1 \tag{1-60}$$

which agrees with the approximations of (1-49) and (1-51), with

$$P_{out,N} \cong \frac{\Lambda_N \eta}{\overline{X}_{nb}} = \frac{\Lambda_N N_{nb}}{\overline{C}_{nb}} \tag{1-61}$$

and

$$P_{out,U} \cong \left\{ \begin{array}{ll} \left(\frac{\Lambda_U}{\overline{X}_{nb}}\right)^{2/\gamma} \Gamma\left(1-\frac{2}{\gamma}\right) & \text{no exclusion} \\ \frac{\Lambda_U \overline{Z}}{\overline{X}_{nb}} = \frac{\Lambda_U \overline{I}}{\overline{C}_{nb}} & \text{with exclusion} \end{array} \right\} \quad P_{out,U} << 1 \tag{1-62}$$

As will be seen in the next section, this division of the outage probability into noise and interference components will facilitate the analysis of UWB/NB coexistence tradeoffs.

1.9. Coexistence Conditions and Tradeoffs

Whether it is appropriate to use different values for Λ_U and Λ_N will depend on the nature of the UWB interference as well as the detector/demodulator processing in the NB receiver. In general, the value of Λ will depend on I_{UWB}/N_{nb} as well as the UWB pulse rate relative to the victim receiver channel bandwidth. For the present, it is assumed that the UWB interference appears noise-like to the NB receiver and, accordingly, only a single value of Λ is used, and it independent of I_{UWB}/N_{nb} .

The goal of this analysis is to apply to results derived above to develop the relationships between P_{tx} and ρ_a , and in the case of the exclusion zone, $d_{\min}$ and n_x . It is assumed that P_{out} is specified (as a receiver performance objective) and $P_{out,N}$ is known, and therefore the maximum permissible value of $P_{out,U}$ is known.

1.9.1. Case 1: No Exclusion Zone

Without an exclusion zone, the UWB interference component of the outage probability is

$$P_{out,U} \cong \left(\frac{\Lambda}{\overline{X}_{nb}}\right)^{2/\gamma} \Gamma\left(1-\frac{2}{\gamma}\right) \quad P_{out,U} << 1 \tag{1-63}$$

Hence,

$$\overline{X}_{nb} \cong \Lambda\left[\frac{\Gamma(1-2/\gamma)}{P_{out,U}}\right]^{\gamma/2} \quad P_{out,U} << 1 \tag{1-64}$$

Applying the normalization factor gives:

$$\overline{C}_{nb} = \alpha P_{tx} (\pi \rho_a)^{\gamma/2} \cdot \Lambda \left[\frac{\Gamma(1-2/\gamma)}{P_{out,U}} \right]^{\gamma/2} \tag{1-65}$$

Dividing both sides by N_{nb} and rearranging gives:

$$\begin{aligned} \frac{\alpha P_{tx}}{N_{nb}} \rho_a^{\gamma/2} &= \frac{\overline{C}_{nb}}{\Lambda N_{nb}} \left[\frac{P_{out,U}}{\pi \Gamma(1-2/\gamma)} \right]^{\gamma/2} \\ &= \frac{1}{P_{out,N}} \left[\frac{P_{out,U}}{\pi \Gamma(1-2/\gamma)} \right]^{\gamma/2} \end{aligned} \tag{1-66}$$

Given the outage specifications, the term on the right-hand side is constant, so (1-66) specifies a tradeoff between P_{tx}, the UWB transmit power that falls within the NB receiver passband, and ρ_a, the average density of active (transmitting) UWB devices. That is,

$$\frac{\alpha P_{tx}}{N_{nb}} \rho_a^{\gamma/2} = K_{nx} \tag{1-67}$$

where K_{nx} is the right-hand side of (1-66).

1.9.2. Case 2: With an Exclusion Zone

With an exclusion zone encompassing an area within which there normally would be n_x active UWB transmitters, the interference component of the outage probability is:

$$P_{out,U} \cong \frac{\Lambda \overline{Z}}{\overline{X}_{nb}} = \frac{\Lambda}{\overline{X}_{nb}} \frac{n_x^{1-\gamma/2}}{\gamma/2-1} \qquad P_{out,U} << 1 \tag{1-68}$$

Applying the normalization factor gives:

$$P_{out,U} \cong \frac{\Lambda N_{nb}}{\overline{C}_{nb}} \alpha P_{tx} (\pi \rho_a)^{\gamma/2} \frac{n_x^{1-\gamma/2}}{\gamma/2-1} \qquad P_{out,U} << 1 \tag{1-69}$$

With $P_{out,N} \cong \dfrac{\Lambda N_{nb}}{\overline{C}_{nb}}$

$$\frac{\alpha P_{tx}}{N_{nb}} \rho_a^{\gamma/2} \cong n_x^{\gamma/2-1} \frac{P_{out,U}}{P_{out,N}} \frac{\gamma/2-1}{\pi^{\gamma/2}} \tag{1-70}$$

Thus, if n_x is specified, then $P_{tx}\rho_a^{\gamma/2}$ is a constant as in the previous case.

An alternative form can be used, substituting $n_x = \pi\rho_a d_{\min}^2$, giving:

$$\frac{\alpha P_{tx}}{N_{nb}} \rho_a \cong d_{\min}^{\gamma-2} \frac{P_{out,U}}{P_{out,N}} \frac{\gamma/2-1}{\pi} \tag{1-71}$$

where now it is $d_{\min}$ rather than n_x that is specified, and $P_{tx}\rho_a$ is a constant.

1.10. Examples

1.10.1. Case 1: No Exclusion Zone

Assume that $P_{out,N} = P_{out,U} = 0.05$, $\gamma = 3$, and $\alpha = 10^{-4}$, which corresponds to the free-space path loss at 1 meter for 2.4 GHz. In this case, the constant for the no-exclusion case is:

$$\frac{1}{P_{out,N}} \left[\frac{P_{out,U}}{\pi\Gamma(1-2/\gamma)} \right]^{\gamma/2} = 0.0092 \tag{1-72}$$

Assume the UWB effective isotropic radiated power spectral density (EIPSD) within the NB receiver passband is –43 dBm/MHz, consistent with the current FCC in-band UWB limit, and that the NB receiver noise figure is 8 dB, in which case:

$$10\log\frac{\alpha P_{tx}}{N_{nb}} = -40 - 43 + 114 - 8 = 23 \text{ dB} \tag{1-73}$$

or a factor of 200. Hence,

$$\rho_a = \left(\frac{0.0092}{200} \right)^{2/3} = 0.0013 \text{ active UWB transmitters/m}^2 \tag{1-74}$$

or roughly one active device in every 28 x 28 m square, on average.

1.10.2. Case 2a: Exclusion Zone with $\mathbf{n_x}$ *Specified*

Using the same assumptions as above, the constant in (1-70) is

$$\frac{P_{out,U}}{P_{out,N}} \frac{\gamma/2-1}{\pi^{\gamma/2}} = 0.09 \tag{1-75}$$

and

$$\rho_a = \left[\frac{0.09}{200} n_x^{\gamma/2-1} \right]^{2/\gamma} = 0.006 \times n_x^{1/3} \text{ active UWB transmitters/m}^2 \tag{1-76}$$

Note that if $n_x = 0.01$, then ρ_a is the same as the non-exclusion zone case (although the approximations used for the exclusion zone case become inaccurate for such low values of n_x).

It is evident that even a small exclusion zone (e.g., $n_x = 1$) significantly increases the allowable UWB active device density. With $\rho_a = 0.006$ and $n_x = 1$, the exclusion distance $d_{\min}$ is about 7.3 meters. The probability that without the exclusion, there would have been at least one active UWB transmitter within this distance is $1 - e^{-n_x}$, or for $n_x = 1$, 63%.

1.10.3. Case 2b: Exclusion Zone with $d_{\mathbf{min}}$ *Specified*

In this case, the constant is:

$$\frac{P_{out,U}}{P_{out,N}} \frac{\gamma/2-1}{\pi} = 0.16 \tag{1-77}$$

and

$$\rho_a = \frac{0.16}{200} d_{\min}^{\gamma-2} = 0.0008\, d_{\min}^{\gamma-2} \tag{1-78}$$

or in this case, with $\gamma = 3$, $\rho_a = 0.0008\, d_{\min}$. If $d_{\min} = 7.3$ meters, then $\rho_a = 0.006$, consistent with the example of case 2a above. To give $\rho_a = 0.0013$, $d_{\min} = 1.625$ meters, corresponding to $n_x \cong 0.01$, but again, in this region, the approximations used for the exclusion zone case are not as accurate as for higher value of n_x (≥ 0.1).

Figure 1-24 shows ρ_a vs. $d_{\min}$ assuming that $P_{tx} = -43$ dBm/MHz within the NB receiver passband. Figure 1-25 shows ρ_a vs. P_{tx} for $d_{\min} = 5$ meters, and Figure 1-26 shown ρ_a vs. P_{tx} for $d_{\min} = 10$ meters. Figure 1-27 shows ρ_a vs. P_{tx} for $d_{\min} = 5$ meters on a logarithmic scale (otherwise the same as Figure 1-25).

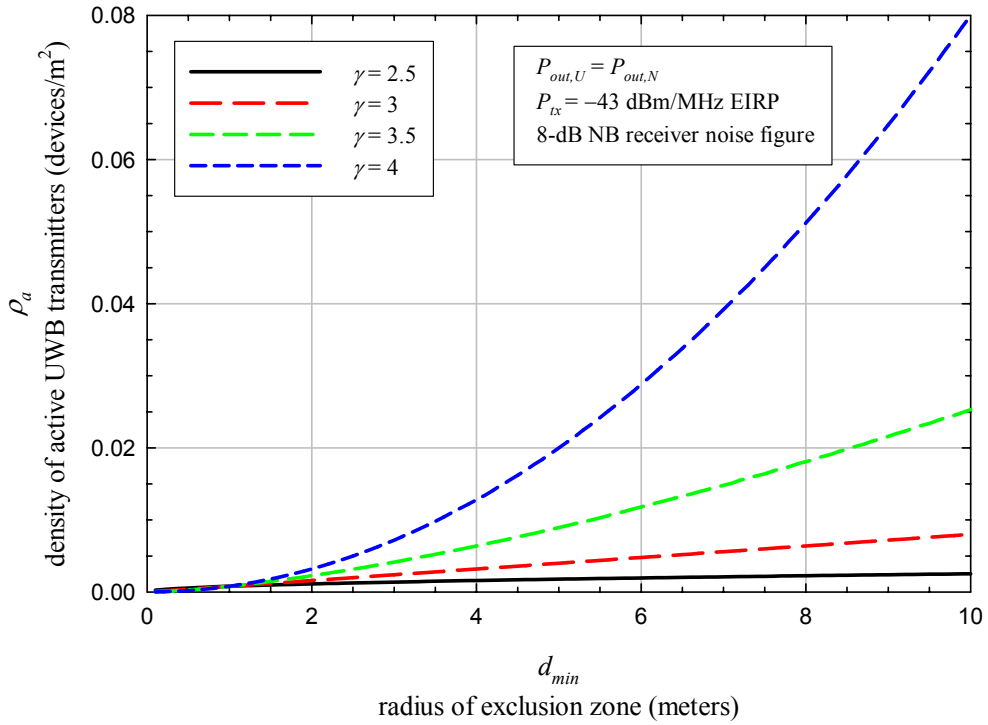

Figure 1-24: *UWB transmitter density vs. exclusion zone radius for –43 dBm/MHz transmit power*

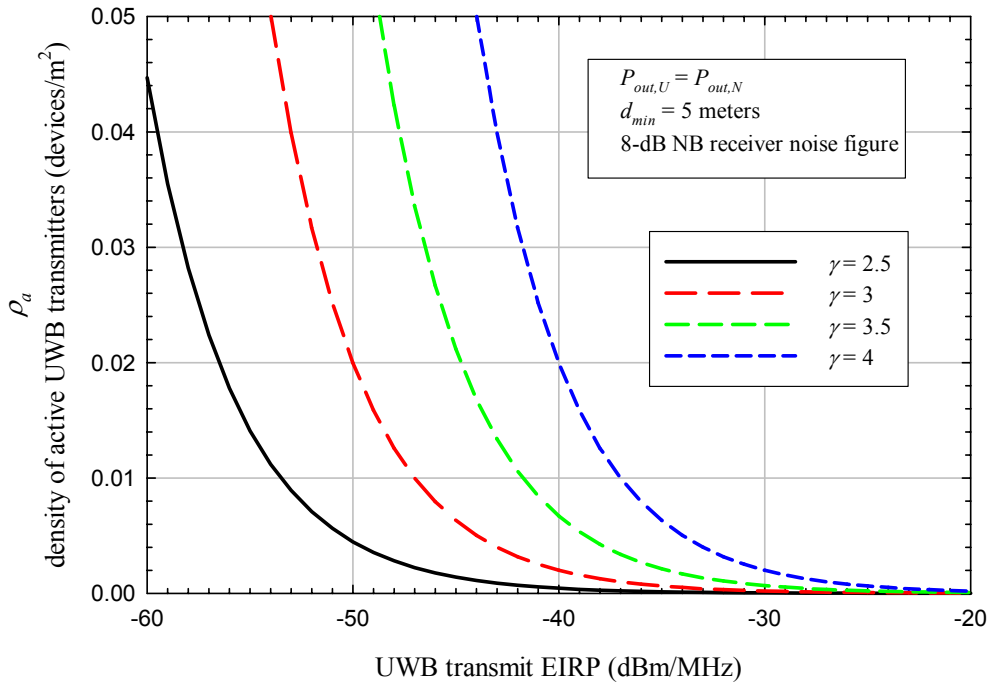

Figure 1-25: *UWB transmitter density vs. transmit power for a 5-meter exclusion zone*

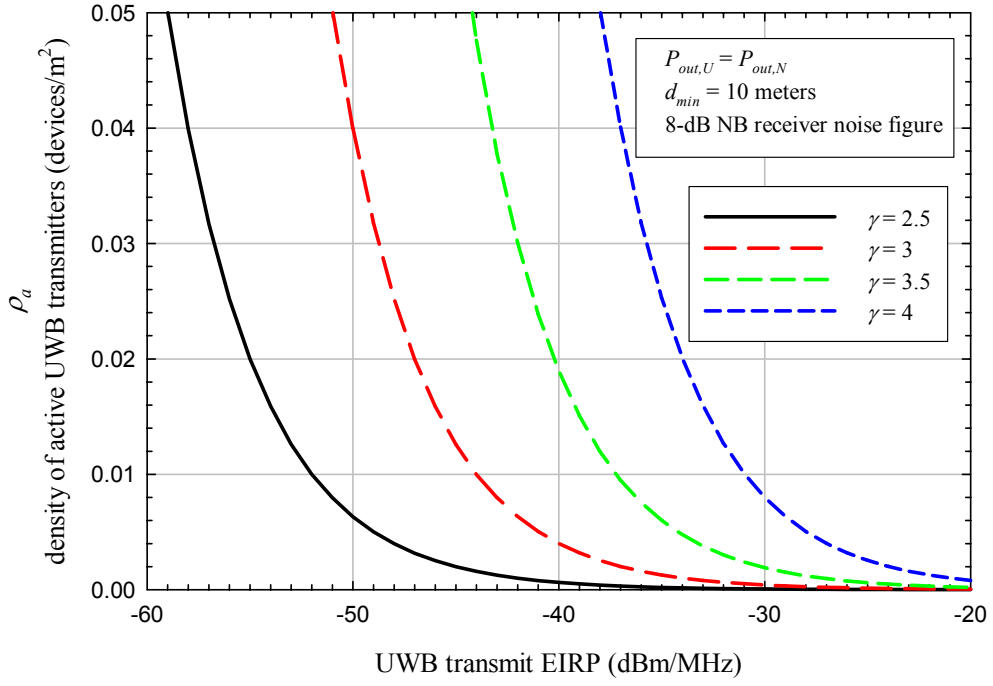

Figure 1-26: *UWB transmitter density vs. transmit power for a 10-meter exclusion zone*

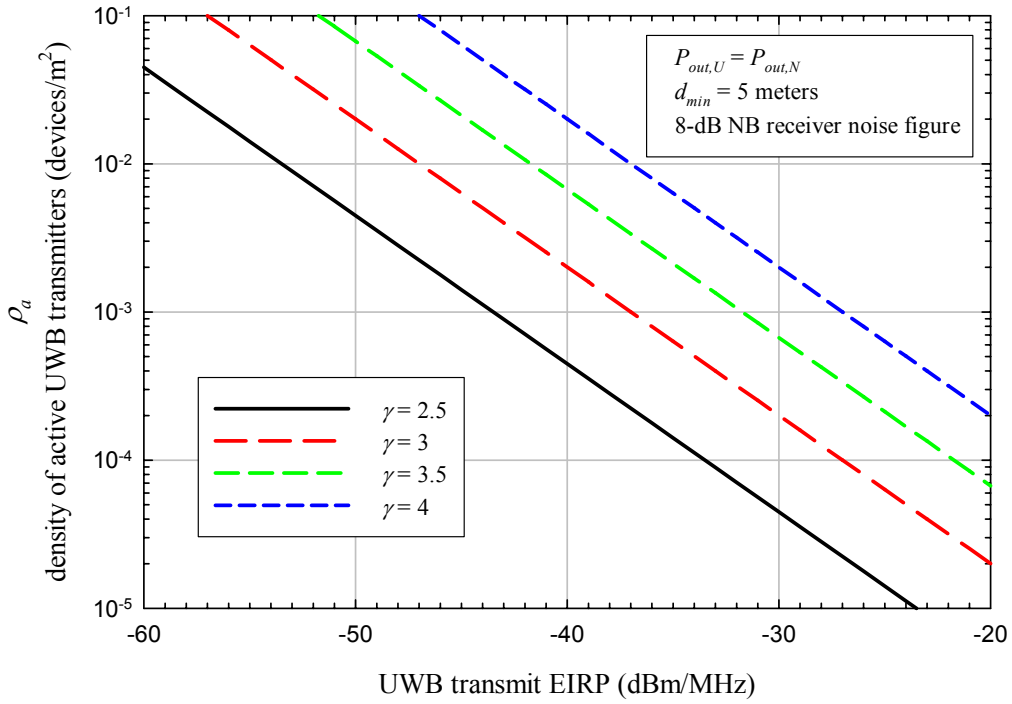

Figure 1-27: *UWB density vs. transmit power for a 5-meter exclusion zone, log scale.*

1.11. The UWB Network Perspective

It is also useful to understand the power vs. density tradeoff from the perspective of the UWB devices, to provide some guidance for UWB network design strategies to minimized interference with narrowband systems.

Consider a UWB network with spatial device density ρ_u and average active transmitter density $\rho_a = a\rho_u$, where a is the average transmit duty cycle. If d_u is the distance between a UWB transmitter and the target UWB receiver, and γ_u is the path loss exponent as seen by the UWB link, then the required UWB transmit power is proportional to $d_u^{\gamma_u}$ and therefore

$$P_{tx} = \beta d_u^{\gamma_u} \tag{1-79}$$

where the constant β depends on a number of factors, including the required power at the UWB receiver, the fraction of the UWB power that falls within the NB victim receiver passband, antenna characteristics, etc.

It is assumed here that the UWB transmission is directed to the nearest neighbor node, and the distance between the transmitter and receiver is denoted $d_{u\min}$. If UWB devices

are randomly-distributed spatially, then $d_{u\min}$ must be modeled as a random variable. To understand the statistics of P_{tx}, the PDF of $d_{u\min}$ is needed.

The probability that there are no UWB devices within distance *r* of the UWB transmitter is

$$\Pr\left(d_{u\min} > r\right) = e^{-\rho_u \pi r^2} \tag{1-80}$$

The PDF of $d_{u\min}$ is therefore

$$f_{d_{u\min}}(r) = -\frac{d}{dr} e^{-\rho_u \pi r^2} = 2r\rho_u r e^{-\rho_u \pi r^2} \tag{1-81}$$

The average value of $d_{u\min}$ is

$$\overline{d_{u\min}} = \int_0^\infty r f_{d_{u\min}}(r) dr = \frac{1}{2\sqrt{\rho_u}} \tag{1-82}$$

and the average value of P_{tx}, assuming just enough UWB power is transmitted to meet the link requirement, is

$$\begin{aligned} \overline{P}_{tx} &= 2\beta\rho_u \pi \int_0^\infty r^{\gamma_u + 1} e^{-\rho_u \pi r^2} dr \\ &= \beta \cdot \Gamma\left(\frac{\gamma_u}{2} + 1\right)\left(\pi\rho_u\right)^{-\gamma_u/2} \end{aligned} \tag{1-83}$$

Hence, it can be generally stated that

$$P_{tx} = K_u \rho_u^{-\gamma_u/2} \tag{1-84}$$

where K_u is a constant that depends on β and the other constants in (1-83) as well as statistical margin factors related to the way in which the UWB network manages its transmit power, routing, etc. If the UWB devices are close together and free-space propagation applies ($\gamma_u = 2$), then $P_{tx} = K_u / \rho_u$.

Note that this general formulation applies not only to UWB communication links but also to UWB radar nets. In that case, $d_{u\min}$ would be the distance from the target to the nearest UWB transmitter.

If it is required that $P_{tx}\rho_a = K_{nb}$ for constant interference impact on the NB receiver, where K_{nb} is a constant, then $P_{tx}a\rho_u = K_{nb}$ and with (1-84),

$$a\rho_u^{1-\gamma_u/2} = \frac{K_{nb}}{K_u} \tag{1-85}$$

or

$$a = \frac{K_{nb}}{K_u}\rho_u^{\gamma_u/2-1} \tag{1-86}$$

Thus, the UWB duty cycle is either independent of ρ_u (for $\gamma_u = 2$), or increases mildly with increasing ρ_u.

If, on the other hand, $P_{tx}\rho_a^{\gamma/2} = K'_{nb}$, which applies to the case of an exclusion zone with a fixed n_x, then $P_{tx}\left(a\rho_u\right)^{\gamma/2} = K'_{nb}$, and

$$a = \frac{K'_{nb}}{K_u}\rho_u^{\gamma_u/\gamma-1} \tag{1-87}$$

and *a* is independent of ρ_u (for $\gamma_u = \gamma$), or changes mildly with ρ_u if $\gamma_u \neq \gamma$.

1.12. Annex to Chapter 1: The Characteristic Function of Combined Interference Power from Multiple Randomly-Distributed UWB Transmitters Outside an Exclusion Zone

This Appendix extends some of the analysis in Appendix 3A of [2] to account for an "exclusion zone" surrounding the victim receiver, within which there will be no interfering transmitters. Some of the material in that appendix is reproduced here for completeness. The model is illustrated in Figure A-1. The victim receiver is at the center of a disc described by an inner circle of radius $\sqrt{n_x}$ and an outer circle of radius $\sqrt{K+n_x}$, so the total area is πK. The average density of active interfering transmitters is assumed to be $1/\pi$, so the average (expected) number of active transmitters within the disc (between the inner and outer radii) is *K*.

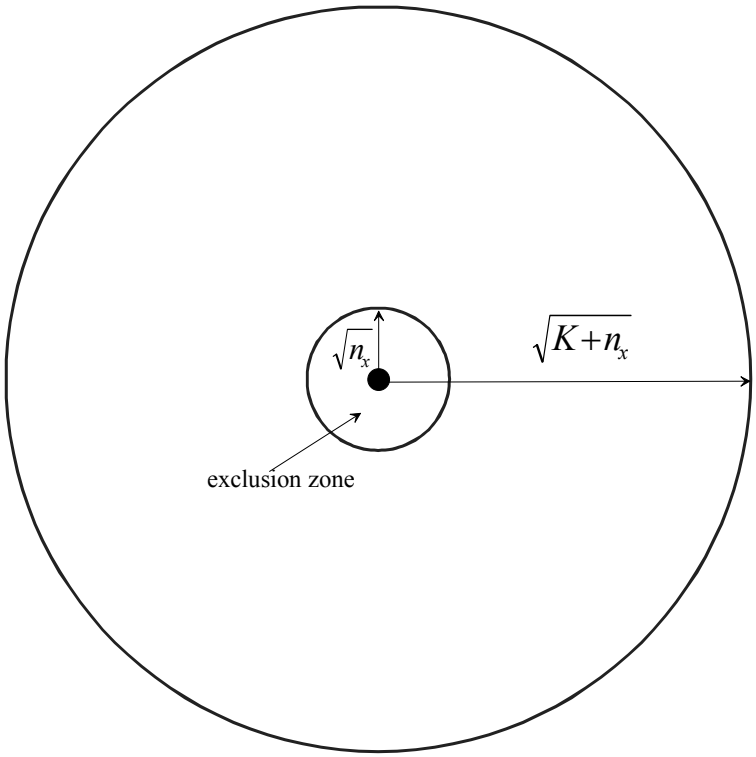

Figure A-1: *Model geometry*

Assuming that interfering transmitters are randomly-distributed over area in a uniform fashion, the *actual* number of active interfering transmitters within the circle at a given time can be modeled as a Poisson-distributed random variable *J* with discrete probability density function (PDF):

$$P_J(k) = \Pr\{J = k\} = \frac{e^{-K} K^k}{k!} \tag{1}$$

where the notation $\Pr\{\cdot\}$ represents the probability of the indicated event. The normalized power received at the base station from the k^{th} interfering transmitter a normalized distance s_k away from it is $z_k = s_k^{-\gamma}$. The total power received from interfering transmitters within the disc is:

$$Z_K = \sum_{k=1}^{J} z_k \,. \tag{2}$$

With interferers that are randomly distributed over area, the pdf of s_k is:

$$f_{s_k}(s) = \frac{2s}{K}, \quad \sqrt{n_x} \le s \le \sqrt{n_x + K}. \tag{3}$$

Hence, the pdf of z_j is:

$$f_{z_j}(z) = \frac{2}{\gamma K} z^{-(\gamma+2)/\gamma}, \quad (K + n_x)^{-\gamma/2} \le z \le n_x^{-\gamma/2} \tag{4}$$

The characteristic function of Z_K is:

$$\Phi_{Z_K}(\xi) = E\left[e^{\xi Z_K}\right] = \int_0^\infty f_{Z_K}(z) e^{\xi z} dz \,, \tag{5}$$

which is the Fourier transform of $f_{Z_K}(z)$. The lower limit is 0 rather than $-\infty$ in this case because Z_K represents power and therefore is non-negative.

Assuming the $\{z_k\}$ are independent and identically-distributed (i.i.d.), (2) and (5) yield:

$$\Phi_{Z_K}(\xi) | J = E\left[\exp\left(\xi \sum_{k=1}^{J} z_k\right)\right] = \left(E\left[e^{\xi z_k}\right]\right)^J \quad . \tag{6}$$

Taking the expectation over J using (1) gives:

$$\Phi_{Z_K}(\xi) = \sum_{n=0}^{\infty} \frac{e^{-K} K^n}{n!} \left[\Phi_{Z_k}(\xi)\right]^n = \exp\left\{K\left[\Phi_{z_k}(\xi) - 1\right]\right\}. \tag{7}$$

Thus, Z_K has a compound Poisson distribution [3]. Using (4) and letting $\nu = 2/\gamma$, the characteristic function of z_k is:

$$\Phi_{z_k}(\xi) = \int_0^{\infty} f_{z_k}(z) e^{\xi z} dz = \frac{\nu}{K} \int_{(K+n_x)^{-1/\nu}}^{n_x^{-1/\nu}} z^{-1-\nu} e^{\xi z} dz \,. \tag{8}$$

The "second characteristic function" of Z_K is defined as the natural logarithm of the characteristic function [4], which in this case is:

$$\Psi_{Z_K}(\xi) = \ln \Phi_{\mathbf{Z}_K}(\xi) = K\left[\Phi_{\mathbf{Z}_K}(\xi) - 1\right] = \left(\nu \int_{(K+n_x)^{-1/\nu}}^{n_x^{-1/\nu}} z^{-1-\nu} e^{\xi z} dz \right) - K \,. \tag{9}$$

Integrating by parts gives

$$\begin{aligned} \Psi_{Z_K}(\xi) &= \left(- z^{-\nu} e^{\xi z} \right) \Big|_{(K+n_x)^{-1/\nu}}^{n_x^{-1/\nu}} + \xi \left(\int_{(K+n_x)^{-1/\nu}}^{n_x^{-1/\nu}} z^{-\nu} e^{\xi z} dz \right) - K \\ &= (K + n_x) e^{\xi (K+n_x)^{-1/\nu}} - n_x e^{\xi n_x^{-1/\nu}} - K + \xi \left(\int_{(K+n_x)^{-1/\nu}}^{n_x^{-1/\nu}} z^{-\nu} e^{\xi z} dz \right) \\ &= K\left(e^{\xi (K+n_x)^{-1/\nu}} - 1 \right) + n_x \left(e^{\xi (K+n_x)^{-1/\nu}} - e^{\xi n_x^{-1/\nu}} \right) + \xi \left(\int_{(K+n_x)^{-1/\nu}}^{n_x^{-1/\nu}} z^{-\nu} e^{\xi z} dz \right) \end{aligned} \tag{10}$$

With $Z = \lim_{K \to \infty} Z_K$, the first term goes to zero since $\lim_{K \to \infty} e^{\xi (K+n_x)^{-1/\nu}} - 1 = \xi (K + n_x)^{-1/\nu}$ and with ξ bounded, $\lim_{K \to \infty} K \xi (K + n_x)^{-1/\nu} = \lim_{K \to \infty} \xi K^{1-1/\nu} = 0$ for $\nu < 1$ ($\gamma > 2$). Hence,

$$\Psi_Z(\xi) = \lim_{K \to \infty} \Psi_{Z_K}(\xi) = n_x \left(1 - e^{\xi n_x^{-1/\nu}} \right) + \xi \int_0^{n_x^{-1/\nu}} z^{-\nu} e^{\xi z} dz \tag{11}$$

For the problem considered here, $\Psi_Z(-\xi)$ (where $\xi > 0$) is of specific interest:

$$\begin{aligned} \Psi_Z(-\xi) &= n_x \left(1 - e^{-\xi n_x^{-1/\nu}} \right) - \xi \int_0^{n_x^{-1/\nu}} z^{-\nu} e^{-\xi z} dz \\ &= n_x \left(1 - e^{-\xi n_x^{-1/\nu}} \right) - \xi^{\nu} \gamma\left(1 - \nu, \xi\, n_x^{-1/\nu} \right) \end{aligned} \tag{12}$$

where $\gamma(a, x) = \int_0^x e^{-t} t^{a-1} dt$ is the incomplete Gamma function [6], and

$$\Phi_Z(-\xi) = \exp\left[n_x \left(1 - e^{-\xi n_x^{-1/\nu}} \right) - \xi^{\nu} \gamma\left(1 - \nu, \xi\, n_x^{-1/\nu} \right) \right] \tag{13}$$

Chapter 1 References

[1] "Physical-Layer Modeling of UWB Interference Effects," J. E. Padgett, J. C. Koshy, A. A. Triolo, January 10, 2003, sponsored by DARPA under contract MDA972-02-C-0056.

[2] "Physical-Layer UWB Interference Impact Analysis," J. E. Padgett, A. A. Triolo, J. C. Koshy, August 8, 2003, sponsored by DARPA under contract MDA972-02-C-0056.

[3] William Feller, *An Introduction to Probability Theory and Its Applications,* second ed., vol. II, New York: Wiley, 1971.

[4] Papoulis, *Probability, Random Variables, and Stochastic Processes,* New York: McGraw-Hill, 1965.

[5] Erdelyi, *et al*, *Tables of Integral Transforms,* vol. 1, New York: McGraw-Hill, 1954.

[6] M. Abramowitz and I. E. Stegun, *Handbook of Mathematical Functions*, U. S. Department of Commerce, National Bureau of Standards, ninth printing, Nov. 1970.

Chapter 2: Effect of UWB Interference on CW Radar Receivers

2.1. Introduction

Frequency modulated (FM) continuous wave (CW) radar and its variants have been important in the development of radar systems due to the simplicity of implementation afforded by these techniques. CW (unmodulated) radar has been used to easily measure the Doppler spread of moving targets without velocity ambiguity at virtually any range. Another advantage of CW radar is its ability to generate an average power with unity peak-to-average power ratio, thus easing the burden on the transmit power amplifier and enabling use of high-efficiency amplification techniques. However, CW radar without modulation is incapable of measuring range. In order to accommodate range measurement, frequency modulation (FM) in many forms (linear, sinusoidal, pulsed linear, coded) can be added. Some of the earliest radar devices to use FW-CW techniques were altimeters. Two early examples of radar altimeters that employed linear FM techniques are the Bendix ALA-52A and the Collins ALT-55 that are used on smaller aircraft.

This chapter analyzes the impact of pulsed UWB interference on the performance of a CW FM radar altimeter. It is assumed that the UWB pulse rate is less than or equal to the IF bandwidth of the radar receiver. The rms altitude estimation error is computed as a function of the carrier-to-interference ratio, where the interference is the average UWB interference power within the receiver IF passband.

2.2. CW Radar Operation

Continuous wave (CW) frequency modulated radar operates by modulating the phase of a sinusoidal carrier and then comparing the phases of the transmitted reference signal and the return echo signal. If we assume the transmitted frequency increases linearly with time, called linear FM, the reflected signal will also have a frequency that increases linearly with time, but delayed by an amount proportional to the target distance. The transmitted and received frequency profiles are shown in Figure 2-1 along with a time-domain plot of the transmitted up-chirp signal.

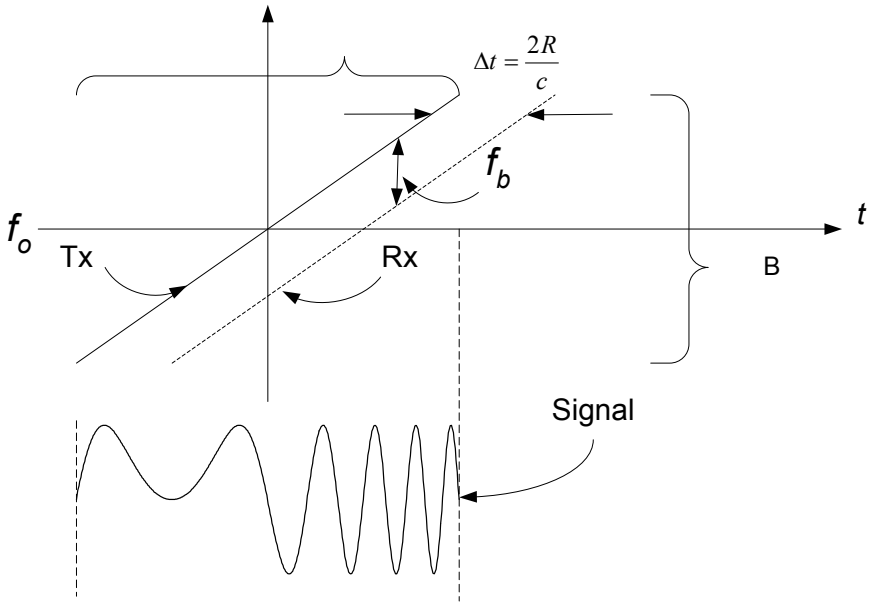

Figure 2-1: *Frequency versus time relation for transmitted and reflected signal of CW LFM radar (up-chirp section).*

The distance to the target can be found by mixing a reference copy of the transmitted signal with the received signal and measuring the resulting beat frequency f_b, which is proportional to the round trip distance to the target. This basic up-chirp waveform can be transmitted in a pulsed manner with duty cycle from 100% (sawtooth frequency versus time waveform) down to a small percentage to conserve transmitted power. An up-chirp waveform can be concatenated with a down-chirp waveform to give a triangular frequency versus time waveform with 100% duty cycle.

In order to measure the beat frequency during a time when the transmitter is on, two antennas can be used, one for transmit, one for receive. A block diagram of a simple FM-CW radar system similar to one given in [3] is shown in Figure 2-2. The transmit feed-through path can be accomplished with controlled coupling from transmit to receive antenna, or with a directional coupler.

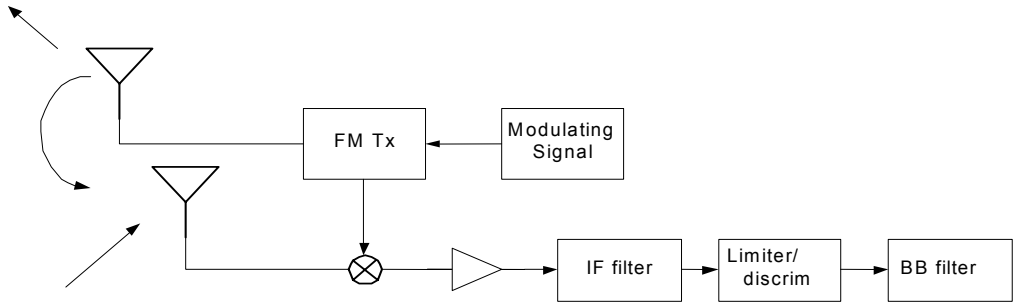

Figure 2-2: *Simplified block diagram of FM radar system.*

The expression for the RF transmitted chirp signal as given in [4] is (assuming we examine a single chirp pulse)

$$s_1(t) = \mathrm{Re}\left\{ A \times \mathrm{rect}\left(\frac{t}{\tau}\right) e^{j2\pi(f_0 t + \alpha(t))} \right\}, \tag{2-1}$$

with the complex baseband equivalent

$$s(t) = A \times \mathrm{rect}\left(\frac{t}{\tau}\right) e^{j2\pi\alpha(t)}. \tag{2-2}$$

The "rect" function is defined here as

$$\mathrm{rect}\left(\frac{t}{\tau}\right) = \begin{cases} 1 & -\frac{\tau}{2} \le t \le \frac{\tau}{2} \\ 0 & elsewhere \end{cases}. \tag{2-3}$$

For a linearly modulated FM (as shown in Figure 2-1), the phase function becomes

$$\alpha(t) = \pi\mu t^2 \tag{2-4}$$

with $\mu = B/\tau$. The spectrum of the baseband equivalent signal can be computed using

$$S(\omega) = A \int_{-\tau/2}^{\tau/2} e^{j\pi\mu t^2} e^{-j\omega t} dt, \tag{2-5}$$

and can be evaluated either through numerical integration or use of the Fresnel integrals *C(x)* and *S(x)*, that are defined as follows

$$C(x) = \int_0^x \cos\left(\frac{\pi\xi^2}{2}\right) d\xi \tag{2-6}$$

$$S(x) = \int_0^x \sin\left(\frac{\pi\xi^2}{2}\right) d\xi \tag{2-7}$$

The baseband spectrum of the linear FM chirp is now

$$S(\omega) = A\sqrt{\frac{\tau}{2B}} e^{-j\frac{\omega^2\tau}{4\pi B}} \left\{ \left[C(a_1) + C(a_2)\right] + j\left[S(a_1) + S(a_2)\right] \right\} \tag{2-8}$$

with

$$a_1 = \sqrt{\frac{2B}{\tau}}\left(\frac{\tau}{2} + \frac{\omega\tau}{2\pi B}\right) \quad a_2 = \sqrt{\frac{2B}{\tau}}\left(\frac{\tau}{2} - \frac{\omega\tau}{2\pi B}\right). \tag{2-9}$$

This baseband spectrum of a linear FM chirp is shown in Figure 2-3. The bandwidth of this system with 30 MHz frequency deviation is approximately 30 MHz.

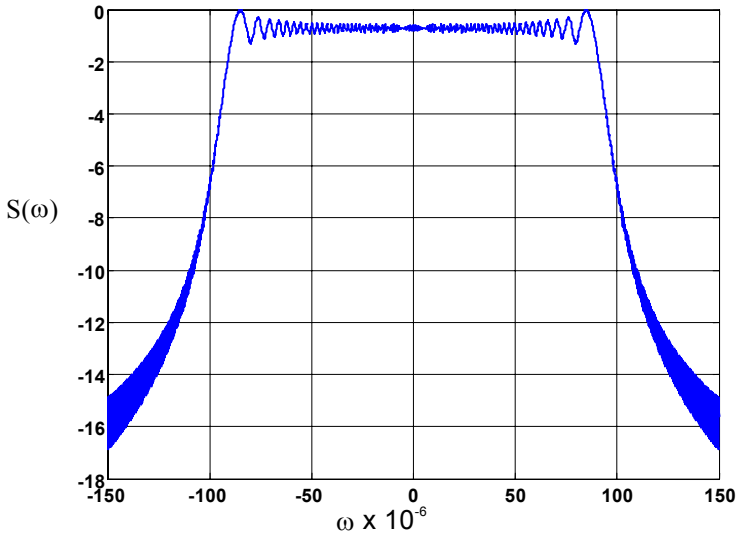

Figure 2-3: *Normalized spectrum of a linear FM chirp with frequency deviation B=30 MHz and pulse width τ=10 μs.*

2.3. Effects of Pulsed UWB Interference on CW FM Radar

It is assumed here that the interferer is present during the period of processing, which in this case is the entire pulse transmission period τ. It is also assumed that the round trip path delay Δt is small compared with the total pulse period τ.

2.3.1. System and Interference Model

As was done in Chapter 5 of [2], the receive chain will be modeled as a filter with a bandwidth equal to that of the narrowest IF filter, but a center frequency equal to the carrier frequency f_0. The frequency conversion (mixing) occurs in this model at the filter output as shown in Figure 2-4. If the narrowest IF has a baseband-equivalent transfer function of $H_{if}(f)$, then the IF-equivalent channel filter in Figure 2-4 has a transfer function of $H_{eq}(f) = H_{if}(f - f_0) + H_{if}^*(-f - f_0)$.

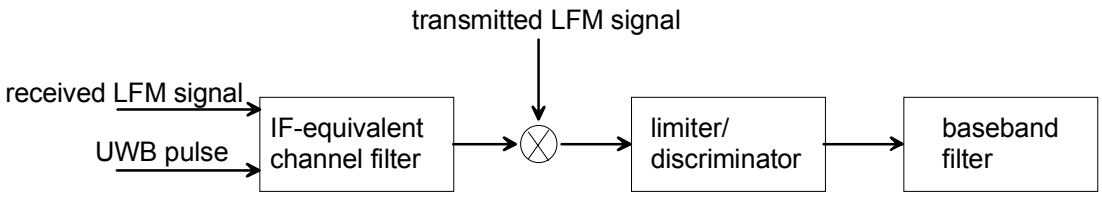

Figure 2-4: *Equivalent receiver model for analysis.*

When a UWB signal with pulse repetition frequency (PRF) much less than the IF bandwidth passes through the filter, each pulse excites the impulse response of the filter and the effect of each pulse is independent of the next. The filter output (mixer input) for a single UWB pulse can be expressed as [1]

$$g_k(t) = \mathrm{Re}\left\{ 2\left|P(f_0)\right| h_{if}(t - T_k) e^{j[2\pi f_0 (t-T_k) + \psi(f_0)]} \right\}. \tag{2-10}$$

where T_k is the arrival time of the k^{th} pulse, $P(f) = \left|P(f)\right| e^{j\psi(f)}$ is the Fourier transform of the UWB pulse waveform, and $h_{if}(t)$ is the baseband equivalent response of the IF filter. It should be noted that $h_{if}(t)$ is in general complex; i.e. $h_{if}(t) = \left|h_{if}(t)\right| e^{j\varphi(t)}$, which represents the complex envelope of the impulse response.

Letting $\beta_k(t) = \psi(f_0) - 2\pi f_0 T_k + \varphi(t - T_k)$, the IF response to the k^{th} pulse can be written as:

$$g_k(t) = 2\left|P(f_0)\right| \left|h_{if}(t - T_k)\right| \cos[2\pi f_0 t + \beta_k(t)] \tag{2-11}$$

In the specific case considered here (the *n*-pole filter), $\varphi(t) = 0$ and $h_{if}(t)$ is real, so $\beta_k(t) = \beta_k = \psi(f_0) - 2\pi f_0 T_k$; i.e., β_k depends only on the pulse arrival time but does not vary over the filter response interval.

2.3.2. Discriminator Output

The UWB pulse interference at the discriminator input can be written generically as a noise term with time varying phase and amplitude

$$n(t) = \mathrm{Re}\left[b(t) e^{j[2\pi f_0 t + \theta(t)]} \right] \tag{2-12}$$

The total signal with both desired LFM and pulsed interference (during a period while the chirped radar signal is on and the interferer is present) is expressed as

$$r(t) = s(t) + n(t) = \mathrm{Re}\left\{ e^{j2\pi f_0 t} \left[A e^{j\phi(t)} + b(t) e^{j\theta(t)} \right] \right\} \tag{2-13}$$

Combining the two exponential terms into a single equivalent exponential term with an equivalent amplitude and phase as was done in [1] gives

$$r(t) = c(t)\,\mathrm{Re}\left[e^{j2\pi f_0 t} e^{j\gamma(t)}\right] \quad , \quad -\tau/2 \le t \le \tau/2 \tag{2-14}$$

with amplitude

$$c(t) = \sqrt{A^2 + b(t)^2 + 2Ab(t)\cos(\theta - \phi)} \tag{2-15}$$

and phase

$$\gamma(t) = \phi(t) + \tan^{-1}\left[\frac{b(t)\sin[\theta(t) - \phi(t)]}{A + b(t)\cos[\theta(t) - \phi(t)]}\right]. \tag{2-16}$$

Assuming an ideal frequency discriminator as the detector in the radar system, the receiver response is obtained by differentiating the phase (dropping all of the explicit time dependencies), giving:

$$\frac{d\gamma}{dt} = \dot{\gamma} = \dot{\phi} + \frac{A\dot{b}\sin(\theta - \phi) + b(\dot{\theta} - \dot{\phi})[b + A\cos(\theta - \phi)]}{c^2} \tag{2-17}$$

A simple *n*-pole filter will be assumed for the IF filter in the radar system, and the filter response will be normalized to have unity bandwidth as was done in [1], and repeated here for convenience

$$h_{if}(t) = B_{if} h_1(B_{if} t), \tag{2-18}$$

which leads to

$$\dot{h}_{if}(t) = B_{if}^2 \dot{h}_1(B_{if} t). \tag{2-19}$$

The bandwidth of the actual IF front-end filter of the radar is B_{if}, and is approximately the same as the total frequency deviation *B* of the chirp (assuming $B >> 1/\tau$).

The normalized unity-bandwidth filter response of the n-pole filter and its first derivative are

$$h_1(t) = \frac{x^n}{(n-1)!} t^{n-1} e^{-xt} \qquad \dot{h}_1(t) = h_1(t)\left(\frac{n-1}{t} - x\right) \tag{2-20}$$

where

$$x = \frac{2\pi(n-1)!}{\Gamma\left(\frac{1}{2}\right)\Gamma\left(n-\frac{1}{2}\right)}. \tag{2-21}$$

We can now write out all of the terms present in the expression of the output of the frequency discriminator so that we can begin discussing the range error that results from the presence of a pulsed interferer. The b and $\dot{b}$ terms in the frequency expression of Equation 2-17 are the time varying amplitude and the first derivative of the pulsed interference term, which are

$$b = 2B_{if}\left|P(f_0)\right|h_1(B_{if}t) \qquad \dot{b} = 2B_{if}^2\left|P(f_0)\right|\dot{h}_1(B_{if}t) \tag{2-22}$$

All that remains in order to apply (2-17) is to find the phase difference term $\theta(t)-\phi(t)$ and its derivative. To do so, the mixing of the desired and interfering signals with the transmitted signal must be considered. The phase of the transmitted signal and its derivative are, respectively, $\alpha(t)=\pi\mu t^2$ and $\dot{\alpha}(t)=2\pi\mu t$. Therefore, with a total two-way propagation delay of Δt, the received phase of the desired signal and its derivative are:

$$\alpha(t-\Delta t)=\pi\mu(t-\Delta t)^2 \qquad \dot{\alpha}(t-\Delta t)=2\pi\mu(t-\Delta t). \tag{2-23}$$

Both the desired signal and the interference due to the UWB pulse are mixed with the transmitted signal, which is proportional to $\cos\left[2\pi f_0 t+\alpha(t)\right]$. The received desired signal is simply a delayed version of this, and is proportional to $\cos\left[2\pi f_0(t-\Delta t)+\alpha(t-\Delta t)\right]$. Multiplying and neglecting the double-frequency term gives the desired signal component of the discriminator input as:

$$s(t)=A\cos\left[\alpha(t-\Delta t)-\alpha(t)-2\pi f_0\Delta t\right]. \tag{2-24}$$

The phase of the desired signal component of the discriminator input therefore is

$$\begin{aligned}\phi(t) &= \alpha(t-\Delta t)-\alpha(t)-2\pi f_0\Delta t \\ &= \pi\mu(t-\Delta t)^2-\pi\mu t^2-2\pi f_0\Delta t \\ &= -2\pi\mu t\Delta t+\pi\mu(\Delta t)^2-2\pi f_0\Delta t\end{aligned}, \tag{2-25}$$

and its derivative is:

$$\dot{\phi}(t)=-2\pi\mu\Delta t. \tag{2-26}$$

Similarly, multiplying the interference term $\cos\left[2\pi f_0 t + \beta_k(t)\right]$ by the transmitted signal and neglecting the double-frequency term, which is rejected by the IF filter, gives

$$n(t) = b(t)\cos\left[\beta_k(t) - \alpha(t)\right] \tag{2-27}$$

Thus, the phase of the interference component at the discriminator input is

$$\theta(t) = \beta_k(t) - \alpha(t), \tag{2-28}$$

and, assuming the impulse response phase $\beta_k(t)$ is invariant with time, and defining $\xi(t) = \theta(t) - \phi(t)$ gives

$$\begin{aligned} \xi(t) = \theta(t) - \phi(t) &= \beta_k + 2\pi f_0 \Delta t - \alpha(t - \Delta t) \\ &= \beta_k + 2\pi f_0 \Delta t - \pi\mu(t - \Delta t)^2 \end{aligned} \tag{2-29}$$

By using the definitions in Equations 2-22 through 2-23, and defining the term

$$\rho \equiv \frac{A}{2B_{if}\left|P(f_0)\right|} \tag{2-30}$$

in Equation 2-17 for the received frequency, we obtain the expression

$$\dot{\gamma} = -2\pi\mu\Delta t + \frac{\rho B_{if}\dot{h}_1(B_{if}t)\sin\xi - 2\pi\mu(t - \Delta t)\left[h_1^2(B_{if}t) + \rho h_1(B_{if}t)\cos\xi\right]}{\rho^2 + h_1^2(B_{if}t) + 2\rho h_1(B_{if}t)\cos\xi}. \tag{2-31}$$

where Δt is round trip delay to the target.

2.4. RMS Range Error vs. Carrier-to-Interference Ratio

To characterize the effect of interference, and relate it to ρ as defined in equation 2-30, we first find the carrier power:

$$C_r = \frac{1}{2\tau}\int_{-\tau/2}^{\tau/2}\left|Ae^{j2\pi\phi(t)}\right|^2 dt = \frac{A^2}{2} \tag{2-32}$$

Assuming the impulse response of the filter decays to zero within the radar pulse interval τ, the energy per pulse of the UWB interferer is

$$E_p = \frac{1}{2}\int_{-\tau/2}^{\tau/2} \left| 2B_{if} \left| P(f_0) \right| h_1(B_{if} t) e^{j\theta(t)} \right|^2 dt = 2B_{if} \left| P(f_0) \right|^2 \tag{2-33}$$

and the total UWB interference power is

$$I_{UWB} = R_u E_p = 2R_u B_{if} \left| P(f_0) \right|^2 . \tag{2-34}$$

This makes the carrier to interference ratio

$$CIR = \frac{A^2}{4R_u B_{if} \left| P(f_0) \right|^2} . \tag{2-35}$$

Defining $N_u = R_u / B_u$, ρ can be expressed in terms of the carrier-to-interference ratio

$$\rho^2 = \frac{R_u}{B_{if}} \frac{A^2}{4B_{if} R_u \left| P(f_0) \right|^2} = \frac{R_u}{B_{if}} CIR = N_u CIR . \tag{2-36}$$

Eq. (2-31) represents the output of a discriminator or frequency counter, and the first term $-2\pi\mu\Delta t$, is the desired signal. Multiplying by the factor $-c/4\pi\mu$ gives the altitude; i.e.,

$$2\pi\mu\Delta t \cdot \frac{c}{4\pi\mu} = \frac{c\Delta t}{2} = R . \tag{2-37}$$

Of interest here is the rms error in the altitude estimate introduced by the UWB signal. To determine this, it is necessary to account for the effect of any filtering or averaging of the discriminator output. For purposes of analysis, this effect can be represented by a baseband filter of bandwidth B_b . In reality, the filtering might be provided by a device such as an analog or digital display, which would be expected to have a time constant measured in terms of tens or hundreds of milliseconds, since the desired signal (which is a voltage proportional to the altitude) is a very low-pass process. If the signal from the altimeter is fed to an autopilot, any high-frequency variations introduce by noise or interference will be filtered for stability.

At this point, the problem becomes very similar to that of an FM receiver as discussed in Chapter 6 of [1] and Chapter 3 of this report. The main differences are the linear frequency modulation format in this case vs. sinusoidal modulation in the other case, and the bandwidth of the final baseband filter. Using the same approach described in Chapter 3 of this report, a closed-form solution for the rms altitude estimation error can be developed.

As in Chapter 6 of [1], let $\overline{E}_{bb}$ represent the average interference energy out of the baseband filter per UWB pulse. The average is taken over (1) uniformly-distributed pulse arrival times relative to the beginning of the chirp, and (2) the phase $\beta_k + 2\pi f_0 \Delta t$, assumed uniformly-distributed over $[0,2\pi]$.

The normalized version of $\overline{E}_{bb}$ is

$$\Lambda(\rho) \equiv \frac{\overline{E}_{bb}}{B} \tag{2-38}$$

which can be found numerically by time-sampling a normalized version of the discriminator output interference time-waveform $\dot{\gamma} - \dot{\phi}$, computing the fast Fourier transform (FFT), then computing the energy over the baseband bandwidth B_b. As shown in Chapter 3, $\Lambda(\rho)$ can also be found in closed form. In either case, the average interference power at the output of the baseband filter is

$$\overline{p}_i = R_u B \Lambda(\rho), \tag{2-39}$$

and the rms interference voltage is $e_{rms} = \sqrt{\overline{p}_i}$. The rms range measurement error therefore is

$$\varepsilon_{rms} \frac{c}{4\pi\mu} e_{rms} = \frac{c\tau}{4\pi B} e_{rms} = \frac{c\tau}{4\pi} \sqrt{N_u \Lambda(\rho)}, \tag{2-40}$$

since $N_u = R_u / B$ and $\mu = B/\tau$.

As shown in Chapter 3, $\Lambda(\rho)$ can be approximated as:

$$\Lambda(\rho) \cong \begin{cases} 2\frac{B_b}{B}(2\pi)^2 P_{xo}(\rho), & \log\rho < 0.16 \\ \frac{4\pi^2}{3}\left(\frac{B_b}{B_{if}}\right)^3 \cdot \frac{1}{\rho^2}, & \log\rho \geq 0.16 \end{cases} \tag{2-41}$$

where $P_{xo}(\rho)$ is the "crossover probability" (the probability that the UWB pulse causes the phase to undergo a net change of $\pm 2\pi$ at the discriminator input; see section 3.5 of this report). An approximation for the crossover probability is derived in section 3.5 for

the case of sinusoidal modulation. For linear FM as considered here, the approximation is (see Annex 2A):

$$P_{xo}(\rho) \cong \begin{cases} \frac{1}{4}\left(1 - \frac{0.51 + \log \rho}{1.7}\right) & \log \rho < -0.51 \\ \frac{1}{4}\sqrt{\frac{0.16 - \log \rho}{0.67}} & -0.51 \le \log \rho < 0.16 \end{cases} \tag{2-42}$$

Figure 2-5 shows $\Lambda(\rho)$ vs. ρ using the numerical (FFT-based) approach and the approximation, for $B_b = 30$ MHz, and the agreement is excellent.

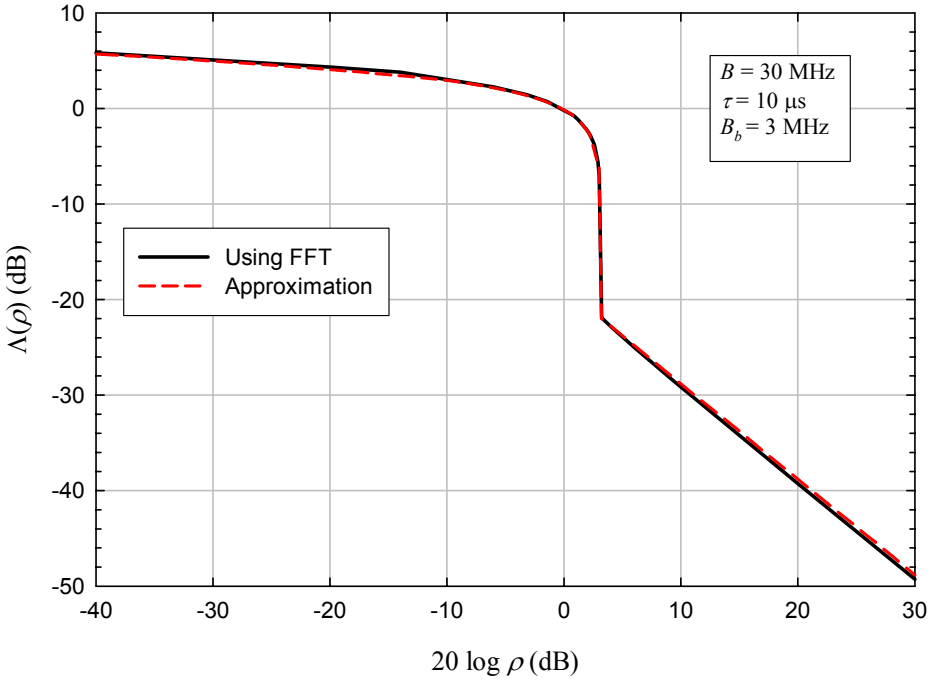

Figure 2-5: *Comparison of closed-form approximation and FFT solution for normalized baseband energy per UWB pulse.*

Using the approximation to $\Lambda(\rho)$, the rms altitude estimation error is:

$$\varepsilon_{rms} = \frac{c}{4\pi\mu} e_{rms} = \frac{c\tau}{4\pi B} e_{rms} = \begin{cases} c\tau\sqrt{\frac{N_u}{2}\frac{B_b}{B}P_{xo}(\rho)} & \log \rho < 0.16 \\ \frac{c\tau}{2\rho}\sqrt{\frac{N_u}{3}\left(\frac{B_b}{B_{if}}\right)^3} & \log \rho > 0.16 \end{cases} \tag{2-43}$$

Figure 2-6 shows ε_{rms} vs. ρ for $\tau = 10\,\mu$s, $N_u = 0.5$, $B = 30$ MHz, and $B_b = 100$ Hz. Note that for $\rho = 0.01$ (–40 dB), $\varepsilon_{rms} \cong 1.8$ m.

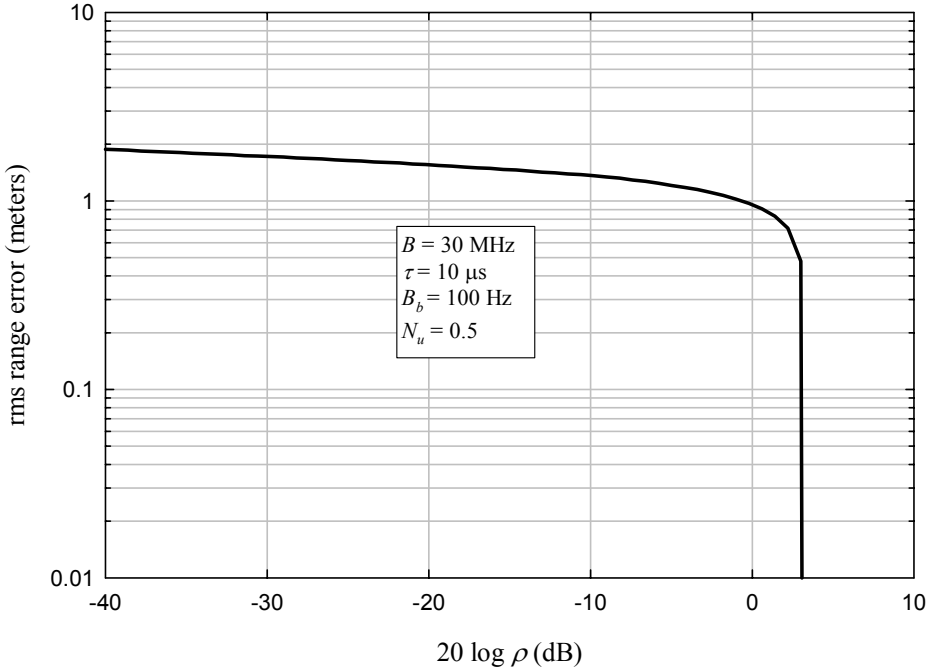

Figure 2-6: *RMS range error with 100 Hz baseband bandwidth and* $N_u = 0.5$.

Figure 2-7 shows the crossover probability based on the approximation, and also the value extracted from the numerical (FFT-based) calculations. As can be seen, agreement is reasonably good. Figure 2-8 shows the rms range error vs. the CIR for several different values of N_u.

Clearly, due to the low-pass nature of the baseband signal being tracked (the aircraft altitude), isolated UWB pulses ($N_u < 1$) do not seem to pose much of a significant threat to the accuracy of the FM radar altimeter, since most of the interference energy is well above the passband of the desired signal and easily filtered out.

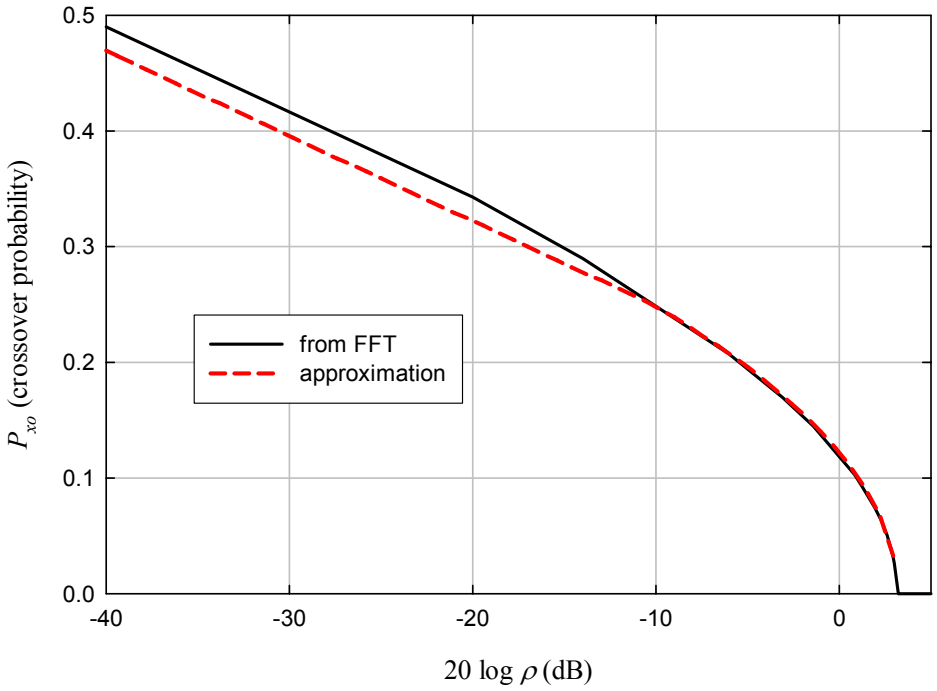

Figure 2-7: *Crossover probability: approximation and value extracted from FFT solution.*

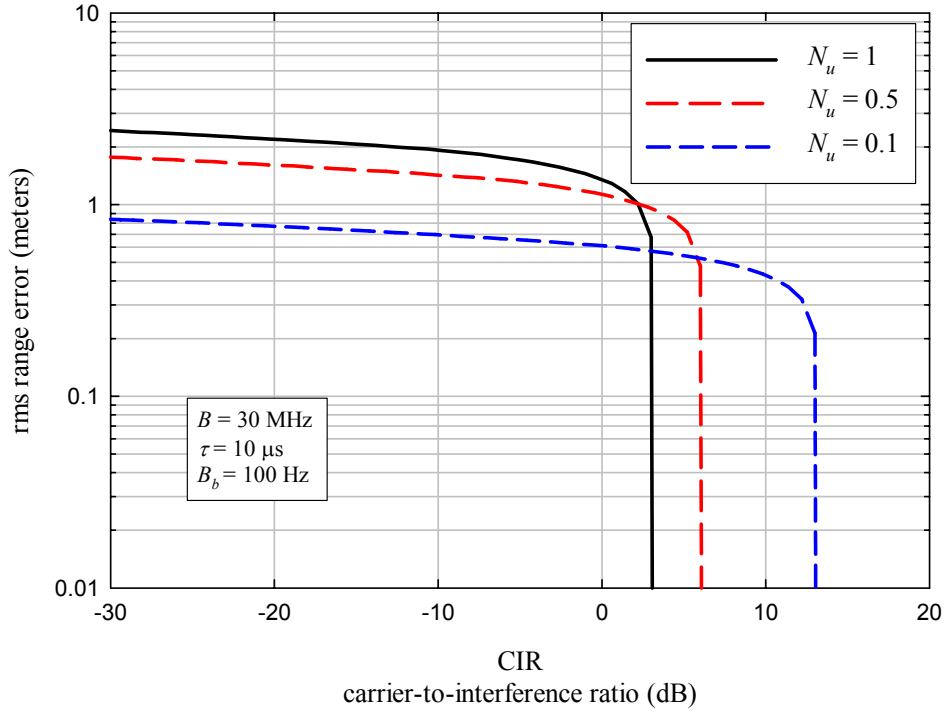

Figure 2-8: *RMS range error vs. CIR for different values of* N_u.

2.5. Conclusions

This chapter has investigated the effect of UWB interference on a CW radar altimeter using linear FM (chirp) modulation. The scope was limited to cases for which $N_u \leq 1$ (the pulse rate is no greater than the IF bandwidth, which in the examples give here was assumed to be 30 MHz). The receiver was assumed to be an ideal discriminator followed by baseband filtering, which may be an integral part of the display or control mechanism associated with altimeter. The effective baseband bandwidth will be very narrow, because the process being tracked (the aircraft altitude) is slowly varying, and any high frequency components at the discriminator output will be due to noise or interference. As a result, most of the energy at the discriminator output due to the UWB pulse is rejected by the baseband filtering and the UWB signal has little effect on the altitude estimate.

UWB signals with pulse rates that are high relative to the IF bandwidth appear as combinations of CW tones and noise-like components. A CW tone within the IF passband can cause a DC component at baseband (at the discriminator output) which cannot be rejected by the baseband filtering. However, CW interference is not unique to UWB signals, and any well-designed altimeter receiver should have capabilities for recognizing and removing the effects of CW interference.

2.6. Annex 2A: Crossover Probability for Linear FM CW Radar Receiver with Pulsed UWB Interference

This discussion relies heavily on Chapter 3, and in particular section 3.5. In the case of the FM CW radar, the UWB signal is mixed with the transmitted LFM signal and it is the change in $\xi(t) = \theta(t) - \phi(t)$ that determines whether a crossover occurs. From (2-29),

$$\xi(t) \equiv \beta_k + 2\pi f_0 \Delta t - \pi\mu(t - \Delta t)^2 \tag{2A-1}$$

and defining

$$\Delta\xi = \xi(t_2) - \xi(t_1), \tag{2A-2}$$

the crossover probability is then

$$P_{xo} = \frac{\langle|\Delta\xi|\rangle}{2\pi}. \tag{2A-3}$$

Letting $\Delta t_1 = t_2 - t_1$ and $\bar{t}_1 = \frac{t_2 + t_1}{2}$, $\Delta\xi$ can be written as

$$\Delta\xi = -2\pi\mu \cdot (\Delta t_1)(\bar{t}_1 - \Delta t) \tag{2A-4}$$

Note that $\mu(\bar{t}_1 - \Delta t)$ is the frequency (relative to f_0) of the reflected signal at time $\bar{t}_1$.

For the approximation, it will be assumed that $\Delta t << \tau$ and $\Delta t_1 << \tau$, where τ is the total duration of the chirp. Assuming $\bar{t}_1 - \Delta t$ to be uniformly-distributed between $-\tau/2$ and $\tau/2$, then

$$\langle|\bar{t}_1 - \Delta t|\rangle \cong \frac{\tau}{4} \tag{2A-5}$$

and

$$\langle|\Delta\xi|\rangle \cong 2\pi\mu \cdot (\Delta t_1) \cdot \langle|\bar{t}_1 - \Delta t|\rangle = \frac{\pi B}{2} \cdot \Delta t_1 \tag{2A-6}$$

and the crossover probability is approximately

$$P_{xo} \cong \frac{\langle |\Delta\xi| \rangle}{2\pi} \cong \frac{B \cdot \Delta t_1}{4}. \tag{2A-7}$$

The term $B\Delta t_1$ is the same as the normalized time "Δt" in section 3.5, and therefore can be approximated, for the 4-pole IF filter used here, as a function of ρ by eq. (3-33), as:

$$B\Delta t_1 \cong \begin{cases} 1 - \dfrac{0.51 + \log\rho}{1.7} & \log\rho < -0.51 \\ \sqrt{\dfrac{0.16 - \log\rho}{0.67}} & -0.51 \le \log\rho < 0.16 \\ 0 & \log\rho \ge 0.16 \end{cases} \tag{2A-8}$$

Hence, the crossover probability is roughly:

$$P_{xo}(\rho) \cong \begin{cases} \dfrac{1}{4}\left(1 - \dfrac{0.51 + \log\rho}{1.7}\right) & \log\rho < -0.51 \\ \dfrac{1}{4}\sqrt{\dfrac{0.16 - \log\rho}{0.67}} & -0.51 \le \log\rho < 0.16 \end{cases} \tag{2A-9}$$

Chapter 2 References

[1] J.E. Padgett, J.C. Koshy, A. A. Triolo, "Physical-Layer UWB Interference Impact Analysis", for Defense Advance Research Projects Agency, Contract MDA972-02-C-0056, August 8, 2003.

[2] J.E. Padgett, J.C. Koshy, A. A. Triolo, "Physical-Layer Modeling of UWB Interference Effects", for Defense Advance Research Projects Agency, Contract MDA972-02-C-0056, January 10, 2003

[3] M.I. Skolnik, *Introduction to Radar Systems*, New York, NY, McGraw-Hill, 1980.

[4] B.R. Mahafza, *Radar Systems Analysis and Design Using Matlab*, Boca Raton, FL, Chapman & Hall, 2000.

[5] M. Schwartz, W.R. Bennett, and S. Stein, Communication Systems and Techniques, Piscataway, NJ, IEEE Press, 1996.

Chapter 3: Detailed Analysis of UWB Pulse Effects on a FM Demodulator

3.1. Introduction and Summary

In Chapter 6 of [1], a sharp threshold effect was observed when pulsed interference is applied to an FM receiver. The purpose of this chapter is to explain the mechanism underlying this phenomenon, and using physical reasoning based on that mechanism, to derive a closed-form approximation to the curve showing the baseband output interference energy per pulse as a function of the carrier-to-interference ratio times the ratio of the pulse rate to the receiver bandwidth (the parameter denoted N_u).

The closed-form expression derived here is

$$\Lambda(\rho) \cong \begin{cases} \dfrac{8\pi\beta f_m B_b}{B_{if}^2}\left(1 - \dfrac{0.51 + \log\rho}{1.7}\right) & \log\rho < -0.51 \\ \dfrac{8\pi\beta f_m B_b}{B_{if}^2}\sqrt{\dfrac{0.16 - \log\rho}{0.67}} & -0.51 \le \log\rho < 0.16 \\ \dfrac{4\pi^2}{3}\left(\dfrac{B_b}{B_{if}}\right)^3 \cdot \dfrac{1}{\rho^2} & \log\rho \ge 0.16 \end{cases}$$

which is shown below, compared to the numerical results obtained with the FFT, discussed in [1]. As can be seen, agreement is excellent.

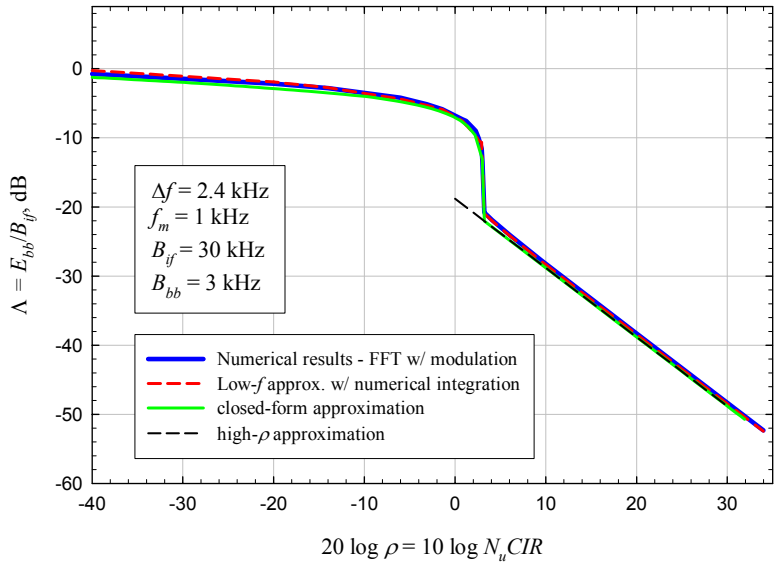

The pronounced threshold effect does not exist if the desired signal is unmodulated. The effect is due to a phase change of 2π radians in the composite signal, which cannot occur in the case considered here if the desired signal is not modulated.

3.2. Review of the FM UWB Interference Model

The desired signal can be expressed as $s(t) = A\cos[2\pi f_0 t + \phi(t)]$, and the phase modulation in the case of a sinusoidal modulating signal is $\phi(t) = \beta \sin(2\pi f_m t + \alpha)$ where $\beta = \Delta f / f_m$ is the modulation index, with Δf being the maximum deviation and f_m being the modulating frequency. The discriminator output due to the desired signal is $\dot{\phi}(t) = 2\pi\Delta f \cos(2\pi f_m t + \alpha)$.

The input to the discriminator due to the interfering pulse can be represented as $n(t) = 2B_{if}|P(f_0)|h_1(B_{if}t)\cos(2\pi f_0 t + \theta)$, where θ is the phase angle between the desired signal and the interfering signal at the beginning of the interfering pulse, $h_1(t)$ is a normalized (unit bandwidth) version of the impulse response envelope of the IF section, and B_{if} is the bandwidth of the IF stages preceding the discriminator.

Of interest here is the phase angle $\gamma(t)$ of the total signal $s(t)+n(t)$ that is applied to the discriminator. Since $\gamma(t)$ depends on the ratio of the desired signal and interference amplitudes (as well as the phase terms), but not on the absolute amplitudes, it is useful to define

$$\rho \equiv \frac{A}{2B_{if}|P(f_0)|} \tag{3-1}$$

in which case the normalized desired signal can be written as $s(t) = \rho\cos[2\pi f_0 t + \phi(t)]$, the corresponding pulsed interference as $n(t) = h_1(B_{if}t)\cos(2\pi f_0 t + \theta)$, and the total input to the discriminator is $r(t) = s(t) + n(t)$. Figure 3-1 shows the basic phasor diagram for understanding the discriminator input and output as a function of the various signal and interference parameters. For simplicity, the phase angle of the desired signal was taken as the reference. The phase angle of the discriminator input is $\gamma(t)$ and the discriminator output is proportional to $d\gamma/dt$ (denoted $\dot{\gamma}$). The term $\gamma - \phi$ is referred to here as the "excess phase" and its derivative $\dot{\gamma} - \dot{\phi}$, or $\frac{d}{dt}(\gamma - \phi)$ is the baseband interference at the output of the discriminator. The phasor diagram in Figure 3-1 shows the excess phase $\gamma - \phi$ and its relationship to the other parameters.

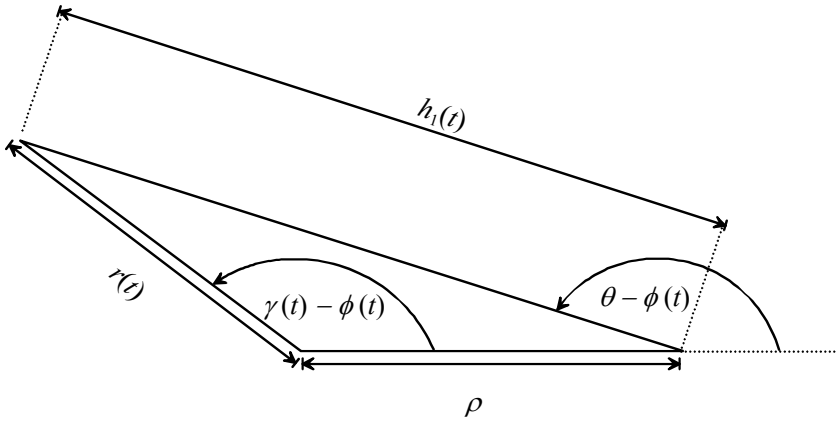

Figure 3-1: *Phasor geometry for pulse interference analysis*

The excess phase and the discriminator output can be expressed as

$$\gamma(t) - \phi(t) = \tan^{-1}\left[\frac{h_1(t)\sin[\theta - \phi(t)]}{\rho + h_1(t)\cos[\theta - \phi(t)]}\right] \tag{3-2}$$

$$\dot{\gamma}(t) - \dot{\phi}(t) = \frac{B_{if}\rho\dot{h}_1(B_{if}t)\sin[\theta - \phi(t)] - \dot{\phi}(t)\{h_1^2(B_{if}t) + \rho h_1(B_{if}t)\cos[\theta - \phi(t)]\}}{\rho^2 + h_1^2(B_{if}t) + 2\rho h_1(B_{if}t)\cos[\theta - \phi(t)]} \tag{3-3}$$

For the interference analysis, it is useful to define a normalized version of the discriminator ouput voltage as:

$$v(t) \equiv \frac{\rho\dot{h}_1(t)\sin[\theta - \phi(t/B_{if})] - \frac{\dot{\phi}(t/B_{if})}{B_{if}}\{h_1^2(t) + \rho h_1(t)\cos[\theta - \phi(t/B_{if})]\}}{\rho^2 + h_1^2(t) + 2\rho h_1(t)\cos[\theta - \phi(t/B_{if})]} \tag{3-4}$$

so that the baseband interference at the discriminator output is

$$i_{bb}(t) = \dot{\gamma}(t) - \dot{\phi}(t) = B_{if} \cdot v(B_{if}t) \tag{3-5}$$

and its Fourier transform is

$$I_{bb}(f) = V(f/B_{if}) \tag{3-6}$$

The total interference energy due to a single pulse at the output of the baseband filter, assumed rectangular with bandwidth B_b, is

$$E_{bb}(\rho,\alpha,\theta) = \int_{-B_b}^{B_b} |I_{bb}(f)|^2 \, df = \int_{-B_b}^{B_b} \left| V\left(\frac{f}{B_{if}}\right) \right|^2 \, df = B_{if} \int_{-B_b/B_{if}}^{B_b/B_{if}} |V(\xi)|^2 \, d\xi \tag{3-7}$$

As described in Chapter 6 of [1], the quantity

$$\Lambda(\rho,\alpha,\theta_k) \equiv \int_{-B_b/B_{if}}^{B_b/B_{if}} |V(f)|^2 \, df = \frac{E_{bk}(\rho,\alpha,\theta_k)}{B_{if}} \tag{3-8}$$

was computed using the fast Fourier transform (FFT), and then averaged over α and θ to give:

$$\Lambda(\rho) = \langle \Lambda(\rho,\alpha,\theta_k) \rangle_{\alpha,\theta} = \frac{\overline{E}_{bb}(\rho)}{B_{if}} \tag{3-9}$$

The parameter ρ can be related to the carrier-to-interference ratio (CIR) by defining

$$N_u \equiv R / B_{if} \tag{3-10}$$

where *R* is the average UWB pulse rate. The average interference power at the final IF filter output is

$$I_{if} = 2B_{if} |P(f_0)|^2 R \tag{3-11}$$

Since the carrier (desired signal) power is $C = A^2/2$, and recalling that $\rho = A / 2B_{if} |P(f_0)|$, the CIR is

$$CIR = \frac{C}{I_{if}} = \frac{A^2}{4|P(f_0)|^2 B_{if} R} = \rho^2 \frac{B_{if}}{R} = \frac{\rho^2}{N_u} \tag{3-12}$$

Hence,

$$\rho^2 = N_u CIR \tag{3-13}$$

The average interference power at the baseband filter output is

$$\overline{I_{bb}} = R \cdot E_{bb} = N_u B_{if}^2 \Lambda(\rho) \tag{3-14}$$

As shown in Chapter 6 of [1], when $\rho >> 1$, the normalized baseband interference energy per pulse is closely approximated by:

$$\Lambda(\rho) = \frac{4\pi^2}{3\rho^2}\left(\frac{B_b}{B_{if}}\right)^3 \quad \rho >> 1 \tag{3-15}$$

Figure 3-2 shows $\Lambda(\rho)$ vs. ρ, computed as described above using the FFT and averaging over θ and α. The extremely sharp threshold at $\rho = 3$ dB, and the flattening-out of the interference energy as $\rho \to 0$ are interesting features and have led to questions about the accuracy of this curve. The purpose of the rest of this Chapter is to develop a more detailed understanding of the relationships and conditions leading to this curve, and to verify it with an approximate analytical solution that does not rely on the FFT.

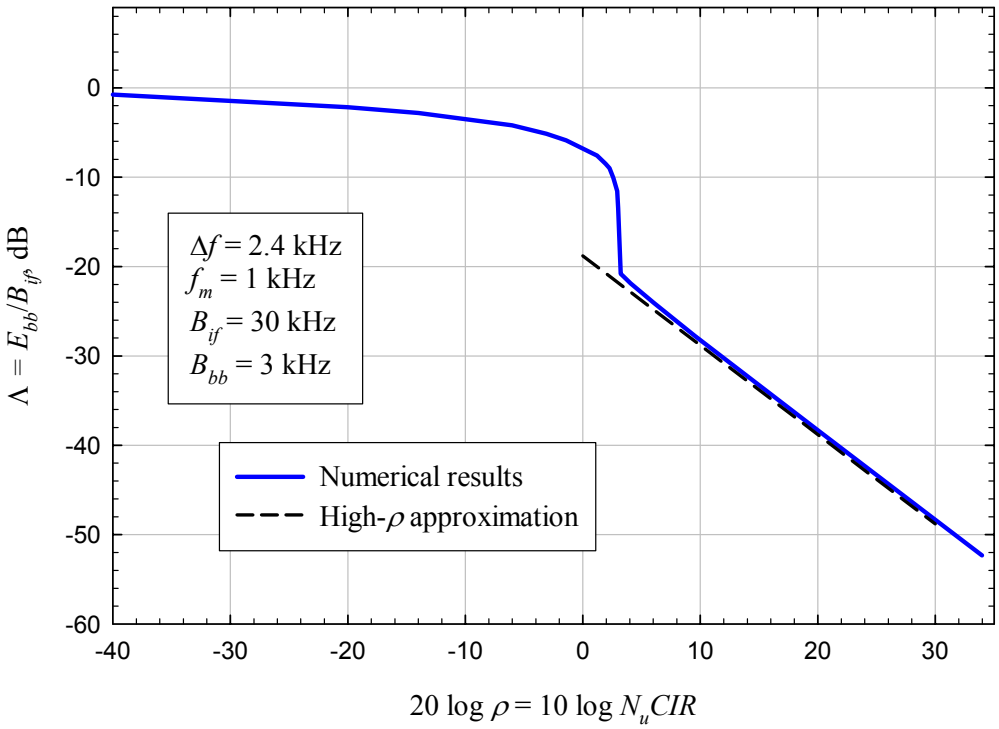

Figure 3-2: *Normalized baseband interference energy per UWB pulse*

3.3. Analysis

Figure 3-1 shows a snapshot in time of the phasor geometry. Since the pulse amplitude is time-varying as shown in Figure 3-3, the phase angle $r(t)$ will vary over time as shown in Figure 3-4, where it was assumed that ρ is small compared to the maximum value of the pulse, which is between 1.4 and 1.5 and is mildly dependent on the number of poles.

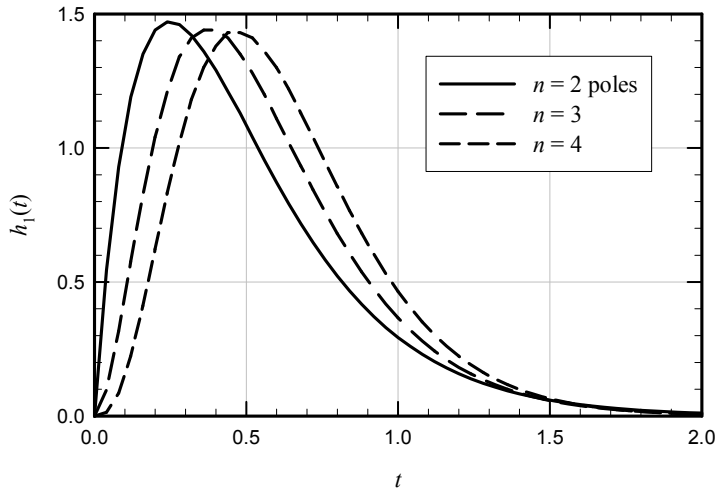

Figure 3-3: *Normalized IF impulse response envelope for n-pole filter*

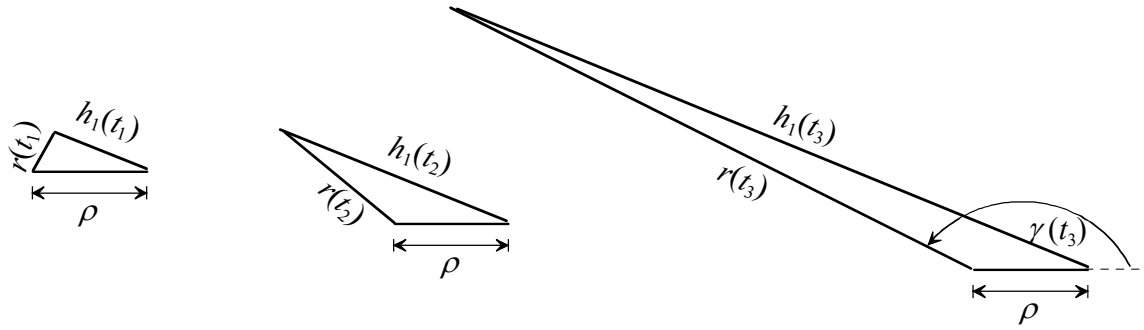

Figure 3-4: *Pulsed interference and total discriminator input at three different times*

As the pulse amplitude grows, the excess phase γ changes, and the highest rate of change occurs when the pulse amplitude $h_1(t)$ is roughly equal to ρ. As $h_1(t)$ grows much greater than ρ, γ approaches θ and $\dot{\gamma}$ becomes very small. After the pulse reaches its peak and decreases, γ begins to change, reaching its maximum rate again when $h_1(t)$ is roughly equal to ρ. As an example, Figure 3-5 shows $h_1(t)$ for a 4-pole filter (left ordinate), and the excess phase $\gamma(t) - \phi(t)$ (right ordinate) for $\rho = 0.1$ and $\theta = 3\pi/4$. Note after the pulse dissipates, $\gamma(t) - \phi(t)$ returns to zero. This means that over the pulse

duration, $\int\left[\dot{\gamma}(t)-\dot{\phi}(t)\right]dt = 0$; that is, the discriminator output interference has no DC component.

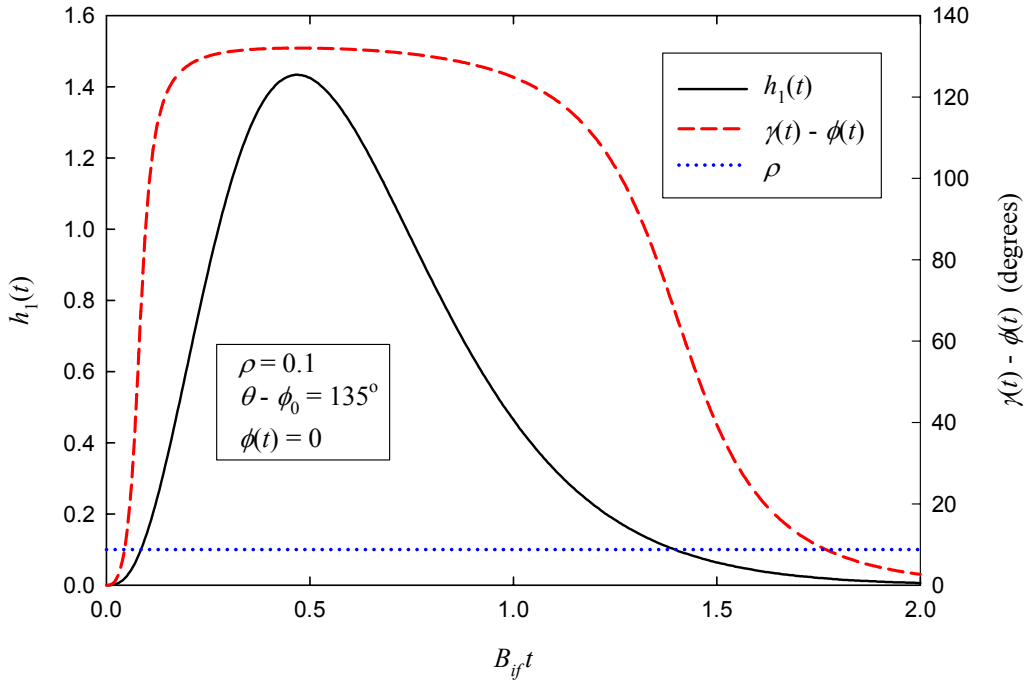

Figure 3-5: *Normalized IF impulse response and excess phase at discriminator input*

If there is modulation on the desired signal, this will no longer be true, and there generally will be a net change in the excess phase over the IF impulse response duration. This can be seen with the help of the example in Figure 3-6. Assume that at some time t_1 the phase of the desired signal is $\phi(t_1)$, and the phase of the IF impulse response due to the UWB pulse is θ. The phase of the composite desired plus interfering signal is $\gamma(t_1)$ as shown in Figure 3-6(a). Note that the excess phase $\gamma(t_1)-\phi(t_1)$ is negative (this is because, in the example shown, the phasor representing the composite signal $r(t)$ will rotate in a clockwise sense as $h_1(t)$ increases). During the duration of the pulse, the phase of the desired signal increases due to the modulation, and at time t_2 the desired signal phase is $\phi(t_2)$. The phase of the composite signal becomes $\gamma(t_2)$ as shown in Figure 3-6(b), shown referenced to $\phi(t_1)$ for comparison with Figure 3-6(a). Using $\phi(t_2)$ as the reference gives Figure 3-6(c).

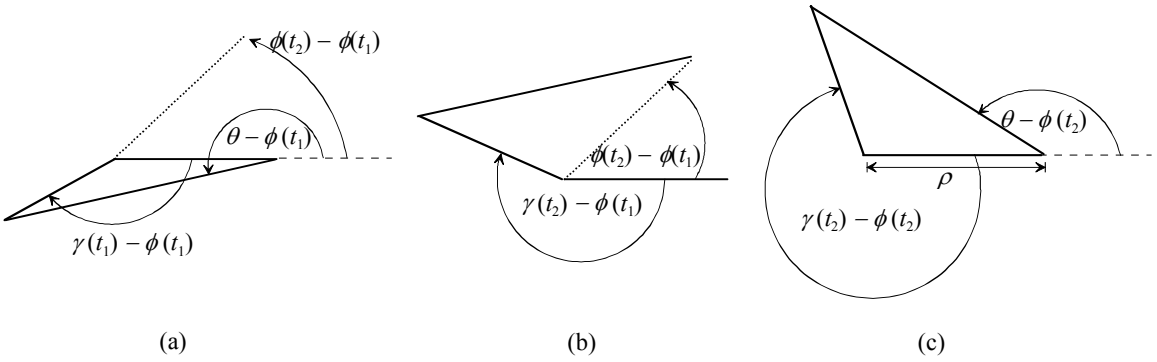

Figure 3-6: *Phasor example with frequency modulation of the desired signal*

Note that the excess phase $\gamma(t) - \phi(t)$ has crossed the $-\pi$ point (negative *x*-axis) and as the pulse amplitude decreases, will continue in a clockwise sense. This means that unlike the case discussed above, $\int [\dot{\gamma}(t) - \dot{\phi}(t)]dt = -2\pi$.

Figure 3-7 shows an example for $\theta = 1.125\pi$, which roughly corresponds to the case illustrated in Figure 3-6. It was assumed that $\rho = 0.01$. Note that the excess phase $\gamma(t) - \phi(t)$, shown on the right-hand ordinate in degrees, starts at 0° and finishes at –360°. The normalized version of its derivative $\dot{\gamma}(t) - \dot{\phi}(t)$, denoted $v_k(t)$, which represents the discriminator output, has a large negative-going spike near $B_{if}t = 0$, and another of lower magnitude but broader in time near $B_{if}t = 2$. Also shown for reference are the normalized IF impulse response envelope $h_1(t)$ and its time derivative. In contrast, Figure 3-8 shows the discriminator output for the same set of parameters, except that the desired signal is not modulated. In this case, the excess phase returns to zero, and the two spikes in the discriminator output are of opposite polarities.

The frequency spectra magnitudes (determined using the FFT) for the modulated and unmodulated cases are shown in Figure 3-9. What is shown on the ordinate is $V(f)/B_{if}$, which is the Fourier transform of the discriminator output interference $\dot{\gamma}(t) - \dot{\phi}(t)$.

Therefore, $\left|V(0)/B_{if}\right| = \left|\int_0^\infty [\dot{\gamma}(t) - \dot{\phi}(t)]dt\right| = 2\pi$ for the modulated case as discussed above, which agrees with the FFT results. Also, $V(0) = 0$ for the unmodulated case, as also predicted in the above discussion.

The important quantity is the interference energy at the baseband filter output per UWB pulse, which is obtained by integrating the energy spectrum of the discriminator output interference across the baseband bandwidth. The energy spectrum is shown in Figure 3-10, and the vertical line represents the baseband bandwidth, assumed to be 3 kHz. The energy within this bandwidth is more than 10 dB higher for the modulated case than the unmodulated case.

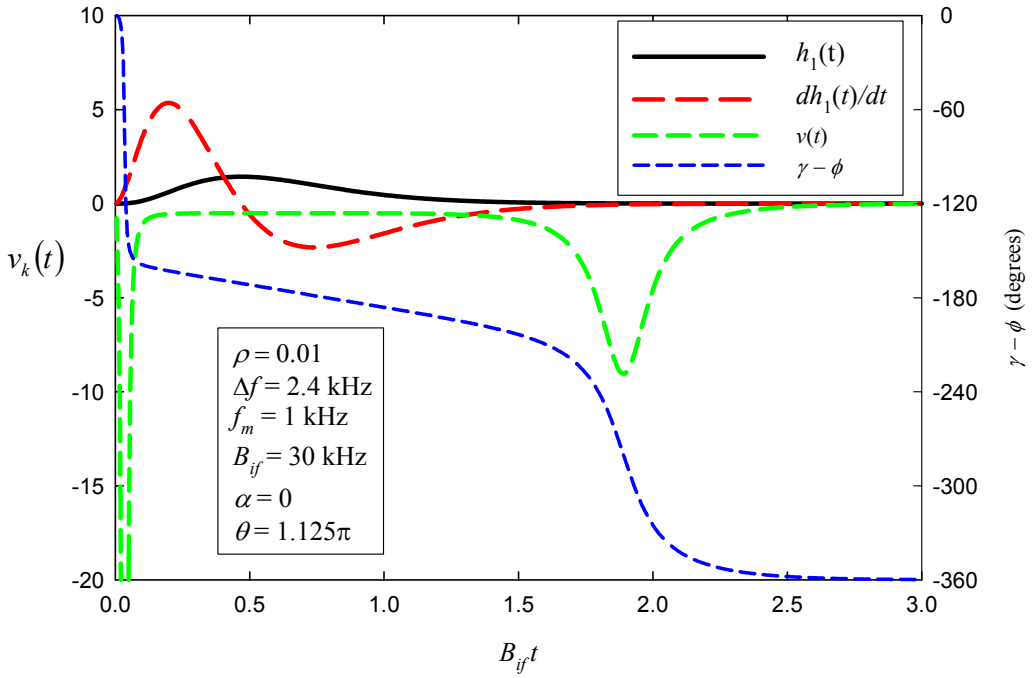

Figure 3-7: *Example of normalized discriminator output and excess phase with modulation*

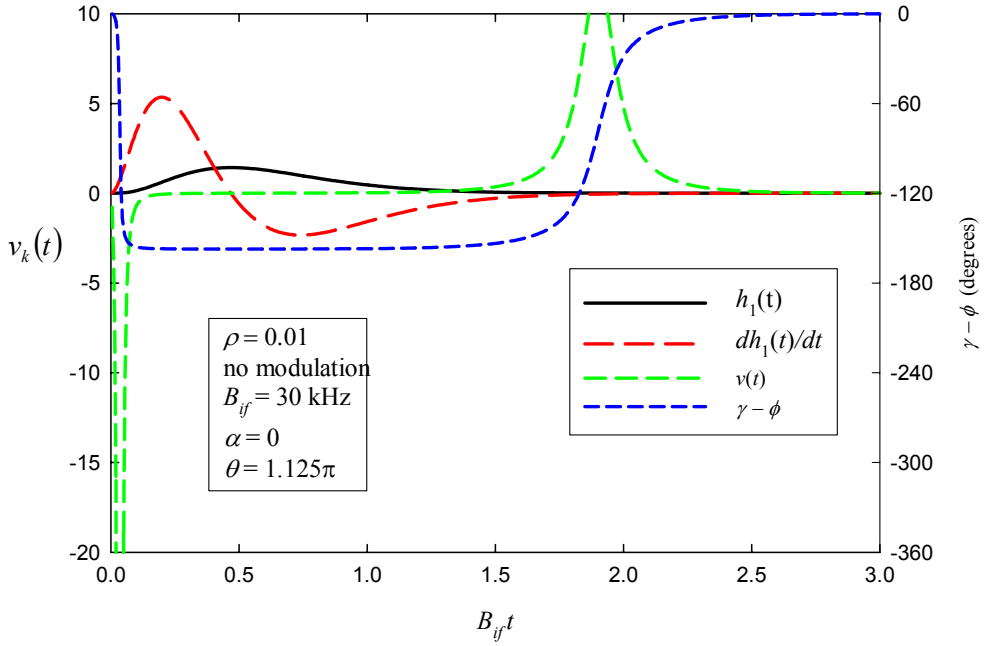

Figure 3-8: *Same parameters as Figure 3-7, except no modulation of desired signal*

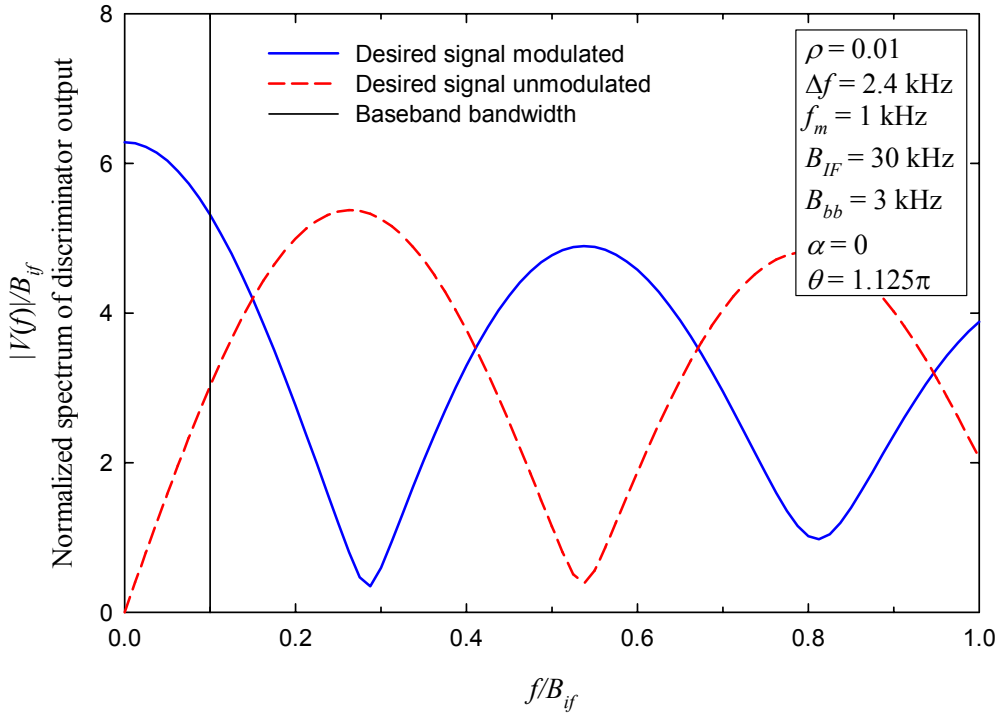

Figure 3-9: *Fourier transform of discriminator output, for modulated and unmodulated cases shown in Figure 3-7 and Figure 3-8*

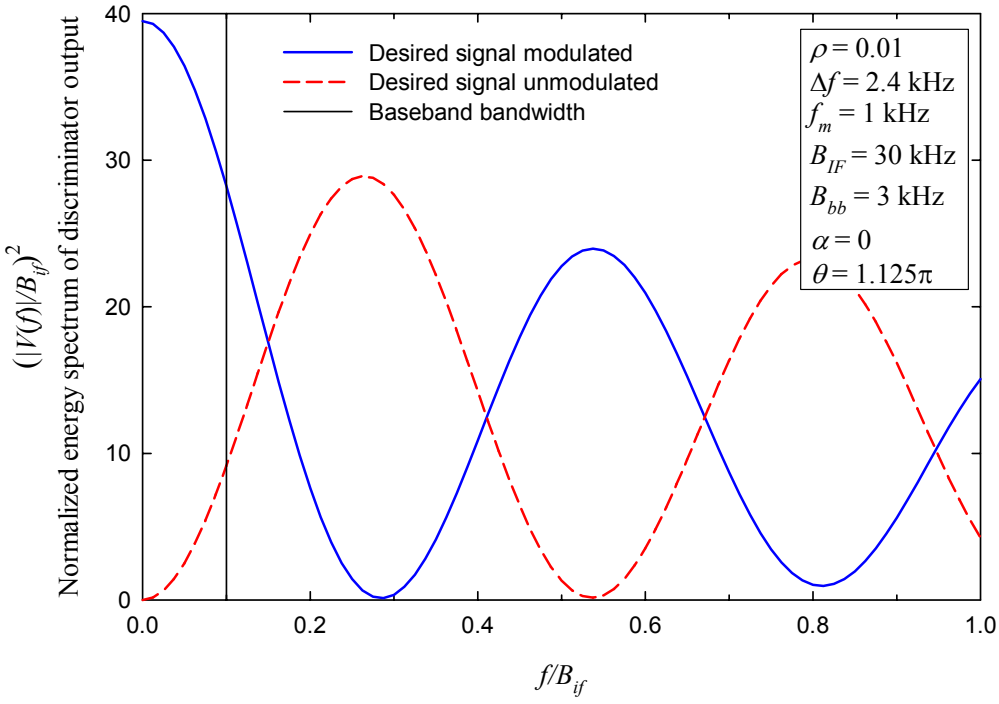

Figure 3-10: *Energy spectrum of discriminator output for modulated and unmodulated cases*

To better understand the conditions required for a non-zero DC value of the discriminator output interference, it is useful to redraw the phasor diagram so that the reference is always the desired signal. The phase change of the desired signal due to frequency modulation is then represented as a rotation of the interference phasor, with magnitude $h_1(t)$, with respect to the desired signal, as shown in Figure 3-11. The rotation direction of the interference phasor in this frame of reference is equal and opposite to the actual phase change due to the modulation. This is illustrated by showing the rotation of the interference phasor as clockwise with a rate of $d\phi/dt$; that is, if $d\phi/dt > 0$, then the interference phasor rotation is clockwise (negative angular change).

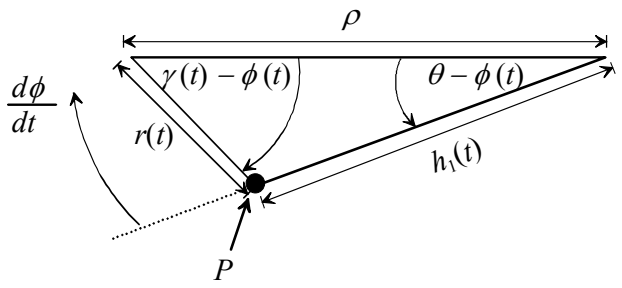

Figure 3-11: *Reference geometry for signal and interference phasors*

In this frame of reference, the excess phase changes by $\pm 2\pi$ and the discriminator output has a non-zero DC value, if the path of the point *P* encircles the origin. An example sequence of phasor snapshots for which this is the case is shown in Figure 3-12. Necessary (but not sufficient) conditions for this to occur are:

- The desired signal is frequency modulated
- ρ is less than the maximum value of $h_1(t)$.

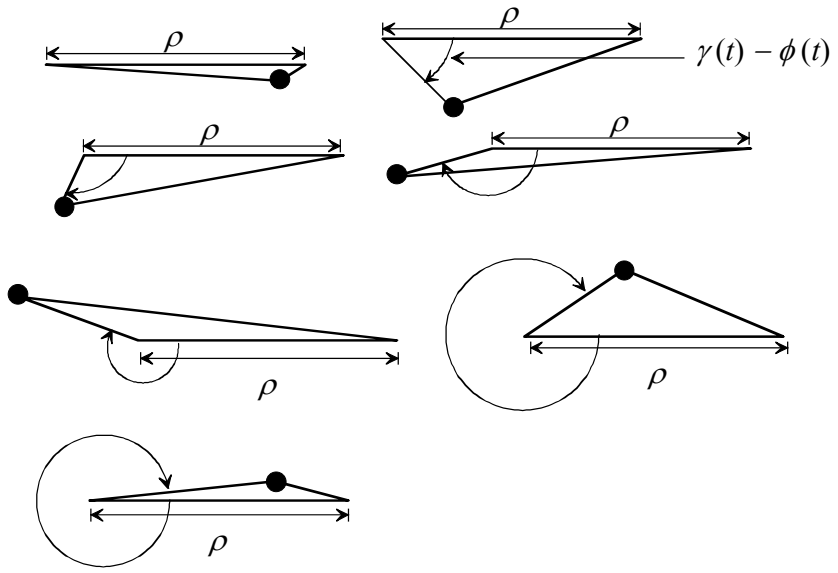

Figure 3-12: *Illustrative example of excess phase trajectory that gives a net non-zero value*

Clearly, if $\rho > h_1(t)_{\max}$, then $|\gamma - \phi|$ can never exceed $\pi/2$ and the composite signal phasor cannot encircle the origin. An example is illustrated in Figure 3-13, and the discriminator output and excess phase for a case roughly corresponding to Figure 3-13 are shown in Figure 3-14.

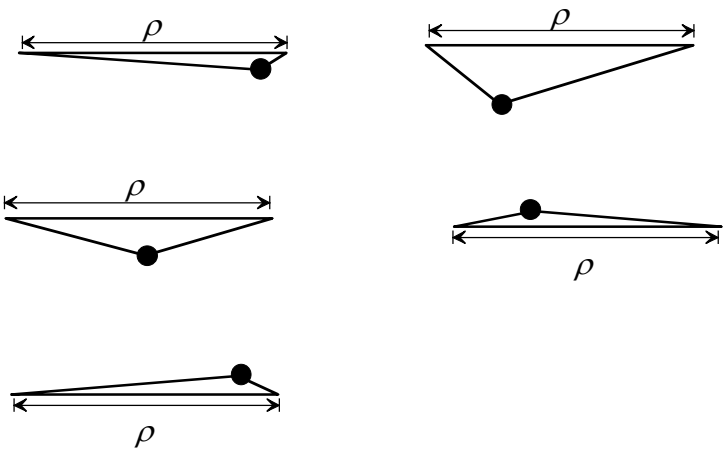

Figure 3-13: *Illustrative example of excess phase trajectory that gives a net zero value*

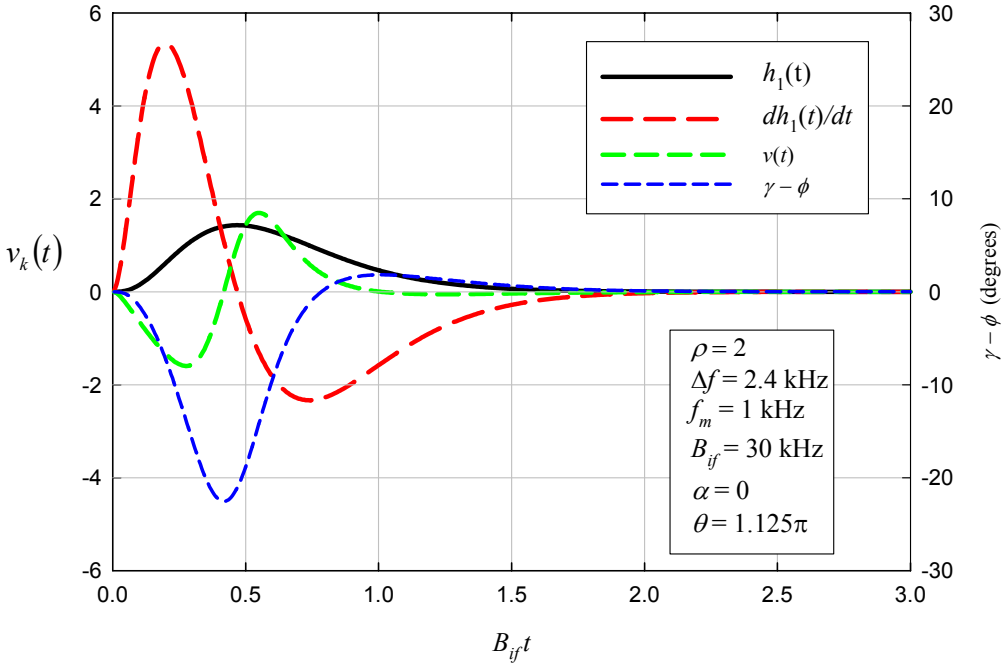

Figure 3-14: *Discriminator output and excess phase for a case roughly corresponding to the phasor diagrams of Figure 3-13*

If the desired signal is modulated and $\rho < h_1(t)_{\max}$, then whether the origin is encircled will depend on ρ, θ, and α, which is the phase of the modulation tone at the time the pulse arrives. The fundamental requirement is that $\theta - \phi(t)$ experience a net rotation in either direction through π radians while $h_1(t) > \rho$.

Let t_1 and t_2 represent the two times for which $h_1(t) = \rho$, so $\Delta t = t_2 - t_1$ is the time interval over which $h_1(t) > \rho$. The phase change of the desired signal during that time is $\Delta\phi \equiv \phi(t_2) - \phi(t_1)$. The conditions for non-zero net excess phase can be easily understood with the help of Figure 3-15. Figure 3-15(a) shows the case in which $\Delta\phi > 0$. The condition that must be satisfied in that case is:

$$\Delta\phi > [\theta - \phi(t_1)] - \pi > 0 \tag{3-16}$$

In the case of Figure 3-15(b), $\Delta\phi < 0$ and the required condition is

$$-\Delta\phi > \pi - [\theta - \phi(t_1)] > 0 \tag{3-17}$$

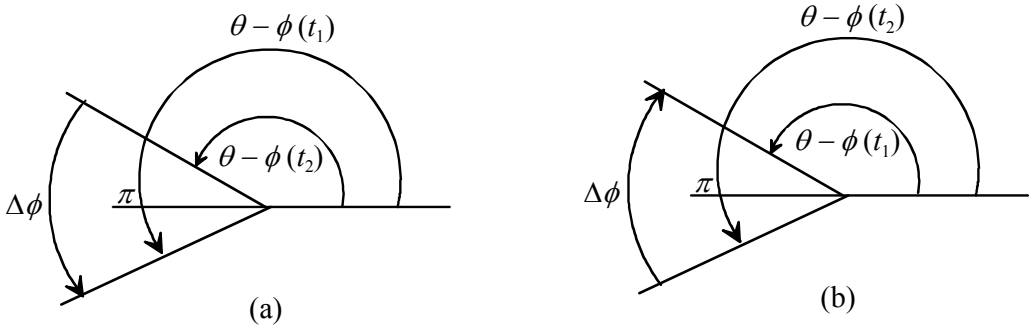

Figure 3-15: *Geometry for the two basic cases leading to non-zero excess phase*

Recalling that $\phi(t) = \beta \sin(2\pi f_m t + \alpha)$ where β is the modulation index, f_m is the modulating frequency, and α is an arbitrary phase, the normalized baseband energy $\Lambda(\rho, \alpha, \theta)$ per UWB pulse for a given value of ρ can be shown as a function of θ for various values of α as shown in Figure 3-16. As indicated, these were computed using the FFT. The rectangular portions of the curves with high magnitude occur for the range of θ which, for a given α, a net excess phase of 2π occurs. Since for $\rho << 1$, $t_1 \cong 0$, $\phi(t_1) \cong \beta \sin(\alpha)$, and it is useful to show $\Lambda(\rho, \alpha, \theta)$ as a function of $\theta - \beta \sin\alpha$ as in Figure 3-17.

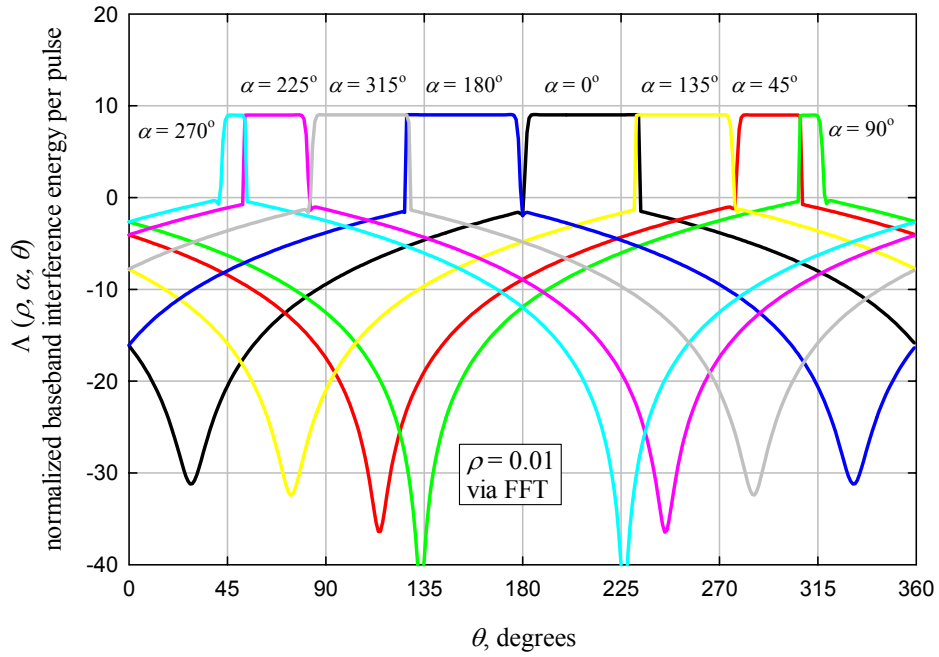

Figure 3-16: *Normalized baseband interference energy per UWB pulse vs. θ and α*

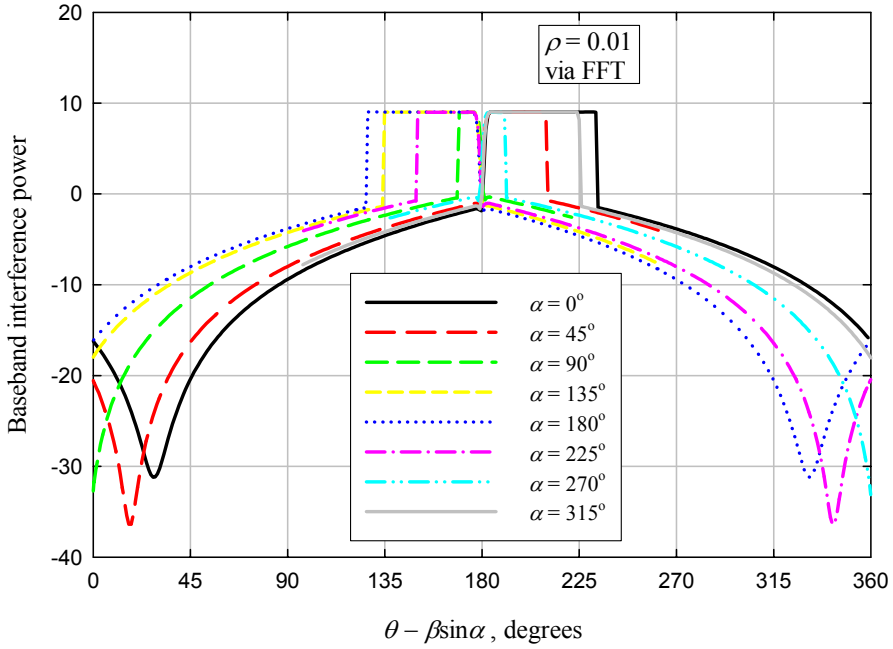

Figure 3-17: *Same as Figure 3-16, except abscissa is $\theta - \beta \sin\alpha$*

3.4. Approximate Solution using Numerical Integration

The next step is to sanity-check the numerical results by computing $\Lambda(\rho,\alpha,\theta)$ using a different approach that does not rely on the FFT. This will also pave the way for a simple closed form expression.

Since $V(f)$ is important only for low values of f (due to the baseband filter) and the values of t for which $h_1(t)$ is significant are less than about 2.5, the Fourier transform kernel can be approximated using the first few terms of its series expansion:

$$e^{-j2\pi ft} \cong 1 - j2\pi ft - 2(\pi ft)^2, \quad ft << 1 \tag{3-18}$$

Hence,

$$V(f) \cong \int_0^\infty v(t)\left[1 - j2\pi ft - 2(\pi ft)^2\right]dt \qquad f << 1 \tag{3-19}$$

The approximation is valid for $f << 1$ because duration of $v(t)$ is limited to roughly $t < 2$.

Letting

$$y_0 = \int_0^\infty v(t)dt \qquad y_1 = \int_0^\infty tv(t)dt \qquad y_2 = \int_0^\infty t^2 v(t)dt \tag{3-20}$$

gives

$$\begin{aligned} |V(f)|^2 &\cong \left[y_0 - 2(\pi f)^2 y_2\right]^2 + (2\pi f y_1)^2 \\ &= y_0^2 - 4(\pi f)^2 y_0 y_2 + 4(\pi f)^4 y_2^2 + 4(\pi f)^2 y_1^2 \end{aligned} \tag{3-21}$$

The interference energy per pulse within the baseband bandwidth is

$$\begin{aligned} \Lambda(\rho,\alpha,\theta) &= \int_{-B_b/B_{if}}^{B_b/B_{if}} |V(f)|^2 df \\ &\cong 2y_0^2 \frac{B_b}{B_{if}} + \frac{8}{3}\pi^2 \left(\frac{B_b}{B_{if}}\right)^3 \left(y_1^2 - y_0 y_2\right) + \frac{8}{5}\pi^4 \left(\frac{B_b}{B_{if}}\right)^5 y_2^2 \end{aligned} \tag{3-22}$$

Figure 3-18 shows the result, which agrees closely with the results obtained using the FFT shown in Figure 3-16.

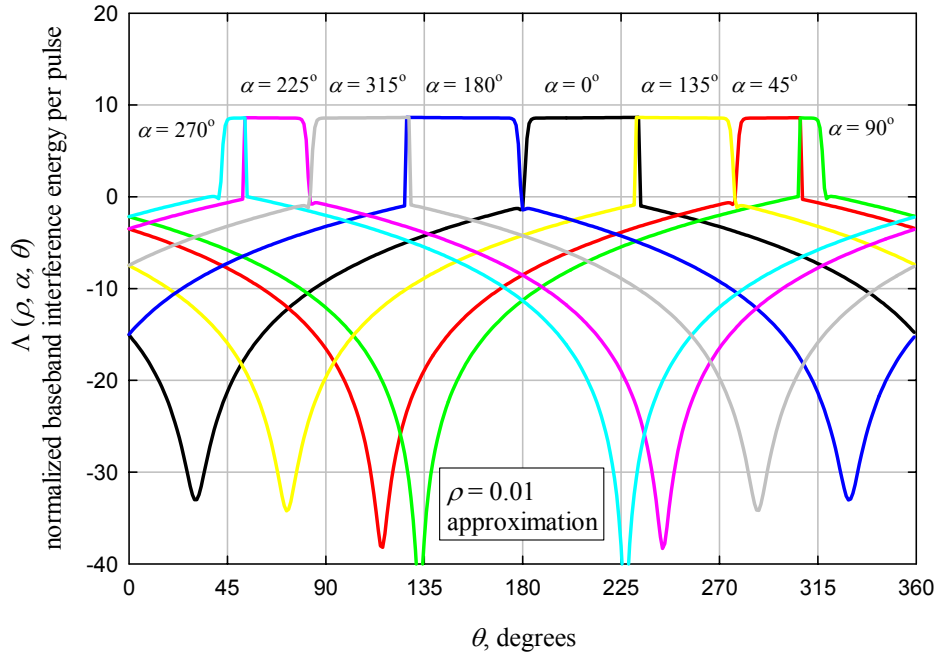

Figure 3-18: *Normalized baseband interference energy per UWB pulse vs. θ and α using the 3-term approximation with numerical integration*

To understand the effects of individual terms, it is useful to define:

$$\begin{aligned}
\Lambda_0(\rho,\alpha,\theta) &\cong 2y_0^2\frac{B_b}{B_{if}} \\
\Lambda_1(\rho,\alpha,\theta) &\cong \frac{8}{3}\pi^2\left(\frac{B_b}{B_{if}}\right)^3 y_1^2 \\
\Lambda_2(\rho,\alpha,\theta) &\cong \frac{8}{5}\pi^4\left(\frac{B_b}{B_{if}}\right)^5 y_2^2 \\
\Lambda_{02}(\rho,\alpha,\theta) &\cong \frac{8}{3}\pi^2\left(\frac{B_b}{B_{if}}\right)^3 y_0 y_2
\end{aligned} \qquad (3\text{-}23)$$

and $\Lambda = \Lambda_0 + \Lambda_1 + \Lambda_2 - \Lambda_{02}$.

Figure 3-19 shows $\Lambda_0 + \Lambda_1$, and as can be seen, the result differs little from Figure 3-18 except that the minima are deeper. Thus, neglecting the y_2 term should have little effect

overall on $\Lambda(\rho)$. Figure 3-20 shows Λ_0, which as would be expected, is non-zero only over a restricted range of θ. When it is non-zero, the above discussion shows that $y_0 = 2\pi$. Since it is assumed here that $B_b/B_{if} = 0.1$, $\Lambda_0 = 0.2 \cdot (2\pi)^2 = 7.9$, or about 9 dB, which agrees with the numerical results shown in Figure 3-20. Figure 3-21 and Figure 3-22 show the first- and second-order terms Λ_1 and Λ_2, respectively, and Figure 3-23 shows the cross term Λ_{02}.

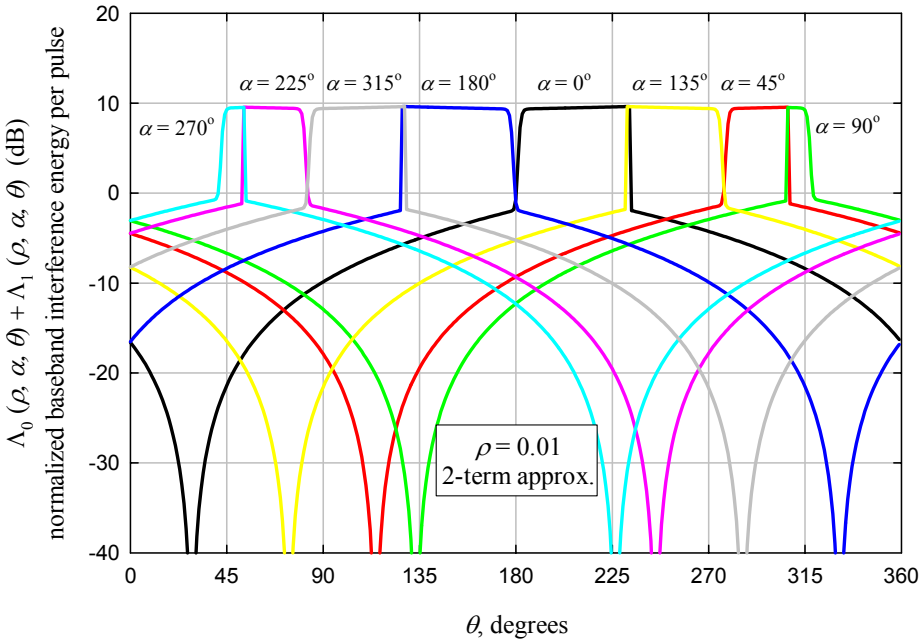

Figure 3-19: *Normalized baseband interference energy per UWB pulse vs. θ and α using the 2-term approximation with numerical integration*

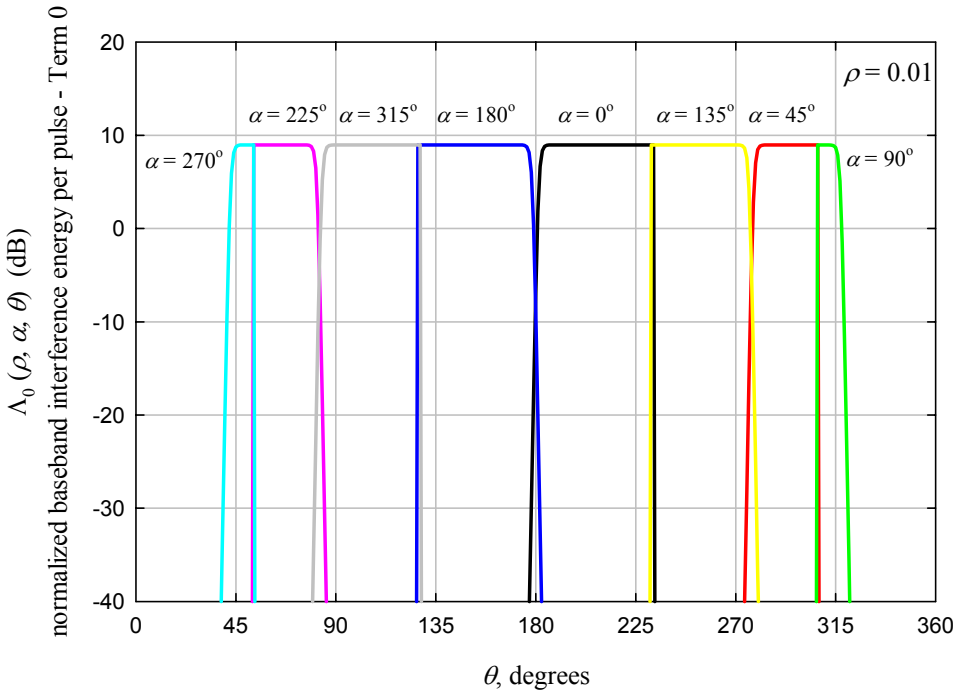

Figure 3-20: *The DC term, from numerical integration*

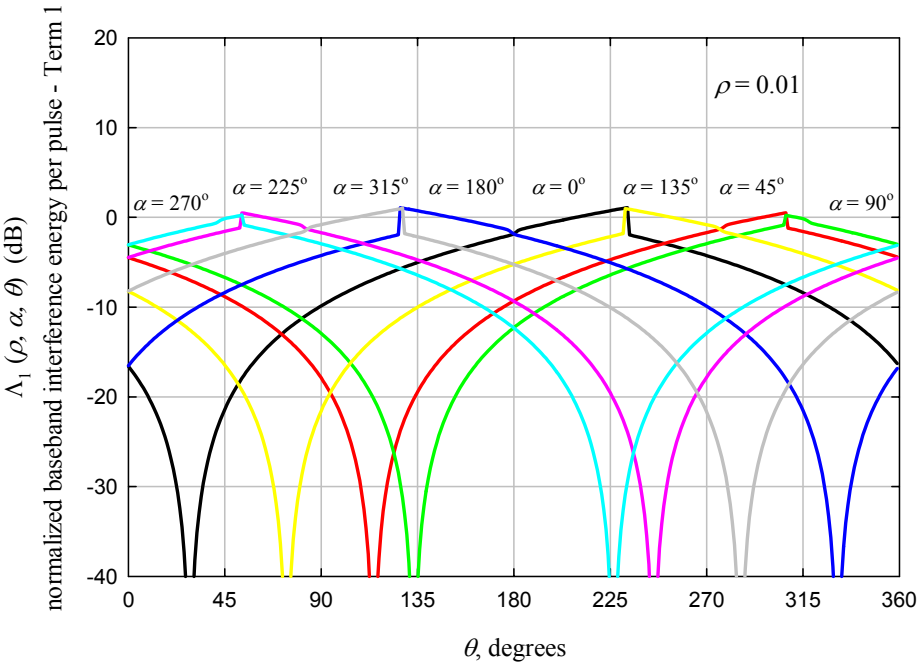

Figure 3-21: *The first-order term* Λ_1 *in the numerical-integration approximation*

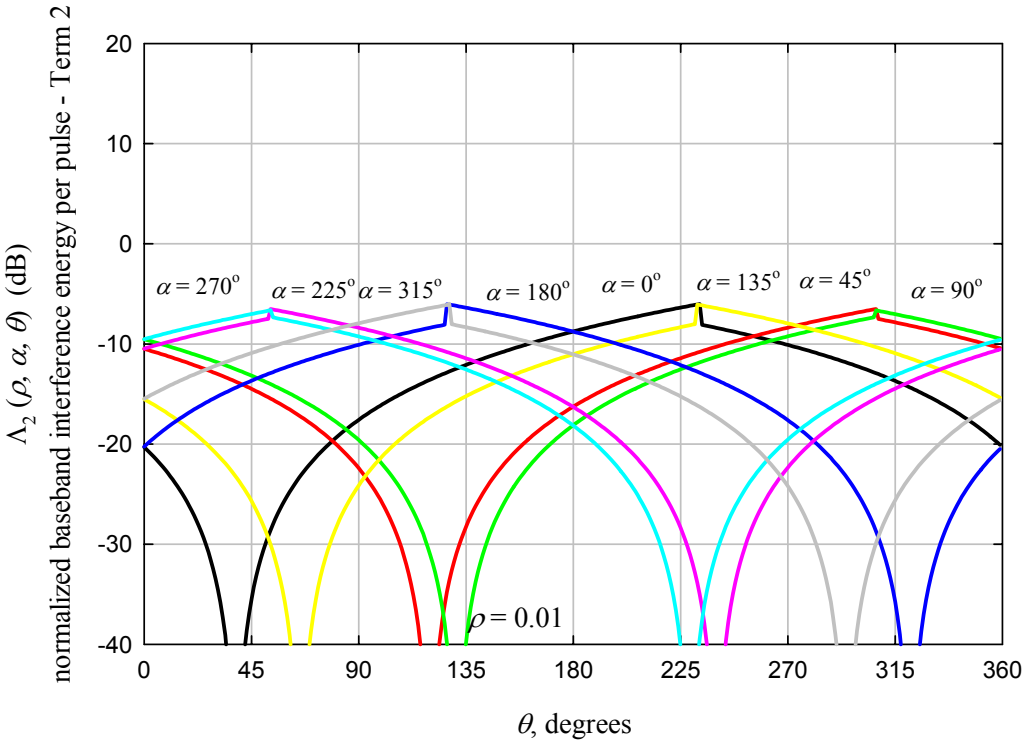

Figure 3-22: *The second-order term Λ_2 in the numerical-integration approximation*

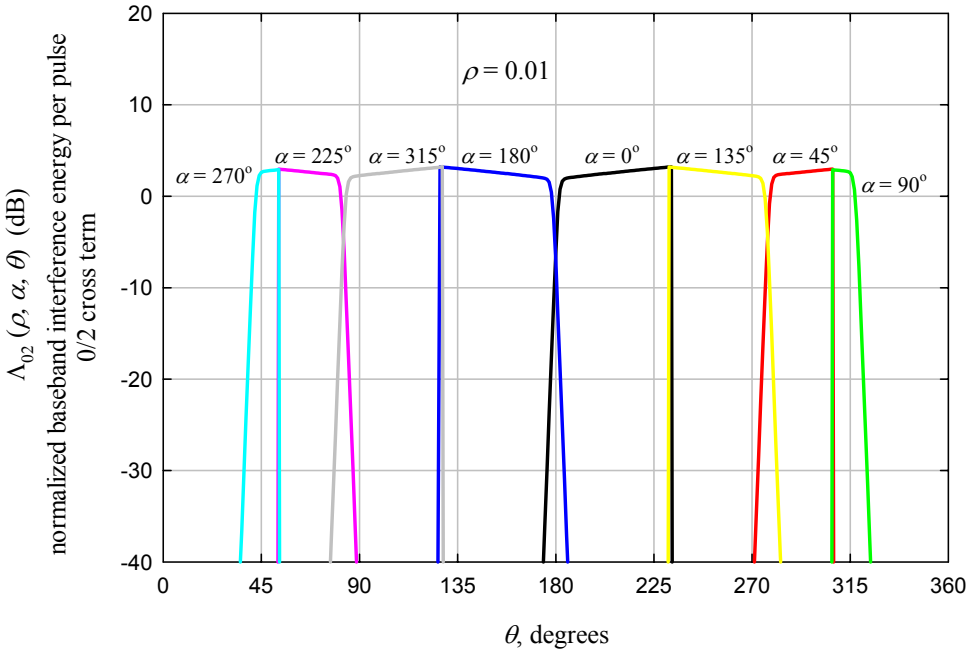

Figure 3-23: *The 0/2 cross term Λ_{02} in the numerical-integration approximation*

It is evident that for combinations of α and θ for which $\Lambda_0 \neq 0$, the baseband interference energy is dominated by the DC term Λ_0. This suggests the approximation:

$$\Lambda(\rho,\alpha,\theta) \cong \begin{cases} \Lambda_0 & \text{when } \Lambda_0 \neq 0 \\ \Lambda_1 & \text{when } \Lambda_0 = 0 \end{cases} \tag{3-24}$$

This "two-term" approximation is shown in Figure 3-24 on a decibel scale and Figure 3-25 on a linear scale. From Figure 3-25 it is apparent that the dominant contributor to the average energy for is the DC term Λ_0, and that the contribution of the first-order term is relatively small, which suggests that the average (over α and θ) normalized interference energy per pulse can be approximated as:

$$\Lambda(\rho) \cong 2\frac{B_b}{B_{if}}(2\pi)^2 P_{XO}(\rho) \qquad \rho < h_1(t)_{\max} \tag{3-25}$$

where $P_{XO}(\rho)$ is the overall average (taken over α and θ) probability or fraction of the time that a "crossover" occurs; that is, either (3-16) or (3-17) is satisfied and the net excess phase is 2π. The restriction on ρ is necessary because no crossover can occur if $\rho \geq h_1(t)_{\max}$. To use this approximation, an expression is needed for $P_{XO}(\rho)$, which is developed in the next section.

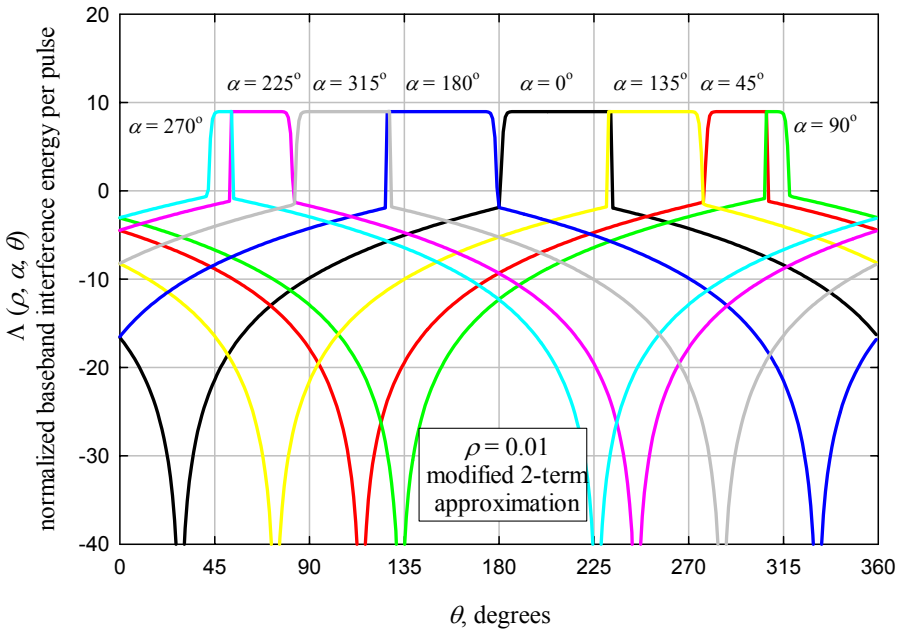

Figure 3-24: Simple 2-term approximation for $\Lambda(\rho,\alpha,\theta)$, dB scale

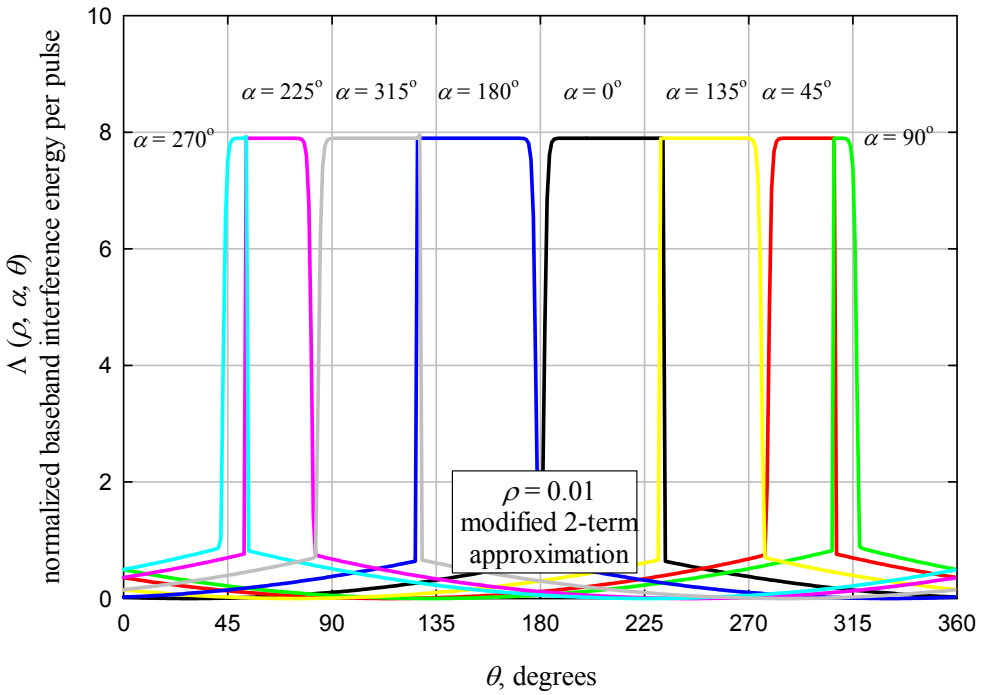

Figure 3-25: Simple 2-term approximation for $\Lambda(\rho,\alpha,\theta)$, linear energy scale

3.5. Crossover Probability and Closed-Form Approximation

The overall curve of $\Lambda(\rho)$ vs. ρ is obtained from averaging $\Lambda(\rho,\alpha,\theta)$ over all θ and α. In the curve shown in Figure 3-2, this was done numerically. Since the goals here are to understand the mechanism leading to the curve of Figure 3-2 and to develop an approximate closed-form expression for that curve, it is desirable to perform that averaging analytically.

Assuming the angle $\theta - \phi(t_1) - \pi$ is uniformly-distributed between 0 and 2π, then the probability of a crossover (the excess phase crosses π in either direction, giving a net excess phase of 2π) is

$$P_{XO} \mid \Delta\phi = \frac{|\Delta\phi|}{2\pi} \tag{3-26}$$

with

$$\Delta\phi(t_2,t_1) = \beta[\sin(\delta+\alpha_1) - \sin\alpha_1] \tag{3-27}$$

where $\delta = 2\pi\left(f_m / B_{if}\right)\Delta t$ is the phase change in the modulating signal during the interval Δt, and α_1 is the phase of the modulating signal at time t_1. Using the appropriate trigonometric identity gives

$$\Delta\phi = 2\beta \sin\frac{\delta}{2}\cos\left(\alpha_1 + \frac{\delta}{2}\right) \tag{3-28}$$

Averaging over a single positive cycle of $\cos x$ gives $\frac{1}{\pi}\int_{-\pi/2}^{\pi/2}\cos x dx = 2/\pi$, so

$$\left\langle\left|\Delta\phi\right|\right\rangle = \frac{4\beta}{\pi}\left|\sin\frac{\delta}{2}\right| \tag{3-29}$$

Therefore, the unconditional crossover probability is

$$P_{XO} = \frac{2\beta}{\pi^2}\left|\sin\frac{\delta}{2}\right| \qquad \beta < 2\pi \tag{3-30}$$

The restriction on β ensures that there is at most a single crossover ($\Delta\phi < 2\pi$). Clearly, the maximum value of $\Delta\phi$ is 2β. Figure 3-26 shows P_{XO} vs. δ, and Figure 3-27 shows P_{XO} vs. Δt. For Δt in the range of interest here (less than about 2.5), $\sin\left(\delta/2\right) \cong \delta/2$ and

$$P_{XO} \cong \frac{2\beta}{\pi}\frac{f_m}{B_{if}}\Delta t \tag{3-31}$$

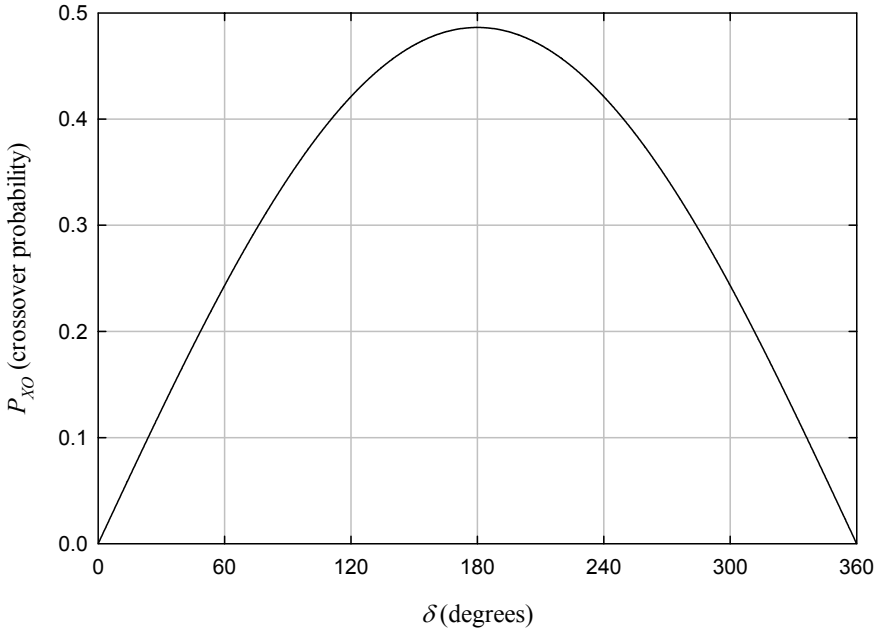

Figure 3-26: *Crossover probability vs. the phase-change angle* δ.

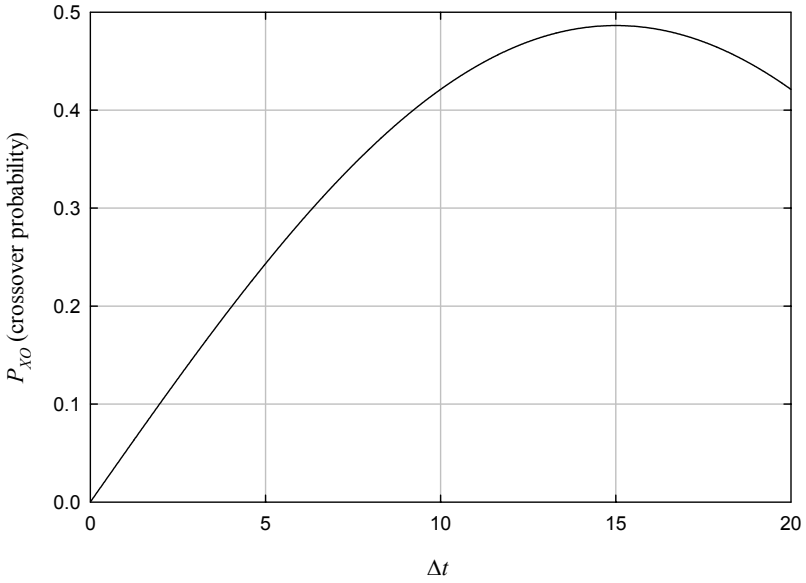

Figure 3-27: *Crossover probability vs.* Δt

To complete the analysis, an expression is needed to relate Δt to ρ. For the 4-pole IF filter used in the examples here,

$$h_1(t) = At^3 e^{-xt} \tag{3-32}$$

where $x = 32/5 = 6.4$ and $A = x^4/3! = 279.6$. Of interest are the two times at which $h_1(t) = \rho$, and the time Δt between them. Figure 3-28 shows $\log_{10} h_1(t)$ vs. *t*, and Δt for $\rho = 0.1$. Figure 3-29 shows Δt vs. ρ and the approximation (determined by regression):

$$\Delta t \cong \begin{cases} 1 - \dfrac{0.51 + \log \rho}{1.7} & \log \rho < -0.51 \\ \sqrt{\dfrac{0.16 - \log \rho}{0.67}} & -0.51 \le \log \rho < 0.16 \\ 0 & \log \rho \ge 0.16 \end{cases} \tag{3-33}$$

Figure 3-30 shows P_{XO} vs. ρ using the approximation for Δt, and Figure 3-31 shows $(2\pi)^2 (B_b / B_{if}) P_{XO}(\rho)$, which is the approximation to $\Lambda(\rho)$ for $\rho < h_1(t)_{\max}$.

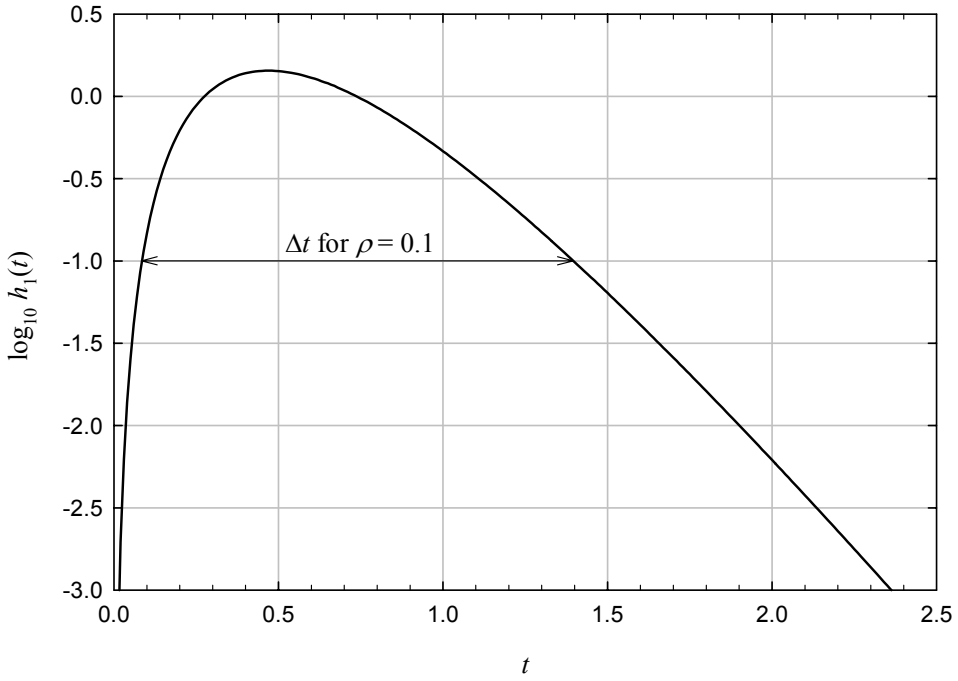

Figure 3-28: $\log_{10} h_1(t)$ *for the 4-pole filter*

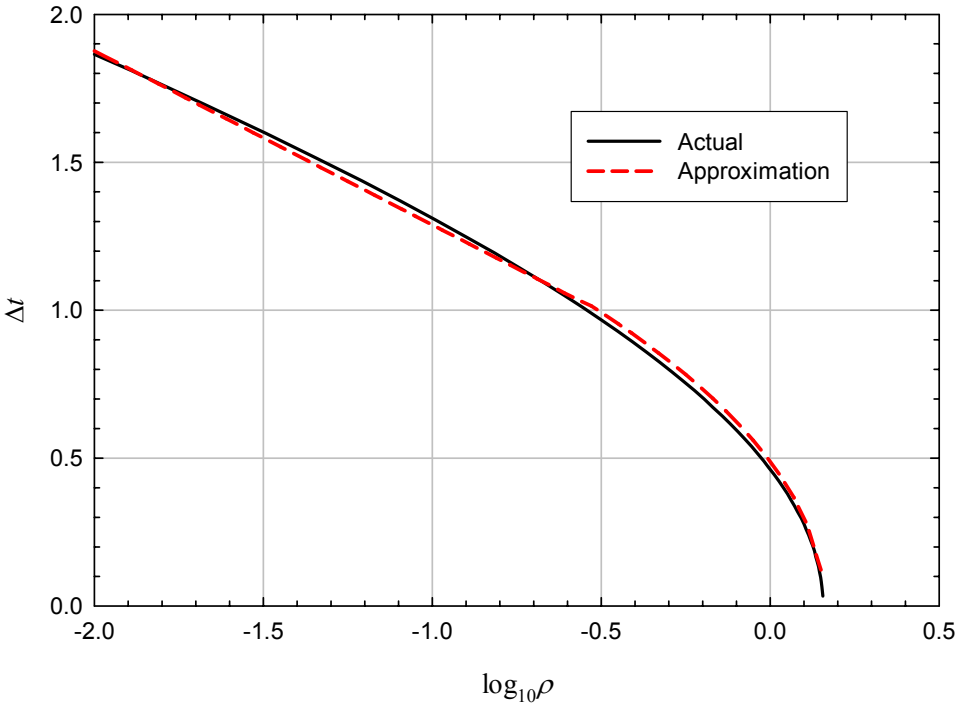

Figure 3-29: *Δt vs. ρ and the approximation*

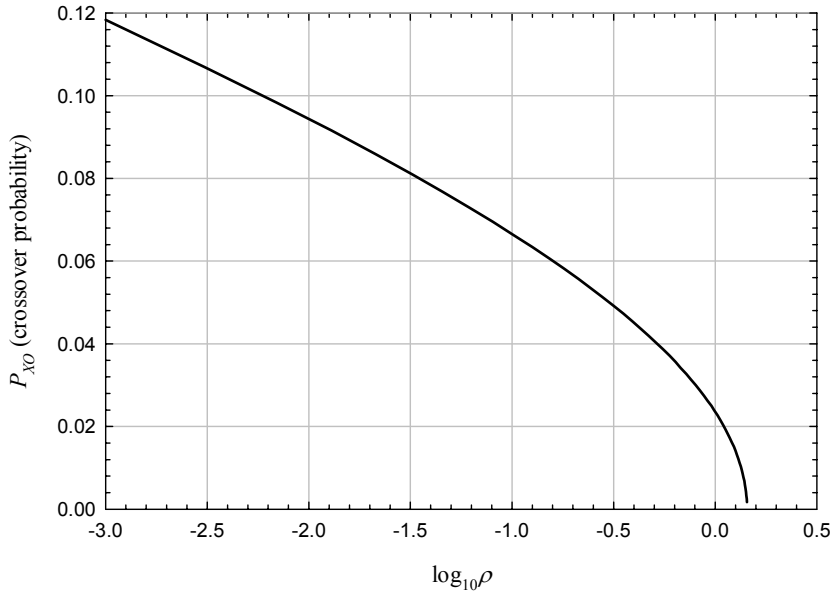

Figure 3-30: *Crossover probability vs. ρ using the approximation for Δt vs. ρ*

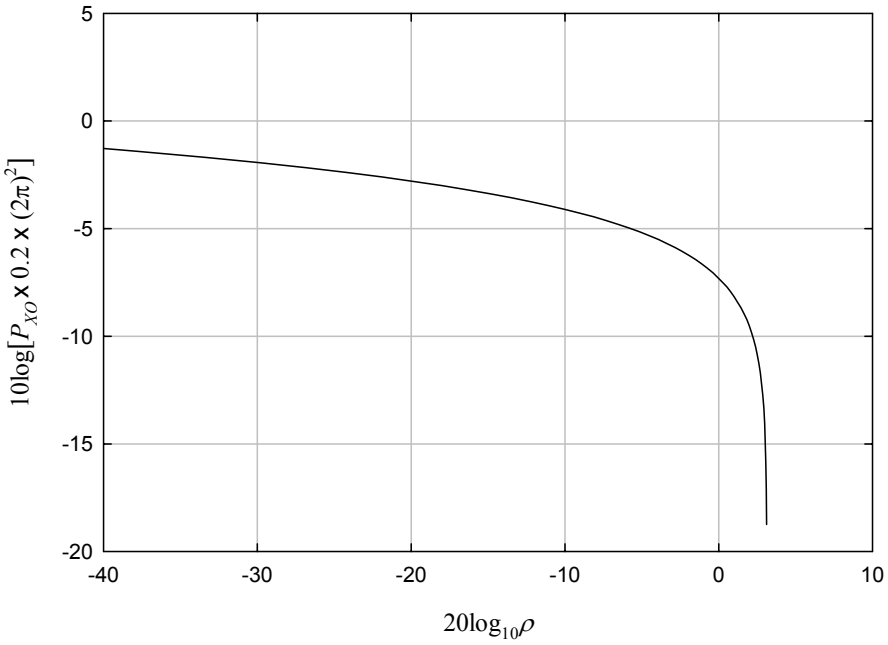

Figure 3-31: $(2\pi)^2(B_b/B_{if})P_{XO}(\rho)$*, the approximation to* $\Lambda(\rho)$ *for* $\rho < h_1(t)_{\max}$.

Figure 3-32 shows the approximation $\Lambda(\rho)$ for $\rho < h_1(t)_{\max}$ compared to the numerical results of Figure 3-2. As can be seen, the agreement is excellent. The high-ρ approximation is $\Lambda(\rho) \cong \frac{4}{3}\pi^2\left(\frac{B_b}{B_{if}}\right)^3 \cdot \frac{1}{\rho^2}$, $\rho >> 1$.

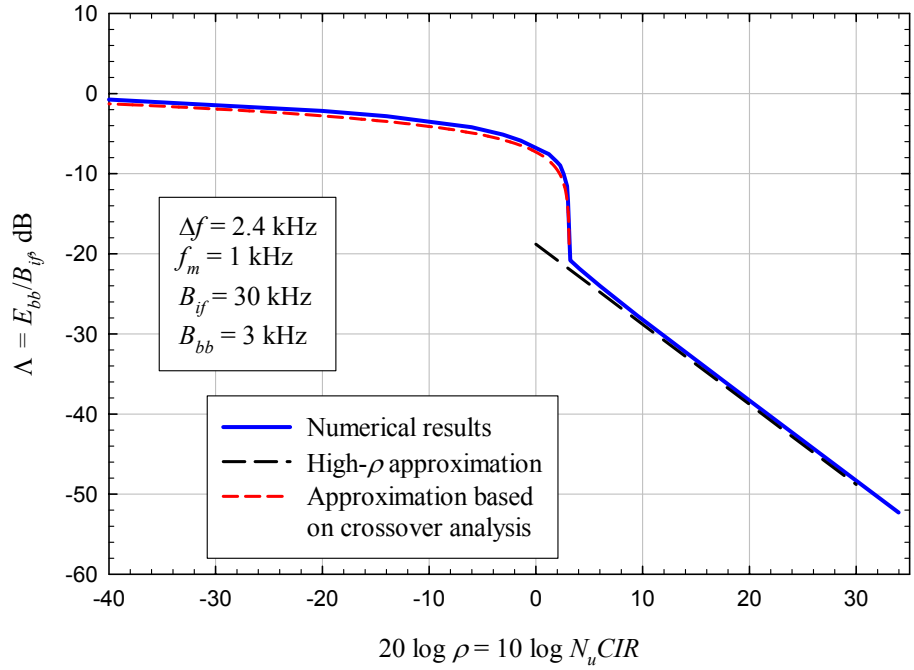

Figure 3-32: *The approximation to* $\Lambda(\rho)$ *for* $\rho < h_1(t)_{\max}$ *compared to the FFT-based results*

All that is left is to check the 3-term approximation against the numerical results for $\rho \geq h_1(t)_{\max}$, in which case $\Lambda_0 = 0$, so $\Lambda \cong \Lambda_1 + \Lambda_2$.

The high-ρ approximation is based on $\rho >> 1$ and ignoring the modulation of the desired signal, giving the normalized discriminator output and its transform as:

$$v(t) \cong \frac{\dot{h}_1(t)\sin(\theta - \beta\sin\alpha)}{\rho} \qquad V(f) \cong j2\pi f H_1(f)\frac{\sin(\theta - \beta\sin\alpha)}{\rho} \tag{3-34}$$

Since $\frac{d}{df}V(f) = -j2\pi\int_0^\infty t v(t) e^{-j2\pi ft}dt$, the y_1 term is

$$\begin{aligned} y_1 &= \int_0^\infty t v(t)dt = -\frac{1}{j2\pi}\left[\frac{d}{df}V(f)\right]_{f=0} \\ &\cong -H_1(0)\frac{\sin(\theta - \beta\sin\alpha)}{\rho} = -\frac{\sin(\theta - \beta\sin\alpha)}{\rho} \end{aligned} \tag{3-35}$$

Figure 3-33, Figure 3-34, and Figure 3-35 show y_1 (computed with numerical integration) and this approximation for $\rho = 1.5$, 2, and 4, respectively.

With the approximation,

$$\Lambda_1(\rho,\alpha,\theta) \cong \frac{8}{3}\pi^2\left(\frac{B_b}{B_{if}}\right)^3 \frac{\sin^2(\theta-\beta\sin\alpha)}{\rho^2} \tag{3-36}$$

Figure 3-36 shown Λ_1 and this approximation for $\rho = 1.5$, and Figure 3-37 shows the second order term Λ_2. Since Λ_2 is more than 10 dB below Λ_1, it can be ignored.

Finally, averaging over θ and α, which are assumed to be independent and each uniform on $(0,2\pi)$, gives:

$$\Lambda_1(\rho) = \langle \Lambda_1(\rho,\alpha,\theta) \rangle_{\alpha,\theta} \cong \frac{4}{3}\pi^2\left(\frac{B_b}{B_{if}}\right)^3 \cdot \frac{1}{\rho^2} \tag{3-37}$$

which is exactly the same as the high-ρ approximation in Figure 3-32. Figure 3-38 compares the high-ρ approximation to the numerical integration result for Λ_1 and for $\Lambda_1 + \Lambda_2$, as well as the numerical FFT results. As can be seen, the high-ρ approximation agrees closely with Λ_1 and is about 0.5 dB below $\Lambda_1 + \Lambda_2$, which in turn agrees closely with the FFT results.

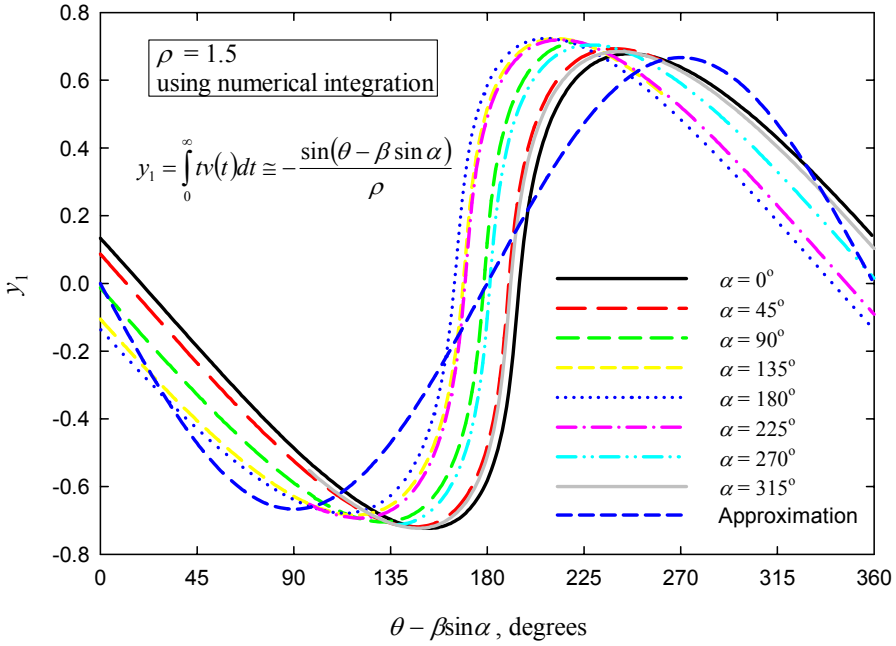

Figure 3-33: *y_1 and the high-ρ approximation for $\rho = 1.5$*

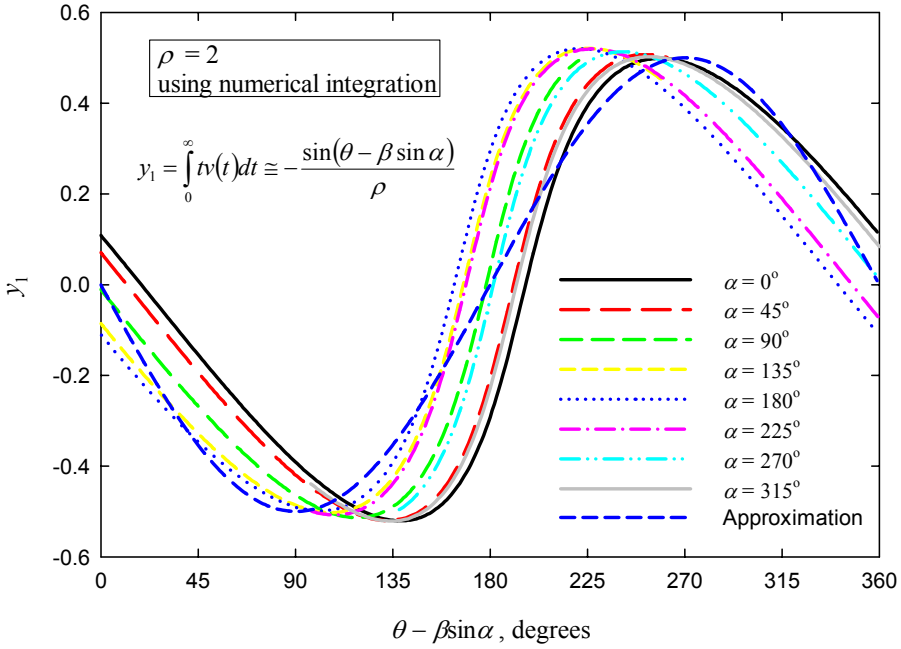

Figure 3-34: *y_1 and the high-ρ approximation for $\rho = 2$*

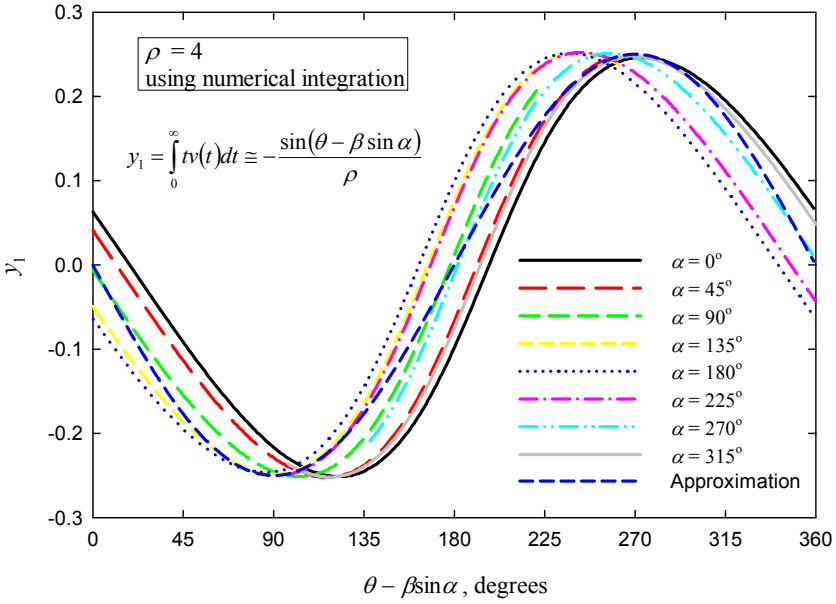

Figure 3-35: *y_1 and the high-ρ approximation for $\rho = 4$*

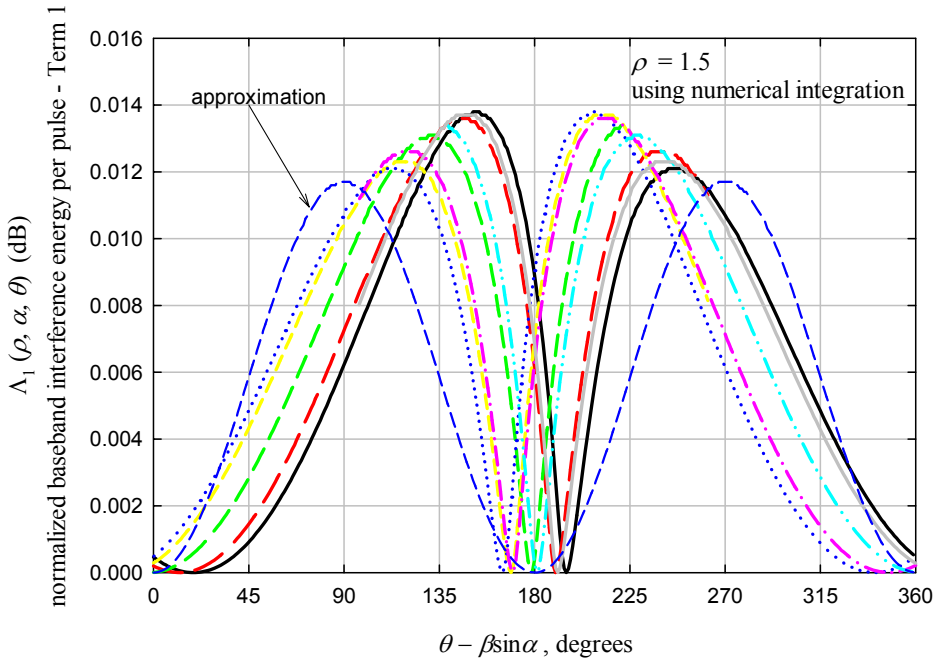

Figure 3-36: *The first-order numerical integration term Λ_1 for $\rho = 1.5$ (linear scale)*

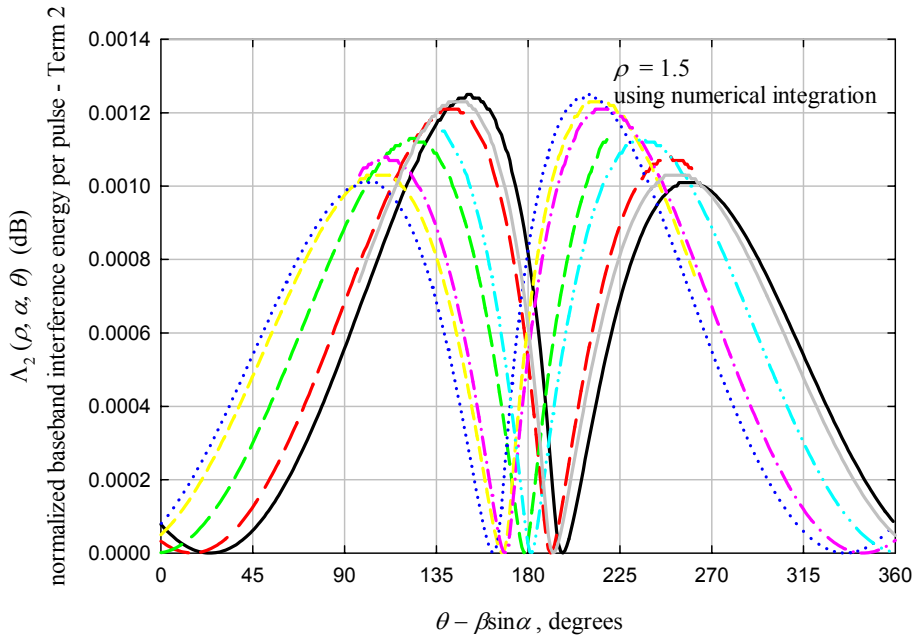

Figure 3-37: *The second-order numerical integration term Λ_2 for $\rho = 1.5$ (linear scale)*

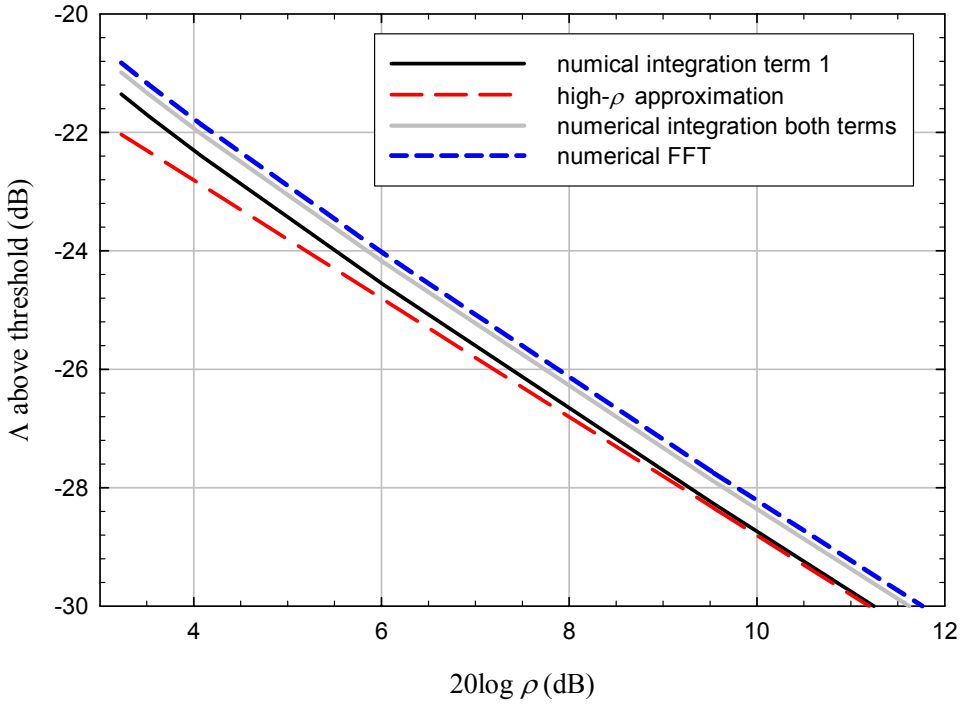

Figure 3-38: *Comparison of the high-ρ approximation and Λ_1 from numerical integration*

The overall closed-form approximation for $\Lambda(\rho)$ can be expressed as

$$\Lambda(\rho) \cong \begin{cases} \dfrac{16\pi\beta\, f_m B_b}{B_{if}^2}\,\Delta t(\rho) & \rho < h_1(t)_{\max} \\ \dfrac{4\pi^2}{3}\left(\dfrac{B_b}{B_{if}}\right)^3 \cdot \dfrac{1}{\rho^2} & \rho \geq h_1(t)_{\max} \end{cases} \tag{3-38}$$

For the particular IF output pulse studied here, Δt is related to ρ approximately by:

$$\Delta t \cong \begin{cases} 1 - \dfrac{0.51 + \log\rho}{1.7} & \log\rho < -0.51 \\ \sqrt{\dfrac{0.16 - \log\rho}{0.67}} & -0.51 \leq \log\rho < 0.16 \\ 0 & \log\rho \geq 0.16 \end{cases} \tag{3-39}$$

$$\Lambda(\rho) \cong \begin{cases} \dfrac{16\pi\beta\, f_m B_b}{B_{if}^2}\left(1 - \dfrac{0.51 + \log\rho}{1.7}\right) & \log\rho < -0.51 \\ \dfrac{16\pi\beta\, f_m B_b}{B_{if}^2}\sqrt{\dfrac{0.16 - \log\rho}{0.67}} & -0.51 \le \log\rho < 0.16 \\ \dfrac{4\pi^2}{3}\left(\dfrac{B_b}{B_{if}}\right)^3 \cdot \dfrac{1}{\rho^2} & \log\rho \ge 0.16 \end{cases} \quad (3\text{-}40)$$

Figure 3-39 shows this approximation, as well as the FFT results, the results from the 3-term Fourier integral approximation, and the high-ρ approximation.

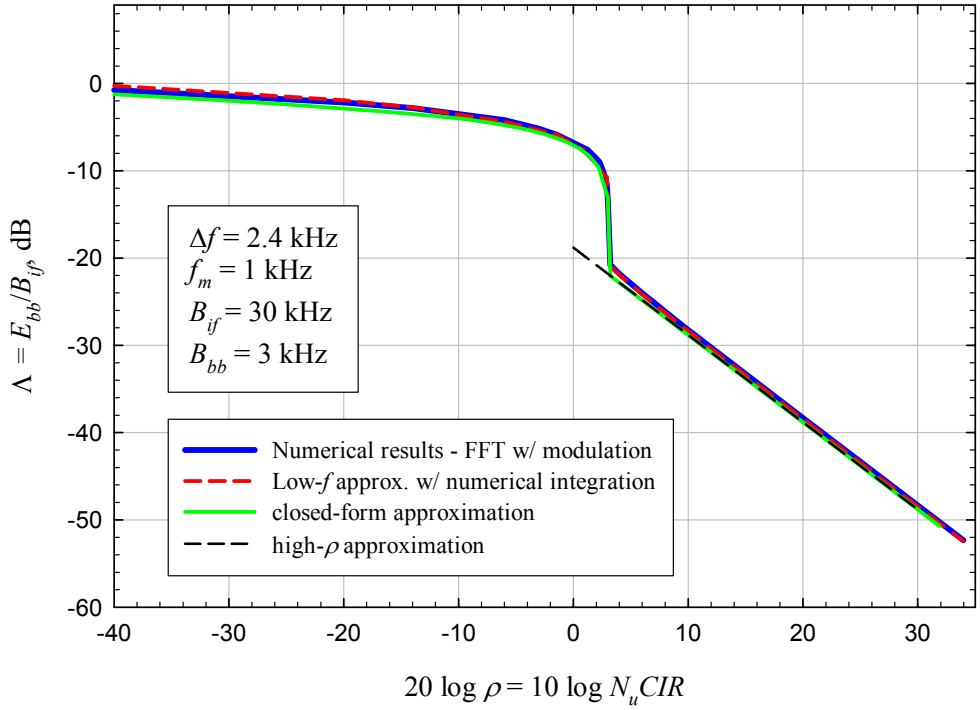

Figure 3-39: *Comparison of closed-form approximation with numerical FFT results and the low-frequency transform approximation using numerical integration*

Clearly, agreement is excellent over the entire range of ρ shown. Just as significant, this approximation has been derived using physical reasoning that clearly explains the mechanism which produces this baseband noise characteristic.

Chapter 3 Reference

[1] "Physical-Layer UWB Interference Impact Analysis," J. E. Padgett, A. A. Triolo, J. C. Koshy, August 8, 2003, sponsored by DARPA under contract MDA972-02-C-0056.